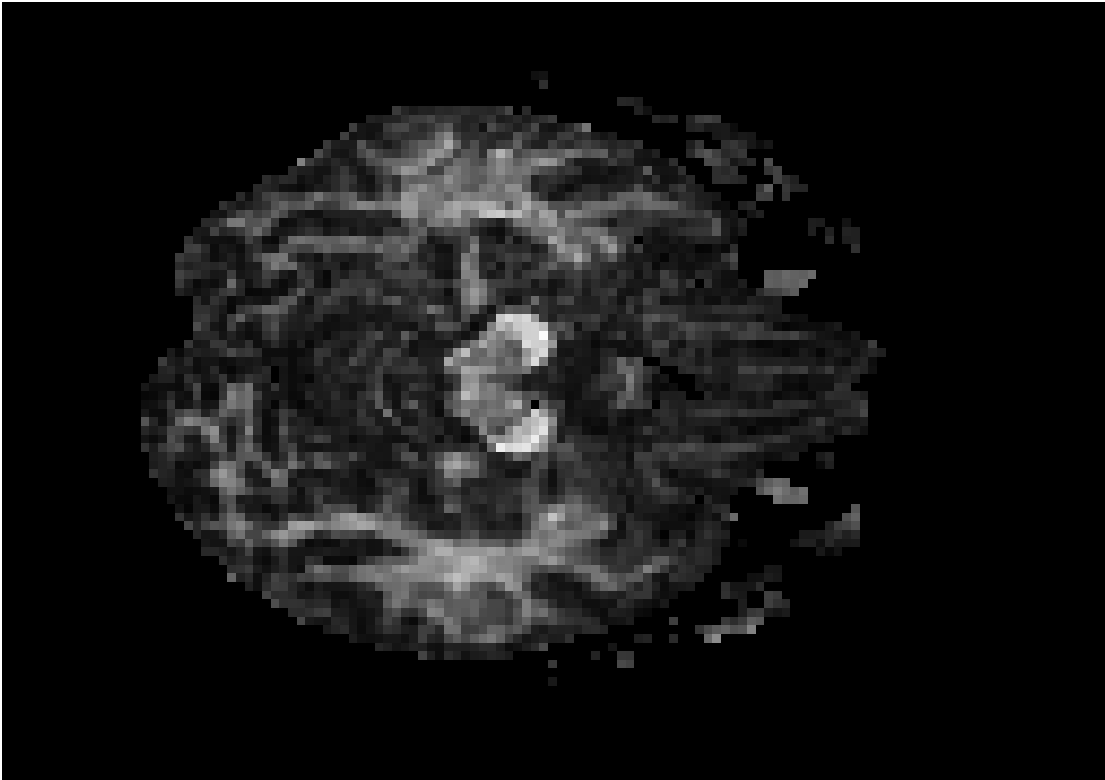# CHALMERS



# Non-Gaussian Diffusion Imaging:

A comparison of the bi-Gaussian and the fourth-order tensor models to diffusion tensor imaging

Master's Thesis in Biomedical Engineering

SOFIA GUNNARSSON

MedTech West

## Abstract

Diffusion weighted imaging (DWI) is a magnetic resonance imaging (MRI) technique that can be used to measure, in vivo, the self-diffusion of water molecules in body tissues. This reveals information about the microstructure of the underlying tissue. The simplest approach to modelling the diffusion at each voxel, known as diffusion tensor imaging (DTI), is as a Gaussian probability density function (PDF). The covariance matrix of this PDF defines a second-order tensor. Whilst this model is adequate for modelling fascicles with a single dominant orientation it is not suitable for more complex tissue architectures; e.g. crossing fascicles. This has driven the development of more sophisticated models such as high-order tensors (HOTs). The aim in fitting such models is to determine: (i) the number fascicles and their orientations and (ii) to extract scalar measures, such as fractional anisotropy (FA), to characterise the tissue microstructure. This knowledge is used for two general types of applications: tractography (visualisation/identification of neural fibre tracts) and the detection/characterisation of diseased tissue.

This thesis explores two non-Gaussian diffusion-modelling approaches. In particular the bi-Gaussian (multi-tensor model with two tensors) and the fourth-order tensor are compared to conventional DTI. In the first part of the thesis synthetic data were generated for a range of signal-to-noise (SNR) values to simulate, for a single voxel, one fibre (for a variety of FA-values), and two crossing fibres (for six FA combinations and a range of crossing angles). Each model was fitted to this data and the quality of the fit evaluated in terms of the three measures: signal deviation, angle deviation and tensor element deviation (in the latter case only when the model matched the structure). The results show that: (i) the fourth-order tensor model consistently has lower signal deviation than the bi-Gaussian and second-order tensor models; (ii) for one fibre both the second-order tensor and the fourth-order tensor models yield low angular deviation, whilst the bi-Gaussian model does not (model-structure mismatch); (iii) for two fibres the angular deviation decreases for both the bi-Gaussian model and the fourth order model with increasing SNR and crossing angle; (iv) the tensor element deviation decreases with increasing SNR.

In the second part of the thesis the concept of FA is explored. In the case of the conventional second-order tensor a standard definition exists for computing a scalar measure of FA from the tensor. FA-definitions for the bi-Gaussian and fourth-order tensor models are explored and compared, empirically (using both the synthetic data and real brain DWI data), to the second-order definition. FA estimation for high-order tensors involves the concept of Z-eigenvalue decomposition. The thesis presents an implementation that is more robust and accurate than the existing open-source implementation. The experimental results for the synthetic data show that: (i) the FA-definition for the second-order tensor in general yields FA-values close to true FA for one fibre and close to the mean value of true FA for two fibres; (ii) the bi-Gaussian FA-definitions all tend to overestimate the true FA for both one and two fibres; (iii) the fourth-order definitions yield FA-values that correlate well with true FA for one fibre and for two fibres with a small crossing angle, but decreases with increasing crossing angle. The results for the real brain data show that FA-maps estimated with the bi-Gaussian model (fitted with

the Levenberg-Marquardt algorithm) yields many undefined values, but that FA-maps estimated with the fourth-order tensor definitions correlate well with the maps estimated with the second order tensor model.

# Acknowledgements

# Contents

iii

# Abbreviations

2DT    Second order Diffusion Tensor

DTI    Diffusion Tensor Imaging

DW    Diffusion Weighted

DWI    Diffusion Weighted Imaging

FA    Fractional Anisotropy

Fascicle    A bundle of fibres

FoO    Fraction of Occupancy

HOT    High Order Tensor

In vivo    Latin for *within the living*

MRI    Magnetic Resonance Imaging

PDF    Probability Density Function

ROI    Region of Interest

SNR    Signal to Noise Ratio

Voxel    Volume element of a 3D digital image; analogous to a picture element (pixel) of a 2D digital image

# 1

# Introduction

T HE RESEARCH DESCRIBED in this thesis was undertaken in the MedTech West centre located at Sahlgrenska University Hospital in Gothenburg, Sweden in 2013. It constitutes part of a larger research project concerned with the development of diffusion imaging tools for the assessment of the visual pathways in the human brain.

This chapter starts with a brief introduction to DWI, and then presents the aim and objective of this thesis, the scope, and finally a description of the structure of this thesis.

## 1.1 Background

An understanding of how the human nervous system, particularly in the brain, is organized has been a long standing area of research. Historically only post mortem and invasive analysis was possible, but now with diffusion weighted MRI (Magnetic Resonance Imaging) (hereinafter denoted DWI) it is possible to visualise the white matter tracts in vivo [1].

With region of interest (ROI) methods it is possible to separate and identify individual tracts. The construction of a 3D-model of the white matter tracts was one of the first applications of DWI. Comparisons of the tractography maps derived from DWI, with structures identified using more invasive methods have shown that DWI is a reliable method for relatively large and homogeneous structures such as the corpus callosum [1].

### 1.1.1 Diffusion Models

The easiest way to model the structure is with DTI (Diffusion Tensor Imaging) which assumes that the diffusion (see section 2.1) PDF can be described with a second order tensor. When a voxel contains crossing, kissing or other multiple fibre directions this model is inappropriate because the second-order tensor describes only an ellipsoid of diffusion with one principal direction. In DWI the resolution is low; one voxel in clinical

DWI typically has a side of one or two millimetres. Since the likelihood that all fibres within one voxel have the same alignment is low, a more complete model is desirable.

DTI utilises a second order tensor to describe the diffusion, and models the signal attenuation as a mono-exponential. However the observed attenuation in tissue is not mono-exponential [2]. Nevertheless, modelling the signal with DTI is still a useful technique and can provide information about the structure of the tissue, with the large advantage of being relatively fast to compute.

Numerous other models have been proposed, including the bi-Gaussian model [2], where the sum of two mono-exponentials model the signal; the multi-Gaussian, similar to the bi-Gaussian but instead a sum of any number of mono-exponentials; DSI, diffusion spectrum imaging; and the high order tensor model, where the conventional second order tensor is replaced with a higher order tensor. These models seek to more accurately describe the hindered diffusion of the water molecules, and thus to yield better reconstructions of the underlying structure.

### 1.1.2 Scalars derived from DWI data

From the data acquired from a DWI-scan and then reconstructed with DTI, it is possible to derive a scalar called FA (Fractional Anisotropy). This is often referred to as a measure of structure or integrity (as discussed in [3]). The possibility to compute a scalar that describes the fibre integrity or fibre structure of each voxel could help determine the progress of diseases like MS (Multiple Sclerosis) or Alzheimer's Disease that cause demyelination of white matter fibres [4]. It is also proposed that FA-maps can provide a method to demonstrate improvement of white matter integrity after tumour removal.

In those cases where the micro-structural integrity is of interest (demyelination, structural damage, etc.), the fibre directions are unimportant [3]. FA is used to help determine a suitable starting point for tractography, because a high FA also is indicative of the structure in the voxel. A high degree of structure is in this context a voxel with highly aligned white matter fibres.

However it can also be argued that a voxel with two clearly distinguishable fascicles is highly structured. Similarly a voxel containing three, four or more fascicles are highly structured when compared with, for example, grey matter. It is clear that structure and integrity are difficult terms to define. Therefore, clinical experts engaged in research in DWI have been consulted throughout this project, to gain an understanding of what it is that they perceive FA to mean.

A standard definition of FA exists for DTI, but not for other reconstruction models. In this thesis we evaluate the various definitions that have been proposed in the literature for a select set of models as outlined in the Aims and Objectives. For models where it is possible to generate multiple FA values, for example the multi-tensor models, the DWI community is not in agreement about whether FA should be expressed as one or several scalars. In this thesis we have adopted the convention that FA is a single scalar when generating FA maps.

## 1.2   Aims and Objectives

The first aim of this research was to compare the conventional Gaussian diffusion model with two non-Gaussian diffusion models, the bi-Gaussian and the fourth-order tensor, for single and crossing fibre architectures.

The second aim of this research was to explore the concept of FA and to evaluate existing FA definitions for the three models chosen in the first aim.

To this end the research had the following objectives:

i) To generate synthetic data to simulate a single voxel, a single fibre (for three different FA values), and two crossing fibres (for six FA combinations, and a range of crossing angles).

ii) To fit each model to this data and evaluate the quality of the fit in terms of the three measures: signal deviation, angle deviation and tensor element deviation.

iii) To review the physical meaning and significance of FA.

iv) To develop a robust and accurate implementation of the Z-eigenvalue decomposition algorithm needed for the FA estimation for high order tensors.

v) To investigate and compare FA definitions for the bi-Gaussian and fourth-order tensor models, empirically (using both the earlier synthetic data and real brain DWI data), to the second-order definition.

## 1.3   Scope

The non-Gaussian diffusion models explored in this research were limited to the bi-Gaussian and fourth-order tensor. The general problem of estimating the number of fascicles and their relative fractions within a voxel was not considered in this thesis.

## 1.4   Structure of the Thesis

The remainder of the thesis is organised as follows:

**Chapter 2**   Briefly reviews the concept of diffusion, describes what DWI (Diffusion Weighted Imaging) is and how it is used to measure diffusion, and presents the three diffusion models explored in this thesis.

**Chapter 3**   Addresses objectives i) and ii) associated with the first aim of the thesis. In particular it evaluates how well the three diffusion models perform in terms of signal deviation, angle deviation and tensor element deviation. The framework used for synthesising the signal is presented and how the quality measures are calculated is described. The resulting measures are presented and the models compared.

**Chapter 4** Addresses objectives iii), iv) and v) associated with the second aim of the thesis. In particular the concept of FA and what it means is discussed. The protocol for synthesising signals with known FA for use in the experiments is described, as well as how to estimate the FA values for the three different models. Z-eigenvalue decomposition of high order tensors is discussed, and a new implementation is presented. Finally the results of the FA value estimation experiments for the different models are presented and compared.

**Chapter 5** Summarises the thesis and the conclusions. Future work and improvements are proposed.

**Appendix** The complete set of results are presented here, in three appendices. The first with the results from model evaluation and the second from synthetic FA-estimations and the third with real data FA-maps.

# 2

# Diffusion Weighted Imaging

T HIS CHAPTER BEGINS by describing diffusion, and the difference between isotropic and anisotropic diffusion. Section 2.2 then describes diffusion weighted imaging (DWI) which is an magnetic resonance imaging (MRI) technique for measuring bulk diffusion in vivo. Section 2.3 describes conventional Gaussian diffusion (the simplest model of diffusion). Finally Section 2.4 describes the two non-Gaussian diffusion models explored in this thesis.

## 2.1 What is Diffusion, and what is DWI?

The term diffusion refers to the random, or Brownian, motion of particles or molecules in a liquid or gas. DWI is an MRI technique that measures the self diffusion of water molecules in body tissue, i.e. the random displacement of the molecules due to thermal agitation. In an unrestricted volume, the diffusion of water is isotropic, the Brownian motion is the same in all directions. However within structured tissue, like the brain white matter, the diffusion is not isotropic, but depends on the direction. Anisotropic diffusion is not restricted to brain white matter, but can be found in other biological tissues also [5]. Herein though the focus is on white matter.

   DWI can be used to perform tractography, that is to identify and visualise the white matter fibre tracts via the main direction of diffusion in each voxel. DWI can also provide information about the progress of a disease or condition, for example a brain tumour, via both tractography and scalar measures (features) describing tissue structure.

## 2.2 How to Measure Diffusion with MRI

In DWI the signal derives from the signal attenuation due to diffusion or more precisely the proton spins dephasing in a spatially varying magnetic gradient [5]. A scan is made

without diffusion weighting ($b = 0$ [1]), providing a reference signal, $S_0$. Then DWI measurements are executed with a diffusion sensitising gradient applied in several directions ($b \neq 0$). A model of diffusion is then fitted voxel-wise to this data. The model makes it possible to quantitatively characterise the diffusion. The complexity of the model together with sampling considerations determines the minimum number of gradient directions. The $b$-value is determined by several factors including the desired resolution, the apparatus and the scanning time.

DWI is an MRI method where the applied magnetic field is not homogeneous as in $T_1$- and $T_2$-weighted images. Instead the pulsed magnetic field is linearly varied causing the protons in the water to precess at different rates. A refocusing gradient pulse of the same magnitude but opposite direction is applied, and those protons that have moved will not be perfectly refocused, causing a detectable signal loss. This diffusion weighted method was introduced by Stejskal and Tanner, who gave name to the Stejskal-Tanner-equation:

$$\frac{S}{S_0} = e^{-T_E/T_2} e^{-\gamma^2 G^2 \delta^2 \left(\Delta - \frac{\delta}{3}\right) D} \tag{2.1}$$

describing the signal attenuation, where $S$ is the signal with applied gradient $G$ and $S_0$ without, $\gamma$ is the gyromagnetic ratio, $\delta$ the duration of the pulses, $\Delta$ the time from the first pulse to the refocusing pulse, $T_E$ the echo time, $T_2$ the spin-spin relaxation time, and $D$ the diffusion-coefficient [5].

To simplify equation (2.1) it is convenient to set $b = \gamma^2 G^2 \delta^2 \left(\Delta - \frac{\delta}{3}\right)$, this is called the $b$-value. Additionally, if the term $e^{-T_E/T_2}$ is assumed to be constant over all gradients, the Stejskal-Tanner equation is reduced to:

$$\frac{S}{S_0} = e^{-bD}. \tag{2.2}$$

In DWI, the conventional way to estimate the diffusion is to model the ADC (Apparent Diffusion Coefficient) with a second order tensor according to

$$ADC = -\log\left(\frac{S}{S_0}\right). \tag{2.3}$$

This has known disadvantages when the underlying structure does not have one main direction of diffusion, but consists of several directed sources of diffusion. Many other approaches have been proposed to address this problem. The bi-Gaussian model and the fourth-order diffusion tensor are two such models. In this thesis they are compared to the second order tensor used in conventional DTI (Diffusion Tensor Imaging) in terms of signal error, angular error and tensor element error. The tensor element error only makes sense when the structure and model matches, for example for DTI when modelling one fibre, and bi-Gaussian when modelling two crossing fibres.

---

[1]$b = \gamma^2 G^2 \delta^2 \left(\Delta - \frac{\delta}{3}\right)$ usually in s/m$^2$. For further explanation of the $b$-value see the following paragraphs and Section 2.2.1

### 2.2.1 The $b-$value

As described previously, the term b-value was introduced in [6] to simplify the Stejskal-Tanner equation, (2.1). This is somewhat misleadingly suggesting that the b-value is less complex than it is. Commonly in literature the b-value is described as a constant value, e.g. 1500 as used in this report, but $b = \gamma^2 G^2 \delta^2 \left( \Delta - \frac{\delta}{3} \right)$. These constituent parameters all have different impacts on the result.

The term $e^{-T_E/T_2}$ in equation (2.1) is often omitted since it generally is considered to be constant over all gradients. Nevertheless it describes the signal's exponential dependency on $T_E$. Increasing $T_E$ will decrease the signal amplitude, and significantly decrease the SNR (Signal to Noise Ratio) for all measurements regardless of the b-value. Considering only unit-norm gradients, $b_{\text{nominal}} = \gamma^2 \delta^2 \left( \Delta - \frac{\delta}{3} \right)$, the relationship between $T_E$ and b-value can be approximated according to

$$T_E \approx \frac{12 b_{\text{nominal}}}{\gamma^2}. \tag{2.4}$$

Increasing the b-value, will also result in a larger minimal $T_E$ and thus decrease the SNR [7]. This is one of the important trade-off's in DTI, a higher b-value is known to increase the contrast between the DW (Diffusion Weighted) gradient directions, but forces $T_E$ to rise and SNR to drop.

If we instead not are considering unit-norm gradients, the b-value can be increased without affecting the $b_{\text{nominal}}$. Since $b_k = b_{\text{nominal}} G_k^2$ the desired gain can be obtained by increasing the gradients to have norm greater than one.

## 2.3 Gaussian Diffusion

Before DWI became a widely-used imaging technique, it had been observed that in diffusion MRI the echo intensity was dependant on the specimen's orientation with respect to the direction of the applied magnetic field gradient, characterised by the diagonal elements of the effective self-diffusion tensor $\mathbf{D}^{\text{eff}}$. $\mathbf{D}^{\text{eff}}$ is a 3 times 3 symmetric matrix with six unique elements. In 1993, Basser, Mattiello and LeBihan in [6] proposed that the off-diagonal elements of $\mathbf{D}^{\text{eff}}$ must be taken into account to fully characterise anisotropic diffusion. In other words, both the eigenvectors and eigenvalues are of importance; not only the eigenvalues. This provided a more general model than the previous, where the diagonal elements non-equality only provided information about the isotropic or anisotropic nature of the structure. An estimation of the fibre tracts orientations and distributions *in vivo*, i.e. tractography, was now possible.

### 2.3.1 DTI

In DTI the PDF (Probability Density Function) of the water molecules diffusion is assumed to be Gaussian. The covariance matrix of this PDF is a second order tensor

(2DT) $\mathbf{D}$ written

$$\mathbf{D} = \begin{bmatrix} D_{xx} & D_{xy} & D_{xz} \\ D_{xy} & D_{yy} & D_{yz} \\ D_{xz} & D_{yz} & D_{zz} \end{bmatrix}. \tag{2.5}$$

The tensor is symmetric with 3 rows and 3 columns, and thus out of those nine elements only six are unique. This covariance matrix describes the diffusion along and correlation between orthogonal axes [5].

Using the Stejskal-Tanner equation the signal with gradient directions $\vec{g}$ (which is included in $\mathbf{b}$) is

$$S = S_0 \cdot e^{-\mathbf{b}:\mathbf{D}} \tag{2.6}$$

where $\mathbf{b} : \mathbf{D}$ is defined according to

$$\mathbf{b} : \mathbf{D} = b \cdot (g_{xx}\mathbf{D}_{xx} + g_{yy}\mathbf{D}_{yy} + g_{zz}\mathbf{D}_{zz} + 2g_{xy}\mathbf{D}_{xy} + 2g_{xz}\mathbf{D}_{xz} + 2g_{yz}\mathbf{D}_{yz}). \tag{2.7}$$

To determine $\mathbf{D}$ at least seven measurements must be performed where one usually is with $b = 0$. The $b = 0$ signal is here denoted $S_0$.

Since DTI utilises a second order tensor to describe the diffusion, it cannot describe more than one main direction (corresponding to the dominant eigenvalue/-vector pair). For complex fibre structures such as crossing, kissing, branching, etc., this disadvantage motivates the use of more complex models.

## 2.4 Non-Gaussian Diffusion

The first proof that the diffusion of water-molecules in the brain tissue is not Gaussian was presented in the $1990s$[1]. Two methods to model the non-Gaussian properties are described here. The first method, the multi-Gaussian model, extends Equation (2.6) to a sum of exponentials. This has been discussed and evaluated in [1], [2], [7]. The second method, the high order diffusion tensor model, can model more complex inter-voxel fibre structures [8]. This model extends the second order tensor to a fourth order tensor, and can thus describe more complex structures.

### 2.4.1 Multi-Gaussian Diffusion

The bi-Gaussian model is an extension of the mono-exponential conventional second order diffusion tensor. A second exponential term is added, thus the signal now is described by

$$S = S_0(A_1 \cdot e^{-b\mathbf{g}:\mathbf{D}_1} + A_2 \cdot e^{-b\mathbf{g}:\mathbf{D}_2}). \tag{2.8}$$

Here $A_1$ and $A_2$ are the fractions of occupancy, i.e. what proportion of the voxel's volume that is assigned to that tensor (fascicle). This can be extended to a multi-Gaussian model, with any number of exponentials, each corresponding to one fascicle's direction.

The simplification utilised in DTI for the relationship between $S_0$ and $S$, transforming the non-linear problem to a linear problem cannot be used here. Estimating the two tensors $\mathbf{D}_1$ and $\mathbf{D}_2$ in Equation (2.8) is more difficult than to estimate $\mathbf{D}$ in Equation (2.6). Additionally, to estimate the scalars $A_1$ and $A_2$, it was demonstrated by [7] that the signals must be acquired over a range of $b-$values to avoid an infinite number of solutions.

### 2.4.2 High Order Diffusion Tensor

In 2002, high angular resolution diffusion imaging (HARDI) was proposed in [9], to describe non-Gaussian diffusion. Over a sphere $N$ discrete gradient directions are sampled. Without assuming the nature of the diffusion, the apparent diffusion coefficient is estimated in all gradient directions. One of the methods proposed to analyse HARDI data is with high order tensors (HOT's).

An advantage of using the high order diffusion tensor is that the 2DT theory can be generalised. The signal is modelled with Equation (2.6) but $\mathbf{D}$ is now a 3-dimensional fourth order tensor, instead of a 3-dimensional second order tensor.

# 3

# Empirical Evaluation of Non-Gaussian Diffusion Models

THIS CHAPTER PRESENTS an empirical evaluation of the two selected non-Gaussian diffusion models – the bi-Gaussian and the 4th-order tensor – and the conventional 2nd-order tensor model used in DTI (Diffusion Tensor Imaging). The aim of the evaluation was to investigate how well the two non-Gaussian models describe single and crossing fibres compared to DTI. Several experiments are presented that evaluate the performance of the three models in terms of signal deviation, angle deviation and tensor element deviation. In the first section the framework used to generate the synthetic data (with prescribed structure, properties, and noise) is described. Section 3.2 describes how the three models were fitted to the synthetic data. In the first section the framework used to generate the synthetic data (with prescribed structure, properties, and noise) is described. Section 3.3 defines the three quality of fit measures and the required adjustments depending on the fibre architecture/structure and model. Section 3.4 presents the fitting results. A discussion of these results is then presented in Section 3.5.

## 3.1  Evaluation Framework

The commonly used evaluation framework of [10] was used in this study. This framework prescribes the steps involved in synthesising signals corresponding to different rotations of a fascicle architecture in a single voxel (for different noise levels), model fitting, and measurement of the goodness of fit. More specifically the framework comprises the following steps:

(i) The structure to synthesise is defined, i.e. the number of fibres and their FA-values (FA is short for fractional anisotropy).

(ii) The gradient directions and $b$-value are defined.

(iii) The number of rotations $N_R$ and Euler angles, noise levels $N_\sigma$, number of noise realisations $N_{RN}$ and crossing angles $N_\phi$ are defined.

(iv) The tensor defined in step (i) is rotated with an angle defined in step (iii).

(v) The diffusion signal is simulated, for underlying structure with one fibre according to the Stejskal-Tanner equation (2.1), or for two fibres according to Equation (2.8).

(vi) The tensors $\mathbf{D}$ is estimated with each model.

(vii) The measures of goodness of fit and derived scalar measures are calculated.

(viii) Steps (v) to (vii) are repeated for a total of $N_{RN}$ Rician noise realisations.

(ix) Steps (iv) to (viii) are repeated for a total of $N_R$ different rotations.

(x) The mean values and standard deviations for the goodness of fit measures and scalar measures are calculated.

In this research the focus lies in how well the FA-maps correlate with the underlying structure. Thus the FoO (Fraction of Occupancy) values have been assumed to be known during the simulations and estimations, and were always set to 0.5 each, such that there are two fascicles of the same fraction in each voxel.

### 3.1.1 Fascicle structures/architecture defined in this study

The fascicle structures/architecture used in this study were all defined in terms of the number of crossing fibres (one or two) and their individual FA-values. Three different FA-values were used: $FA_{high} = 0.94$, $FA_{medium} = 0.51$ and $FA_{low} = 0.18$. For one fibre this resulted in three FA-structures: high, medium and low, and for two crossing fibres in six: high-high, high-medium, high-low, medium-medium, medium-low and low-low.

The three different FA-values defined three diffusion tensors, one high, one medium

and one low according to the following

$$\mathbf{D}_{high} = \begin{pmatrix} 17 & 0 & 0 \\ 0 & 1.01 & 0 \\ 0 & 0 & 1 \end{pmatrix} \cdot 10^{-4} \tag{3.1}$$

$$\tag{3.2}$$

$$\mathbf{D}_{medium} = \begin{pmatrix} 17 & 0 & 0 \\ 0 & 10 & 0 \\ 0 & 0 & 5 \end{pmatrix} \cdot 10^{-4} \tag{3.3}$$

$$\tag{3.4}$$

$$\mathbf{D}_{low} = \begin{pmatrix} 1.4 & 0 & 0 \\ 0 & 1.1 & 0 \\ 0 & 0 & 1 \end{pmatrix} \cdot 10^{-4}. \tag{3.5}$$

Their magnitudes are based on the largest diffusivity [1] experimentally found along a fibre [3]. Each was used as an initialisation tensor $\mathbf{D}_{init}$ to generate the synthetic signals and were appropriately rotated to create the desired fibre-crossing structure. Due to symmetry, it suffices to define the acute angle of intersection between two fascicles to be from 0° to 90° in steps of 10°.

### 3.1.2 Gradient Directions

The gradient directions used in the study are the 81 evenly distributed directions defined in [11]. This was chosen to assure that the tensor-element estimation is robust. For DTI it was shown in [12] that at least 30 unique sampling directions are necessary to estimate the six unique elements. For the fourth order tensor, as described in Section 3.2.3, we have fifteen unique elements to estimate requiring a larger set of sampling directions. The $b$-value was chosen to be 1500 s/mm$^2$ which is a value that can be found in the clinical settings [7].

### 3.1.3 Noise

The noise in measured MRI (Magnetic Resonance Imaging) signals is commonly assumed to be of Rician distribution [13]. Therefore we added Rician noise to the synthetically generated signals for values of $\sigma \in [0.02, 0.14]$ in steps of 0.02, where $\sigma = 1/\text{SNR}$. This resulted in $N_{RN} = 7$ noise realisations with SNR $\in [7.1, 50]$. In [3] a lowest SNR for practical use and a given $b$-value was suggested according to

$$\text{SNR}_{min} = \frac{3}{e^{-b \cdot 10^{-3}}} \tag{3.6}$$

---

[1] Diffusivity has unit m$^2$/s and describes how fast the molecules diffuse

where $b$ is in $\mathrm{mm}^2/\mathrm{s}$. With a $b$-value of 1500 $\mathrm{mm}^2/\mathrm{s}$ this means that in practical use the SNR for that $b$-value should be larger than 14. Given that when we generate the synthetic signal we can choose what SNR-range to use, it was chosen to cover this smallest value with margin, thus covering a range from more noise than preferred to very little noise.

The Rician noise was generated and added to the noise-free signal $S$ according to

$$S_{\mathrm{noise}} = \sqrt{(S + n_1)^2 + (n_2)^2} \tag{3.7}$$

where $S_{\mathrm{noise}}$ is the noisy signal, $n_i = \sigma\delta_i$ and $\delta \in [0,1]$ is a normally distributed pseudo-random number. For each noise level the procedure was repeated $N_{\mathrm{RN}} = 25$ times each time for new $\delta$. In this way seven noise level sets of synthetic signals were generated, giving a total of $25 \times 7$ noise-realisations.

### 3.1.4 Procedure for creating rotations of the crossing fibre signals

Since the number of gradient directions is finite, the fibre orientation in relation to the gradient directions has an impact on the signal intensity. For example, in the extreme case with only one gradient direction applied, a fibre perpendicular to the gradient direction generates a stronger signal than a parallel one would, see equation (2.6) and (2.7). To limit the signal-dependence on the fibre-gradient-orientation relation, multiple rotations of each crossing fibre signal were generated.

Each diffusion tensor $\mathbf{D}$ was rotated with a rotation matrix $\mathbf{R}$ to obtain $\mathbf{D} = \mathbf{R}\mathbf{D}_{\mathrm{init}}\mathbf{R}^{\mathrm{T}}$, where $\mathbf{R}$ was defined by combining the three rotational matrices according to equation (3.8), one for rotation about each axis, $\mathbf{R}_x$, $\mathbf{R}_y$ and $\mathbf{R}_z$. The three rotation matrices are shown in Equations (3.9) – (3.11) where $\alpha$, $\beta$ and $\gamma$ are the angles to rotate around the x-, y- and z-axis respectively. $\mathbf{D}_{\mathrm{init}}$ is an initialisation tensor with elements defined to achieve a desired FA-value, as described in Section 3.1.1.

$$\mathbf{R} = \mathbf{R}_x\mathbf{R}_y\mathbf{R}_z \tag{3.8}$$

$$\mathbf{R}_x = \begin{pmatrix} 1 & 0 & 0 \\ 0 & \cos(\alpha) & -\sin(\alpha) \\ 0 & \sin(\alpha) & \cos(\alpha) \end{pmatrix} \tag{3.9}$$

$$\mathbf{R}_y = \begin{pmatrix} \cos(\beta) & 0 & \sin(\beta) \\ 0 & 1 & 0 \\ -\sin(\beta) & 0 & \cos(\beta) \end{pmatrix} \tag{3.10}$$

$$\mathbf{R}_z = \begin{pmatrix} \cos(\gamma) & -\sin(\gamma) & 0 \\ \sin(\gamma) & \cos(\gamma) & 0 \\ 0 & 0 & 1 \end{pmatrix} \tag{3.11}$$

The rotation procedure was performed in the same way for both one fibre and two fibre synthetic signals. Rotations corresponding to the following intervals $\alpha \in [0, \pi/2]$,

$\beta \in [0, \pi/2]$ and $\gamma \in [0, 2\pi]$ were considered. For $\alpha$ and $\beta$ the intervals were evenly divided into three steps each and $\gamma$ for four. Thus the fibres were rotated a total amount of 36 times.

## 3.2 Fitting the Models

The Gaussian diffusion model (DTI) and the two non-Gaussian models (the fourth order tensor model and the bi-Gaussian model) were fitted to each synthetic signal in turn as described below.

### 3.2.1 DTI (Second order tensor model)

The estimate of the tensor $\mathbf{D}$, denoted $\hat{\mathbf{D}}$, was estimated using a linear least squares fit of the diffusivity function $d(\vec{g_i})$ with respect to the six unique elements in $\hat{\mathbf{D}}$ according to

$$\min_{\hat{\mathbf{D}}} \left\{ \sum_{i=1}^{N} \left( d(\vec{g_i}) - \hat{d}(\vec{g_i}) \right)^2 \right\}. \qquad (3.12)$$

The relation between the diffusivity function and the logarithm of the signal is linear, viz.

$$d(\vec{g_i}) = -\frac{1}{b} \log \left( \frac{S_i}{S_0} \right) \qquad (3.13)$$

and the relation between the measured signal and estimated tensor is

$$\hat{S}_i = S_0 e^{-b\vec{g_i}\hat{\mathbf{D}}\vec{g_i}^T}. \qquad (3.14)$$

### 3.2.2 Bi-Gaussian Model

The bi-Gaussian model was fitted using non-linear least squares (Levenberg-Marquardt algorithm) to obtain estimates for the two second order tensors $\mathbf{D}_1$ and $\mathbf{D}_2$ according to

$$\min_{\hat{\mathbf{D}}_1, \hat{\mathbf{D}}_2} \left\{ \sum_{i=1}^{N} \left( S_i - \hat{S}_i \right)^2 \right\} \qquad (3.15)$$

where $N$ is the number of gradient directions. The relationship between the measured signal and estimated tensors is given by

$$\hat{S}_i = 0.5 e^{-b\vec{g_i}\hat{\mathbf{D}}_1\vec{g_i}^T} + 0.5 e^{-b\vec{g_i}\hat{\mathbf{D}}_2\vec{g_i}^T} \qquad (3.16)$$

which cannot be expressed as a linear least squares problem as was the case for DTI.

To initialise the minimisation, three approaches were investigated:

1. Ranged random initialisation [9], where the initial guess is two second order tensors of three dimensions, whose elements are of $10^{-4}$ order of magnitude. The order of magnitude is based on the free diffusion of water at $37°$ [7] [6].
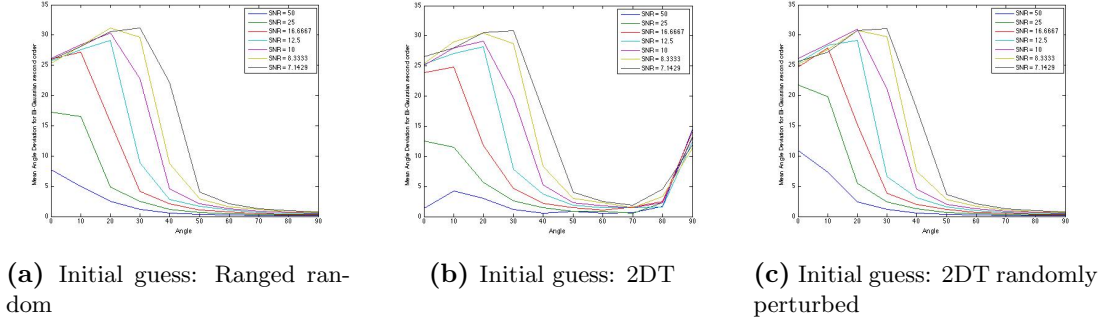
**(a)** Initial guess: Ranged random

**(b)** Initial guess: 2DT

**(c)** Initial guess: 2DT randomly perturbed

**Figure 3.1:** Angle deviation as a function of fibre crossing-angle for the bi-Gaussian tensor estimation of different initialisation methods.
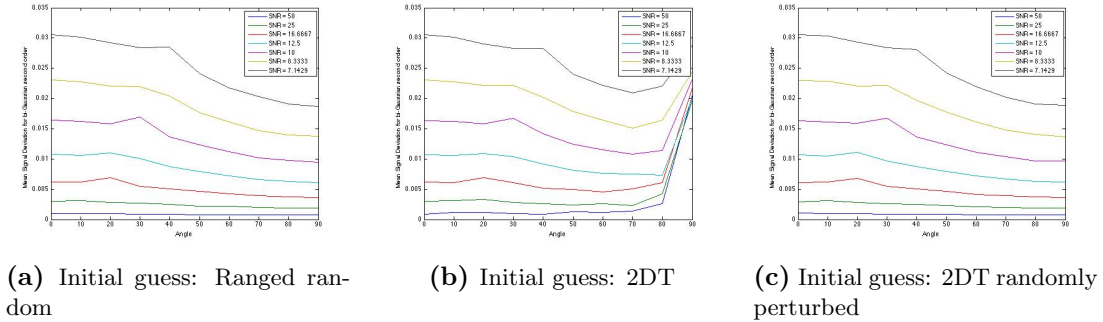


**(a)** Initial guess: Ranged random

**(b)** Initial guess: 2DT

**(c)** Initial guess: 2DT randomly perturbed

**Figure 3.2:** Signal deviation as a function of fibre crossing-angle for the bi-Gaussian tensor estimation of different initialisation methods.

2. A conventional 2nd-order tensor is estimated, which is used as the initial guess for both bi-Gaussian tensors [14].

3. To avoid local minima, a conventional 2nd-order tensor is estimated and randomly perturbed (a random number in the range $[-1, 1] \times 10^{-4}$ is added to each tensor element) as initial guess. This is repeated twenty-five times (no improvement was detected with more than 25 repetitions).

The angular deviation for the three initialisation methods is shown in Figure 3.1. For angles lower than $50°$ the results are similar, but for larger angles the two random initialisations are superior. With the DTI initialisation the optimisation step found local minima for large crossing angles, which resulted in a larger angular deviation. The signal deviation, see Figure 3.2, shows the same pattern. For low angles the methods' deviations are similar, but for higher angles the DTI initialisation yields larger deviation. The computation times for method 1 and 2 are significantly lower than for method 3.

15

### 3.2.3  Fourth Order Tensor Model

One method for indexing the elements of a (fourth order) tensor $A$ is by four indices $i_1, \ldots i_4$, one for each order, $i_m \in [1,2,3]$ for three dimensions. But the diffusion tensor has an inherent symmetry by definition (similar to the symmetry in DTI) which makes the fourth order, three dimensional tensor possible to represent with fifteen unique elements. Each can be represented by a lower case letter with two indices, here $a_{kl}$ where $k,l \in 0, \ldots, 4$ and effectively determine the number of 1's and 2's (and therefore also 3's) for $A_{i_1 i_2 i_3 i_4}$. One way to interpret the indices for A is to translate 1,2 and 3 to x,y and z respectively.

**Example**   The element $A_{1123}$ of the supersymmetric tensor $A$ can also be represented by the element $a_{21}$ in the fifteen element long vector **a**.

For the fourth order model the fitting introduced in [15] that ensures that the fourth order tensor is PSD (Positive Semi-Definite) was used. The estimated signal was then fitted, using non-linear least squares, to the Cartesian tensor orientation distribution function (CT-ODF) according to

$$\min_{\lambda} \left\{ \sum_{i=1}^{N} \left( \frac{S_i}{S_0} - \hat{S}_i \right)^2 \right\} \tag{3.17}$$

and the estimated signal is defined according to

$$\hat{S}_i = \int_{S_2} \sum_{j=1}^{M} \lambda_j p(\vec{g_i}; \vec{c})^2 B(\vec{v}, \vec{g}, b) d\vec{v} \tag{3.18}$$

where $B$ is the response function and the kernel is a fourth order tensor defined by $\lambda$. The author of [15] has developed an open source software package which was used to perform the fourth order tensor fit.

## 3.3  Measures of Goodness-of-Fit

For each synthetic signal, the three models were fitted and three goodness-of-fit measures calculated for each. The calculation of these measurements depends not only on the underlying structure (represented by the synthetic signal), but also on the model used. This section describes how the calculations of the measures were performed.

### 3.3.1  Signal Deviation

Signal deviation $\Delta S$ provides a measure of the percentage deviation between the measured signal $S$ and the signal $\hat{S}$ estimated by the model; i.e.

$$\Delta S = \frac{1}{N} \sum_{i}^{N} \frac{S_i - \hat{S}_i}{S_i}. \tag{3.19}$$

$\hat{S}$ was calculated according to Equation (3.14) for DTI, Equation (3.15) for the bi-Gaussian model and Equation (3.18) for the fourth order tensor model.

### 3.3.2  Angle Deviation and Estimation of the Main Direction

The angle deviation measure $\Delta\phi$ gives the angular difference between the simulated structure's direction or directions and the estimated direction. In [16] a mean angle error was used for validation of the results. Since DTI yields one main direction, bi-Gaussian two and the fourth order tensor theoretically up to thirteen directions the angular deviation was defined in three different ways.

 The number of fibres were assumed to be known when estimating the angle deviation for the fourth order tensor model; i.e. the problem of estimating how many crossing fascicles are contained in a single synthetic signal was not considered in this thesis (as noted in Section 3.1).

**Angle Deviation for Single Fibre Simulations**

When simulating one single fibre, the underlying structure can be described with one clearly defined main direction $\phi$. For the simplest case, DTI, the angle deviation was defined as the absolute difference in degrees between the estimated second order tensor's main direction and the simulated fibre's direction. The eigenvector $\vec{e}_{\max}$ corresponding to the largest eigenvalue $\lambda_{\max}$ is directed in the estimated fibre's main direction $\hat{r}$ such that $\vec{e}_{\max} = \hat{r}$. The angle deviation for DTI was defined according to

$$\Delta\phi = \left| \phi - \hat{\phi} \right|. \tag{3.20}$$

The angle between two vectors was determined according to

$$\left| \phi - \hat{\phi} \right| = \arccos\left( \frac{r \cdot \hat{r}}{\sqrt{r^2 \cdot \hat{r}^2}} \right) \tag{3.21}$$

where $r$ is the ground truth main direction and equal to the main eigenvalue's corresponding eigenvector. Since $\arccos(x) \in [0, 180]$ and the acute angle was sought, $\phi = 180 - \phi$ if the resulting angle was larger than $90°$.

 For the bi-Gaussian model, the two tensors both gave one estimated main direction each, $\hat{\phi}_1$ and $\hat{\phi}_2$. The angle deviation was calculated according to

$$\Delta\phi = \frac{1}{2} \sum_{i=1}^{2} \left| \phi - \hat{\phi}_i \right| \tag{3.22}$$

where the angular difference and directions were calculated in the same way as for DTI, see Equation (3.21).

 As previously mentioned, the estimation of the number of fibres was not within the scope of this thesis. Thus so for the fourth order tensor model one main direction was sought. This was, in the same way as for the conventional second order tensors, found

by the maximum eigenvalue and it's corresponding eigenvector. The generalisation of eigenvalues and eigenvectors of two-dimensional matrices into symmetric matrices of even order are called Z-eigenvalues and Z-eigenvectors and is described in Section 4.4. The angle deviation was then calculated in the same way as for DTI, according to Equation (3.20).

**Angle Deviation for Simulations with two Crossing Fibres**

When the underlying structure was two simulated crossing fibres with main directions $r_1$ and $r_2$ the angle deviation for DTI was defined according to

$$\Delta\phi = \frac{1}{2}\sum_{i=1}^{2}\left|\phi_i - \hat{\phi}\right| \tag{3.23}$$

where $|\phi - \hat{\phi}|$ was defined in the same way as for one simulated fibre, see Equation (3.21).

For the bi-Gaussian and fourth order tensor models the angle deviation for the two estimated directions $\hat{r}_1$ and $\hat{r}_2$ had to be be combined with the right ground truth directions $r_1$ and $r_2$ which was achieved by minimising the sum of the possible differences as follows

$$\Delta\phi = \frac{1}{2}\min\left\{\left|\phi_1 - \hat{\phi}_1\right| + \left|\phi_2 - \hat{\phi}_2\right|, \left|\phi_1 - \hat{\phi}_2\right| + \left|\phi_2 - \hat{\phi}_1\right|\right\}. \tag{3.24}$$

### 3.3.3 Tensor Element Deviation

The tensor element deviation $\Delta D$ was only calculated when the model and underlying structure matched, i.e. when estimating one simulated fibre with DTI or two simulated fibres with the bi-Gaussian model. It is defined according to

$$\Delta D = \frac{1}{n}\sum_{i=1}^{n}\left|D_i - \hat{D}_i\right| \tag{3.25}$$

where $n$ is the number of tensor components in the model.

## 3.4 Results

For all setups the three measures of quality were plotted as a function of SNR and in the case of two fibres, the crossing angle as well. The complete set of figures can be found in Appendix A. A representative selection of results is presented below.

### 3.4.1 Results for One Fibre-Structure
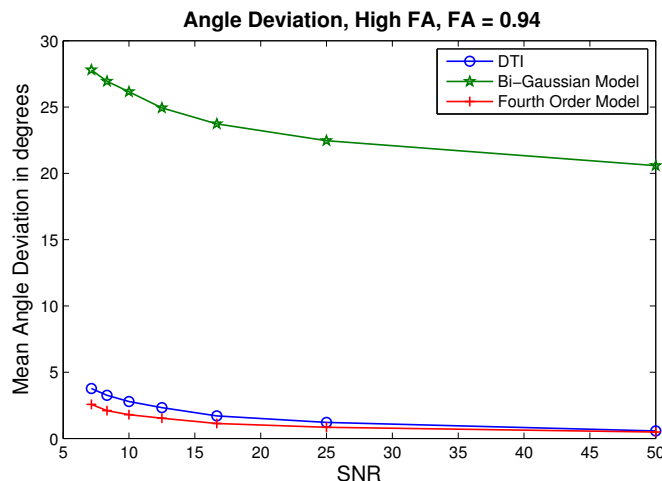


**Figure 3.3:** Mean angle deviation, one fibre. Ground truth FA= 0.94. The bi-Gaussian model's large angle deviation is because the model approximates two tensors when the underlying structure is composed of only one.

A summary of the number of times that the two non-Gaussian models yielded smaller deviation than DTI, and that the fourth order tensor model yielded smaller deviation than the bi-Gaussian is presented in Table 3.2 (note that the percentage was calculated over all SNR-levels). This shows that the fourth order model yielded smaller angular deviation than the bi-Gaussian for all FA-values, and compared to DTI the deviation is smaller for the high FA-value but not medium and low. The bi-Gaussian model had the largest deviation for all three FA-values. Figure 3.4 presents the angle deviations for each component tensor of the bi-Gaussian model separately. For high and medium FA the best fit-deviation is lower than 20° for all SNR-levels and lower than 10° for SNR above 14. Compared to the results in Figure 3.3 this is low. So the bi-Gaussian model seems to, in the case of medium or high FA-values, fit one of the two tensors well, but the second one poorly.

In Figure 3.5 the mean signal deviation for the low FA-value and all models is shown which indicates that all models give a similar deviation which decreases with increasing SNR. In table 3.2 the models are compared, which shows that DTI gives the smallest signal deviation in a majority of the estimations for one fibre simulations.

19

**Table 3.1:** The percentage of times the bi-Gaussian and the fourth order tensor models had lower angle deviation than DTI, and that the fourth order model had smaller deviation than the bi-Gaussian model (H = high FA, M = medium FA, and L = low FA).

|  | H | M | L |
|---|---|---|---|
| Bi-Gaussian | 1% | 2% | 13% |
| Fourth Order | 68% | 41% | 26% |
| Fourth Order better than bi-Gaussian | 99% | 95% | 81% |

**Table 3.2:** The percentage of times the bi-Gaussian and the fourth order tensor models had lower signal deviation than DTI, and that the fourth order model had smaller deviation than the bi-Gaussian model (H = high FA, M = medium FA, and L = low FA).

|  | H | M | L |
|---|---|---|---|
| Bi-Gaussian | 23% | 7% | 20% |
| Fourth Order | 11% | 4% | 19% |
| Fourth Order better than bi-Gaussian | 26% | 18% | 34% |

The tensor element deviation for DTI is shown in Figure 3.6. The magnitude of the tensor element deviation is of the same order of magnitude as the ground truth tensor elements, and the smallest deviation was obtained for low FA.
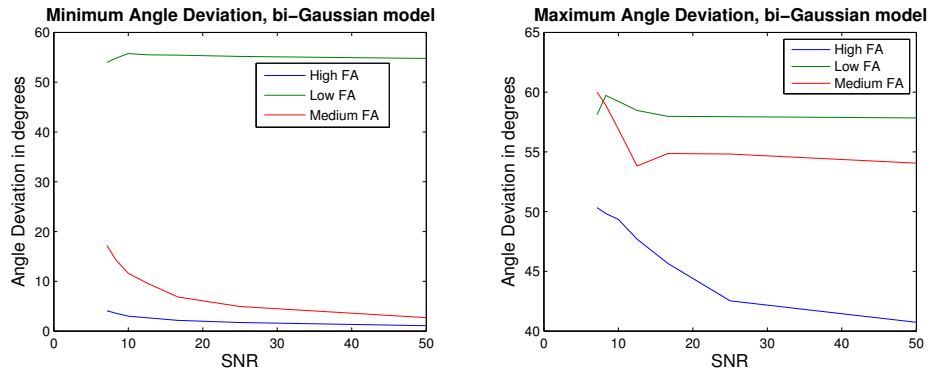
**Figure 3.4:** Angle deviation for the two main directions of the two tensors estimated with bi-Gaussian model, to the left the direction with lowest angle deviation, to the right the largest deviation.
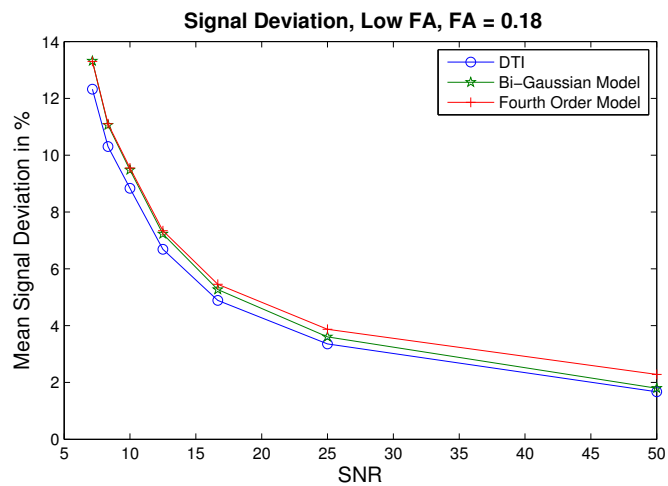


**Figure 3.5:** Mean signal deviation, one fibre. Ground truth FA= 0.18
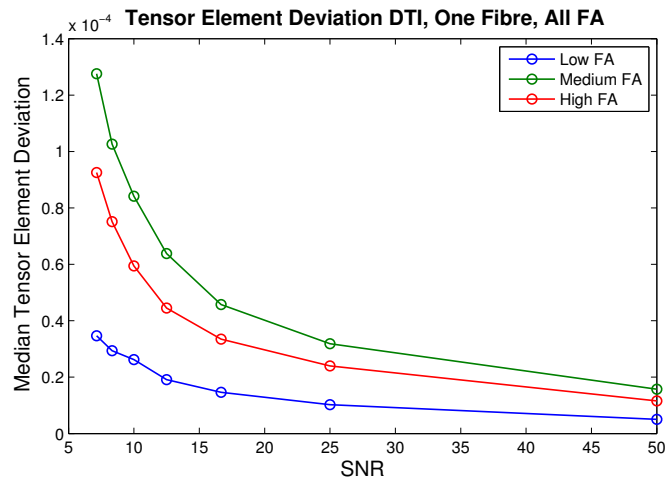
**Figure 3.6:** Median tensor element deviation, one fibre, DTI. Ground truth $FA_{low} = 0.18$, $FA_{medium} = 0.51$ and $FA_{high} = 0.94$.

### 3.4.2 Results for Two Fibre-Structure

**Angle Deviation**
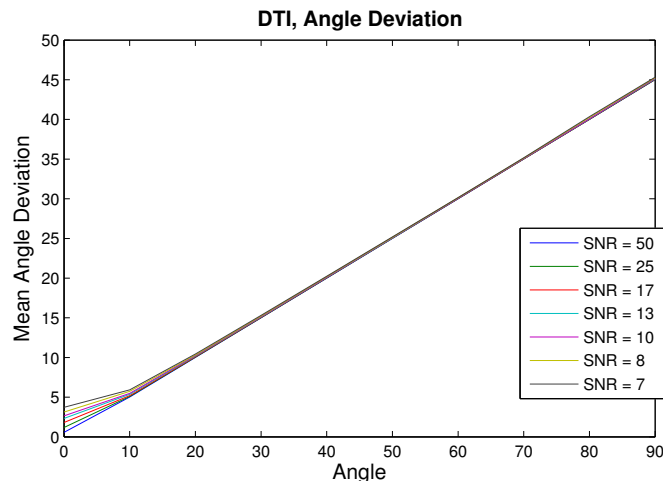


**Figure 3.7:** Angle deviation as function of fibre crossing angle. Ground truth $FA_1 = 0.94$ and $FA_2 = 0.94$.

In Figure 3.7 a typical result for the angle deviation with DTI is shown. Note that the deviation is computed as the average of the deviations of the direction estimated by the model and the two ground truth directions (see Equation (3.23)). The deviation was shown to increase almost linearly with increasing crossing angle, showing a precise but not accurate behaviour [2]. The estimated direction was close to the direction directly in-between the two simulated fibre directions (see Figure 3.8). All simulated FA-values showed the same trends but with decreasing mean-FA the dependence of SNR increased (see Figure 3.9 where both ground truth FA-values are medium and low, $FA_1 = 0.51$ and $FA_2 = 0.18$).

The bi-Gaussian model (note that this is the model used to synthesise the signal) performed best when both fibres had high FA and high crossing angle. When the crossing angle is low, the structure approaches the behaviour of one fibre in which case the bi-Gaussian model was shown to give high angular deviation (see Section 3.4.1). For the structure of two high-FA fibres Figure 3.10 shows the angular deviation as a function of the crossing angle.

For the fourth order tensor model, as described earlier, the number of fibres and their fraction of occupancy were not estimated but assumed to be known. In the same manner as for the bi-Gaussian model, when the angle decreases and approaches parallel fibres, the structure cannot be distinguished from one fibre. So for parallel fibres the model

---

[2]Precision means that the standard deviation is small but says little about how accurate the result is, while accuracy means that the mean value is a good estimate but nothing about the spread of the results (the deviation).
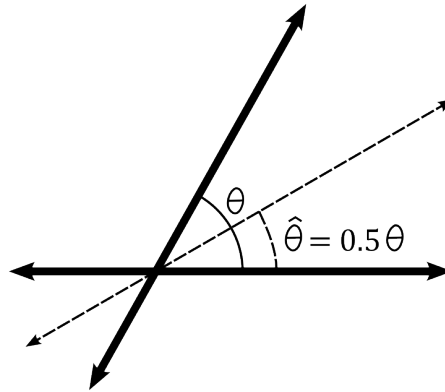
**Figure 3.8:** The dashed line represents the estimated direction with DTI when the underlying structure, represented by the two filled lines, is two crossing fibres
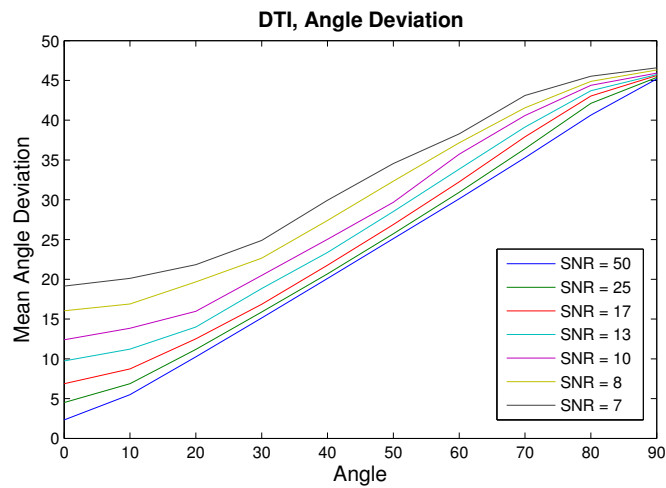


**Figure 3.9:** DTI, angle deviation as function of fibre crossing angle. Ground truth $FA_1 = 0.51$ and $FA_2 = 0.18$.

and the structure does not match. As can be seen in Figure 3.11 the angle deviation was small for crossing angles over 70° and large for smaller angles. For all simulations the deviation was larger for smaller crossing angles and vice versa, but with decreasing FA this change is less distinct.

A comparison between the angular deviations for all of the models is presented in Table 3.3 where all crossing angles were taken into account. It can be seen that the bi-Gaussian model only gave a majority of lower angular deviations when both fibres had high FA-values, and the fourth order model never had the majority of lowest angular deviations. However, since these models do not estimate the number of fibres and for low crossing angles this is a problem (as shown by the results in Section 3.4.1), the same comparison was done but only for crossing angles larger than 60°. The results are
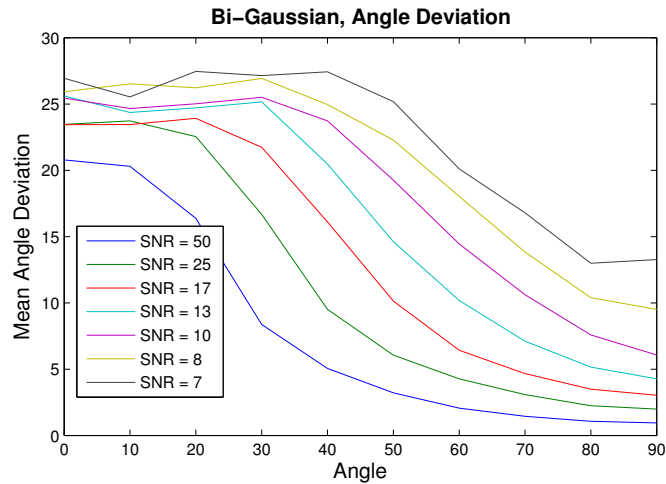
**Figure 3.10:** Bi-Gaussian model, angle deviation as function of fibre crossing angle. Ground truth $FA_1 = 0.94$ and $FA_2 = 0.94$.
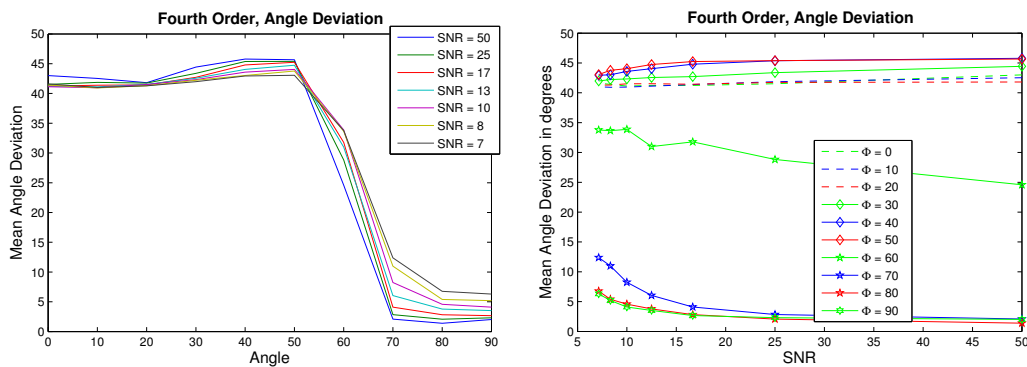


**(a)** Fourth order model, angle deviation as function of fibre crossing angle.

**(b)** Fourth order model, angle deviation as function of SNR.

**Figure 3.11:** Angle deviation as function of fibre crossing angle for fourth order tensor estimation. Ground truth $FA_1 = 0.94$ and $FA_2 = 0.94$.

presented in Table 3.4. For those angles the fourth order model gave lower angular deviation for all FA-values, and the bi-Gaussian model as well except when both FA-values are low. Additionally the fourth order model gave, in a majority of the measurements, a lower angular deviation than the bi-Gaussian model.

**Signal Deviation**

For DTI the signal deviation decreased with increasing SNR, but as can be seen in Figure 3.12 crossing angle has a large impact. This is expected due to the model-structure mismatch. The crossing angle had most impact when both fibres had high FA-value.

25

**Table 3.3:** The percentage of times (over all SNR levels and crossing angles) the bi-Gaussian and the fourth order tensor model had a lower angle deviation than DTI, and that the fourth order model had a lower deviation than the bi-Gaussian model. LL, ML, etc. refers the ground truth FA value, Low-Low, Mean-Low and so on.

|  | LL | ML | MM | HL | HM | HH |
|---|---|---|---|---|---|---|
| Bi-Gaussian | 23% | 35% | 38% | 41% | 46% | 61% |
| Fourth Order | 44% | 43% | 38% | 38 % | 42% | 32% |
| Fourth Order better than bi-Gaussian | 81% | 62% | 50% | 46% | 44% | 29% |

**Table 3.4:** The percentage of times (over all SNR levels and crossing angles larger than or equal to 60°) the bi-Gaussian and the fourth order tensor model had a lower angle deviation than DTI, and that the fourth order model had a lower deviation than the bi-Gaussian model. LL, ML, etc. refers the ground truth FA value, Low-Low, Mean-Low and so on.

|  | LL | ML | MM | HL | HM | HH |
|---|---|---|---|---|---|---|
| Bi-Gaussian | 33 % | 63% | 70% | 73% | 80% | 97% |
| Fourth Order | 72 % | 88% | 80% | 85% | 97% | 81% |
| Fourth Order better than bi-Gaussian | 81% | 77% | 73% | 66% | 72% | 55% |

When the SNR was high (how high depended on the FA-value, with higher FA the SNR-level was higher) the signal deviation increased with increasing crossing angle, but for low SNR the relation was reversed (this can be seen in Figure 3.13 where the SNR limit is 10).

The bi-Gaussian model and fourth order model performed similarly for all combinations of FA-values. The signal deviation decreased with increasing SNR, and for high-high, high-medium and medium-medium FA-structures, i.e. when no fibre had low FA-value, the signal deviation decreased with increasing crossing angle (see Figure 3.14). When instead one fibre or more had low FA, the crossing angle did not have any effect on the mean signal deviation (see Figure 3.15) and very little on the variance (see Figure 3.16). In Figure 3.15 and Figure 3.14 the bi-Gaussian model and fourth order model are similar but at least one difference can be noticed, i.e. the bi-Gaussian model has for SNR from 17 and above, a lower signal deviation.

In the same way as for the angle deviation the total differences were summarised, and the bi-Gaussian and fourth order model were compared to DTI. The results for all angles can be seen in Table 3.5, and as can be seen DTI gives the lowest signal deviation

26
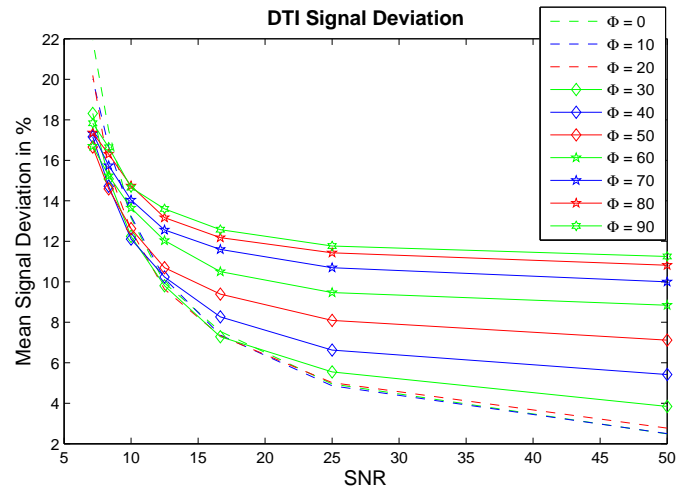
**Figure 3.12:** Signal deviation for DTI. Ground truth $FA_1 = 0.94$ and $FA_2 = 0.94$.
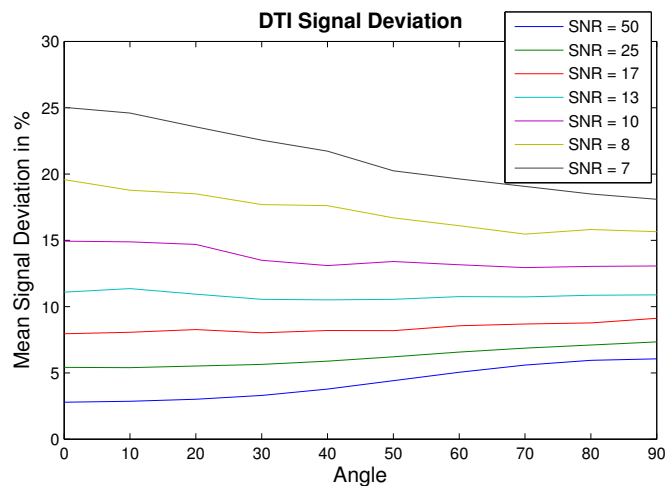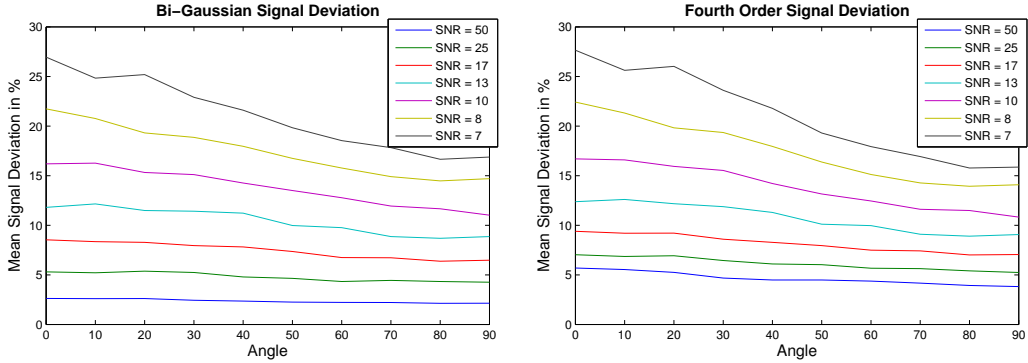


**Figure 3.13:** Signal deviation as function of fibre crossing angle for DTI. Ground truth $FA_1 = 0.94$ and $FA_2 = 0.51$.

in a majority of the cases, with exceptions for high-high and high-low FA-values. In the last row it can be seen that the fourth order model had a lower signal deviation than the bi-Gaussian model in a majority of the estimations.

For crossing angles larger than 60° see Table 3.6. Here we can see that in agreement with the plots for cases when at least one fibre had low FA, the results for one or more low FA-fibres in Table 3.6 and Table 3.5 are almost the same. For high-high structure, both the bi-Gaussian model and the fourth order model give lower signal deviation, but the high-medium structure still had lowest signal deviation with DTI. In both these tables it can be seen that the bi-Gaussian model in a majority of the estimations had

27

**(a)** Bi-Gaussian model, ranged random initialisation, signal deviation as function of fibre crossing angle.

**(b)** Fourth order model, signal deviation as function of fibre crossing angle.

**Figure 3.14:** Ground truth $FA_1 = 0.94$ and $FA_2 = 0.94$.
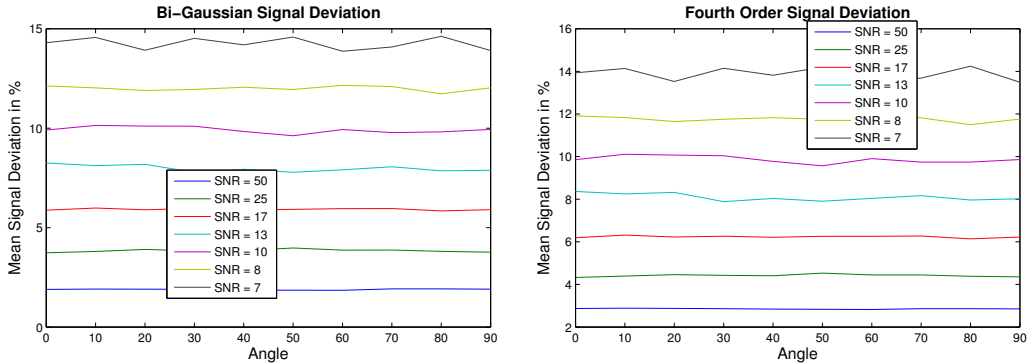


**(a)** Bi-Gaussian model, ranged random initialisation, signal deviation as function of fibre crossing angle.

**(b)** Fourth order model, signal deviation as function of fibre crossing angle.

**Figure 3.15:** Ground truth $FA_1 = 0.94$ and $FA_2 = 0.18$.

lower deviation than the fourth order model.

**Tensor Element Deviation**

For the synthetic signal with two fibres, the only tensor element deviation that could be calculated was when the model used was the bi-Gaussian. In all cases the tensor element deviation's order of magnitude was reasonable, i.e. smaller than the ground truth tensor element. For all simulations except for the medium-medium FA-values, the deviation decreased with increasing SNR, e.g. see Figure 3.17. Similarly to the signal deviation, when one fibre had low FA-value, the deviation was not dependent on the crossing angle (see Figure 3.18). For high-high and high-medium FA, the deviation decreased with
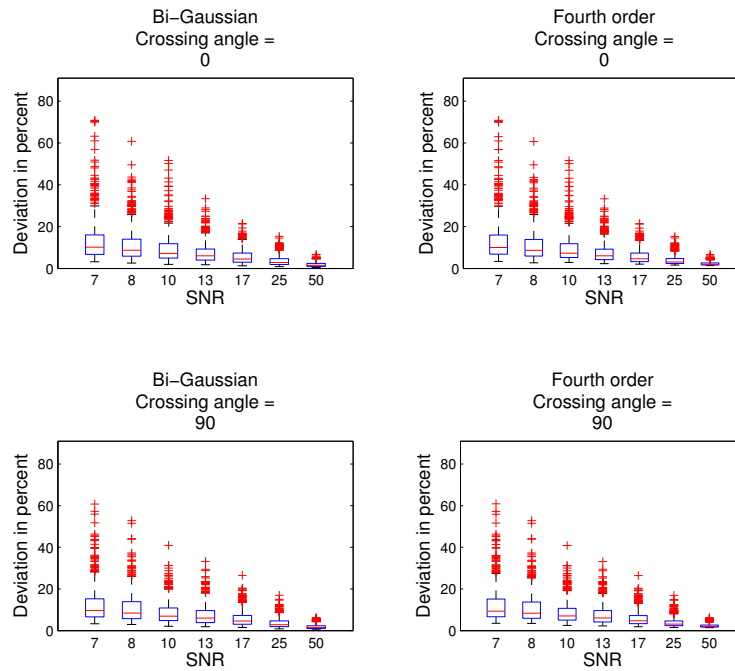
**Figure 3.16:** Boxplots of mean of signal deviation for the bi-Gaussian and Fourth order model. Parallel and perpendicular fibres. Ground truth $FA_1 = 0.18$ and $FA_2 = 0.18$.

**Table 3.5:** The percentage of times (over all SNR levels and crossing angles) the bi-Gaussian and the fourth order tensor model had a lower signal deviation than DTI, and that the fourth order model had a lower deviation than the bi-Gaussian model. LL, ML, etc. refers the ground truth FA value, Low-Low, Mean-Low and so on.

|  | LL | ML | MM | HL | HM | HH |
|---|---|---|---|---|---|---|
| Bi-Gaussian | 20% | 24% | 9.6% | 55% | 29% | 55% |
| Fourth Order | 20% | 19% | 5.2% | 52% | 24% | 50% |
| Fourth Order lower than bi-Gaussian | 35% | 40% | 22% | 33% | 33% | 30% |

increasing crossing angle.

**The Impact of SNR**

For the synthetic data with $FA_1 = FA_2 = 0.51$, SNR's impact on the angle deviation depended on the simulated crossing angle (see Figure 3.19). For crossing angles above

**Table 3.6:** The percentage of times (over all SNR levels and crossing angles larger than or equal to 60°) the bi-Gaussian and the fourth order tensor model had a lower signal deviation than DTI, and that the fourth order model had a lower deviation than the bi-Gaussian model. LL, ML, etc. refers the ground truth FA value, Low-Low, Mean-Low and so on.

|  | LL | ML | MM | HL | HM | HH |
|---|---|---|---|---|---|---|
| Bi-Gaussian | 20% | 24% | 10% | 56% | 42% | 84% |
| Fourth Order | 20% | 19% | 6.8% | 53% | 45% | 87% |
| Fourth Order better than bi-Gaussian | 35% | 41% | 24% | 34% | 41% | 33% |

70° the angle deviation decreases with increasing SNR, but for crossing angle lower than 60° the relationship is reversed. A similar behaviour occurred for $FA_1 = FA_2 = 0.18$, the low-low fibre configuration, where increasing the SNR increased the angle deviation (see Figure 3.20).
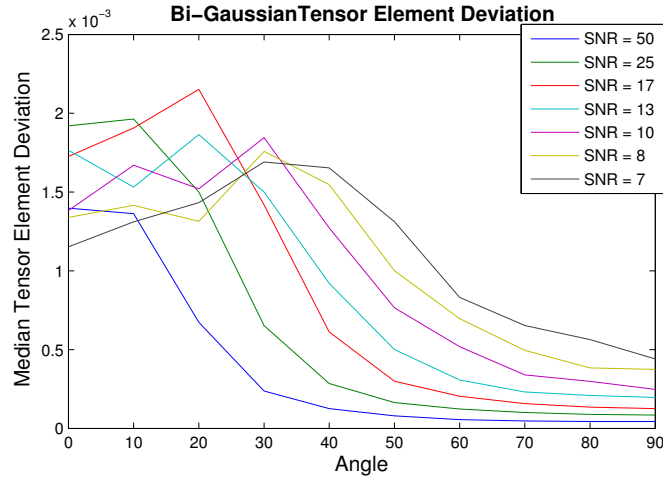
**Figure 3.17:** Bi-Gaussian model, tensor element deviation as function of fibre crossing angle. Ranged random initialisation. High-high FA fibre structure.
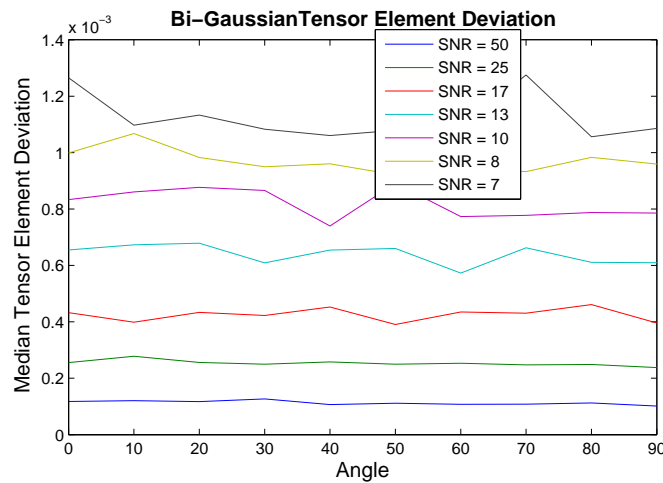


**Figure 3.18:** Tensor element deviation for bi-Gaussian model estimation. Ground truth $FA_1 = 0.94$ and $FA_2 = 0.18$. Bi-Gaussian model, tensor element deviation as function of crossing angle. Ranged random initialisation.

31
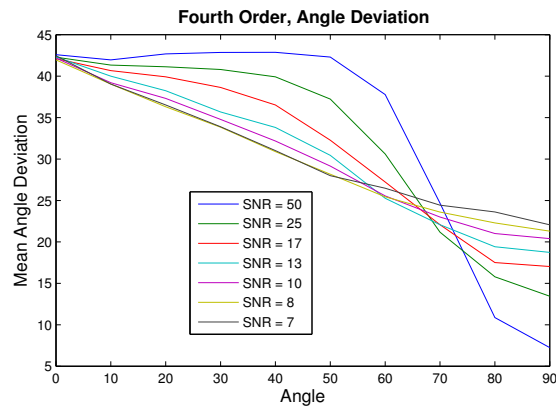
**Figure 3.19:** Angle deviation for fourth order tensor estimation. Ground truth $FA_1 = 0.51$ and $FA_2 = 0.51$.
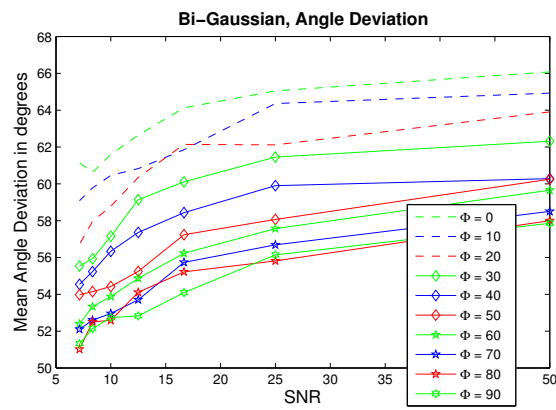


**Figure 3.20:** Random initialisation, angle deviation for bi-Gaussian model estimation. Ground truth $FA_2 = 0.18$ and $FA_2 = 0.18$.

## 3.5 Discussion of Quality of Fit Results

The angular deviation plots show that both the bi-Gaussian model and the fourth order model yielded more accurate direction estimates with increasing crossing angle. They also show that for small crossing angles the direction estimate is inaccurate. As previously mentioned, the synthetic signal from two parallel fibres and one fibre cannot be distinguished, and the fourth order model had as low angular deviation as DTI for one fibre. This indicates that the fourth order model used here, needs to be complemented with an estimation of the number of fibres, and preferably their fraction of occupancy as well.

For one fibre, the model-structure mismatch for the bi-Gaussian model meant that DTI generated lower deviation in both signal and angle. However the fourth order model had the lowest angular deviation for the high FA-simulations.

The tensor element deviation could not be used to compare the different models, but was useful in evaluating the different initialisation methods for the bi-Gaussian model. It also makes sense in this case to compare relative values and not absolute, since some tensor elements could be very small and others big.

The value of signal deviation as a quality measure is debatable. All models minimise with respect to the signal, and for SNR of 10 and above, they all result in the same range of deviation. When providing a value of how well your model performs, when the underlying structure is unknown, this measure is often the only available one, since you then do not know the ground truth directions of the fibre bundles, or the tensor element values, etc.

The angle deviation is more informative. It provides information about how well the model actually reconstructs/estimates directions, and which is used (important in tractography). To do a more complete analysis of the fourth order model, estimation of the number of fibres should also be taken into consideration, as well as a larger variety of medium FA-values. Not only could the explicit FA values be within a range from e.g. $[0.3, 0.7]$ but several different eigenvalue-relations that all generate the same FA could be used, to evaluate how that relation affects the resulting directions.

The effect of noise should also be considered. It was shown in the simulations that crossing fibres with medium and low FA-values can generate a larger angular deviation with increasing SNR. In practice this could lead to the detection of false fibre tracts in tractography.

# 4

# FA - A Measure of Structure

T HIS CHAPTER EXPLORES the concept of fractional anisotropy (FA). Its meaning and significance from the perspective of diffusion weighted imaging are discussed in Section 4.1 and Section 4.1.2. Section 4.2 describes how signals with known FA were generated for the purpose of empirically evaluating FA estimation with the conventional second order tensor model (DTI), the bi-Gaussian model, and the fourth-order tensor model. Section 4.3 describes how FA is estimated for these three models. Section 4.4 presents the Z-eigenvalue decomposition method needed to estimate FA using the fourth-order tensor model, as well as a new implementation of the method developed by the author. Section 4.5 presents the results of the FA estimation experiments for the different models. Finally Section 4.6 discusses these results, draws conclusions, and offers suggestions for improved FA estimation.

## 4.1 What is FA?

Fractional anisotropy, FA, is a scalar that for each voxel provides information about how anisotropic the diffusion within that voxel is. This scalar can then be interpreted in terms of fibre-integrity or structure. A standard definition of FA exists for DTI. Generalisations have been proposed for the bi-Gaussian and fourth order model, but there has not been a general method accepted throughout the DWI (Diffusion Weighted Imaging)-community.

FA-maps can be used as a tool to find regions of interest; for example to locate the area in which a tractography should be started (the seed points). In that case the correlation between high FA and white matter-fibres is utilised. It can also be used to determine progression of a disease like MS (Multiple Sclerosis); the condition causes demyelination of the fibres which in turn decreases the FA-values which as shown in [17]. In the same way it could be used to confirm that a treatment has the desired effect, that the white matter integrity is improved which is indicated by increased FA-values.

That FA does not consistently represent fibre integrity is known. In [3] it is pointed out that the decrease of FA in white matter-areas with crossing fibres is natural. In this section five FA-definitions for the non-Gaussian models are evaluated, including how the FA-value is altered with crossing fibres.

### 4.1.1 Properties of FA

There are two properties of FA that must be fulfilled. FA ultimately is a measure of the anisotropy of diffusion within the voxel, which means two things. Firstly, that if the diffusion is isotropic, i.e. the Brownian motion is independent of direction, FA should be very low, preferably zero. Secondly, if the diffusion has one dominant direction, effectively if all white matter fibres are aligned, FA should be high, preferably one, since this is the most anisotropic environment.

The first case, with isotropic diffusion, can also be regarded as the case where the white matter fibres are oriented in all (infinite) directions within the voxel. FA can take values in the range of $[0, 1]$, so between the two extreme cases from one to infinite directions when the structure decreases, the FA-value must in some way decrease with increasing number of directions.

### 4.1.2 What to expect from FA

FA is a scalar invariant; i.e. it is rotationally and translationally invariant. In order to evaluate whether a certain method gives a good FA value or not, a 'good FA-value' must be defined. FA-values have two main applications, in tractography and in progression of a disease. For the tractography application the main issue is to distinguish between structured and unstructured tissue, such that the structured tissue has an FA-value that is sufficiently higher than the FA-value for unstructured tissue. In the disease progression application, the change over time is of interest. The FA-values from one session to another must make it possible to highlight the areas where the degree of myelination has changed since the last scan(s). So all increases or decreases of the FA-value are of importance.

In order to specify the desired behaviour of FA, discussions have been held with Dr. Ylva Lilja MD and PhD-student at Sahlgrenska University Hospital, and with Mohammad Alipoor Lic. and PhD-student at Chalmers University of Technology. Y. Lilja's research is within preoperative imaging of the optic nerves before neurosurgery with the aim to improve the knowledge of the anatomy and function of nerve tracts in the brain as a tool to aid in risk assessment before surgery. M. Alipoor research is within signal processing, he is involved in a project related to DWI analysis, with the aim to develop new and effective methods for tractography and the analysis of fascicles in the brain. Examples of their work include [18] and [10]. It was during these discussions concluded that FA should give information about the fibre integrity; e.g. about the demyelination of the white matter fibres. Even if the voxel of interest contains several crossing fibres, the FA should be able to provide information of the fibre integrity. However, when the number of fibre-direction increases and approaches

infinity, the FA-values should decrease. In a voxel with an infinite number of direction the FA should approach zero. From one fibre-direction to infinite fibre-directions the FA should decrease from one to zero. Whether this change should be linear, exponential, or something else is an open question.

## 4.2 Generating Signals to Estimate FA from

For the synthetic signal the same synthetic signal and structure as described in Section 3.1 was used.

The real data was obtained at Sahlgrenska University Hospital, with one $b = 0$ acquisition, and a single-shell [1] with $b = 800$ s/mm$^2$ and 32 gradient directions. An experimentally determined threshold of 20 % of maximum $S_0$ was set to remove the voxels outside the brain. To find an informative and known structure, a region of interest-mask was drawn by a physician to locate a volume containing the optic chiasm [2]. The slice that contained the selected voxels was then processed.

## 4.3 Calculating FA

Prior to the FA-estimations the three models were fitted to the signal as described in Section 3.2. An additional method, not previously described, was also used to fit the fourth order model to the signal, described in Section 4.3.3. The FA definitions for the three models are described in Section 4.3.1, 4.3.2 and 4.3.3.

### 4.3.1 FA for DTI

FA values for DTI were computed using the standard definition based on the eigenvalues of the estimated tensor, viz.

$$\text{FA} = \sqrt{\frac{1}{2}\frac{(\lambda_1 - \lambda_2)^2 + (\lambda_1 - \lambda_2)^2 + (\lambda_2 - \lambda_3)^2}{\lambda_1^2 + \lambda_2^2 + \lambda_3^2}} \tag{4.1}$$

where $\lambda_i$ is the $i$th eigenvector's eigenvalue. By definition FA $\in [0,1]$, where 0 reflects an isotropic voxel and 1 a highly anisotropic voxel.

### 4.3.2 FA for the Bi-Gaussian Model

For the bi-Gaussian model two second order tensors $\mathbf{D}_1$ and $\mathbf{D}_2$ were estimated, from which two FA-values $\text{FA}_1$ and $\text{FA}_2$, one for each tensor, were calculated according to Equation (4.1). These two values were combined in the following three ways to obtain a single FA value: $\text{FA}_\text{mean} = \text{mean}(\text{FA}_1,\text{FA}_2)$, $\text{FA}_\text{max} = \text{max}(\text{FA}_1,\text{FA}_2)$ and $\text{FA}_\text{min} = \text{min}(\text{FA}_1,\text{FA}_2)$.

---

[1]The number of shells is determined by how many different $b$-values are used, often referred to as single-shell acquisition for one $b$-value and multi-shell acquisitions for more than one $b$-value.

[2]The optic chiasm is the area in the brain where the optic nerves, whom stretches from the eyes to the chiasm, partially cross each other and on the other side of the chiasm becomes the optic tracts.

### 4.3.3 FA for the Fourth Order Model

For the fourth order model the concept of Z-eigenvalue decomposition was used to define FA. Two methods were used to find the fourth order tensor, the first method is described in Section 3.2.3. The second method fits the fourth order tensor to the ADC (Apparent Diffusion Coefficient, see Equation (2.3))-profile with the diffusivity function

$$
\begin{aligned}
d(g) &= \log\left(\tfrac{S}{S_0}\right) \\
&= -b \sum_{i,j,k,l=1}^{3} \left(g_i g_j g_k g_l D_{ijkl}\right).
\end{aligned}
\tag{4.2}
$$

This is essentially a generalisation of the method used to fit the tensor in DTI. The fourth order tensor was fitted to the ADC with least squares fit

$$
\min_{\mathbf{D}} \left\{ \sum_{i=1}^{N} \left( d(g_i) - \hat{d}(g_i) \right)^2 \right\}
\tag{4.3}
$$

where $N$ is the number of gradient directions [13].

For the fourth order model, the conventional eigenvalue-decomposition cannot be used to obtain eigenvalues from which to define FA. Eigenvalues and eigenvectors are defined only for square matrices. However a generalisation, called Z-eigenvalue-decomposition was introduced in [13] for symmetric tensors of even order. This decomposition is discussed in more detail in Section 4.4. The resulting Z-eigenvalues $\lambda_i$ are the basis of two FA definitions found in the literature for the fourth order model.

The first definition, introduced in [13], is

$$
\mathrm{FA_{Qi}} = \sqrt{\frac{\nu}{\nu - 1}} \sqrt{\frac{\sum_{i=1}^{\nu} (\lambda_i - \lambda_{\mathrm{mean}})^2}{\sum_{i=1}^{\nu} \lambda_i^2}}
\tag{4.4}
$$

where $\lambda_{\mathrm{mean}} = \frac{1}{\nu} \sum_{i=1}^{\nu} \lambda_i$. The second definition, introduced in [18] is

$$
\mathrm{FA_{MA}} = \frac{\lambda_{\mathrm{max}}}{\nu \lambda_{\mathrm{mean}}}.
\tag{4.5}
$$

Both definitions range from 0 to 1.

## 4.4 Z-Eigenvalue Decomposition

In this section the author's implementation of the Z-eigenvalue decomposition method is described. This implementation is based on previous implementations described in Section 4.4.2. The definitions and theory in this section are drawn from [19] and [13].

### 4.4.1 Theory of Z-eigenvalues

An $m$th order n-dimensional tensor $\mathbf{A}_{i_1,\ldots,i_m}$ is supersymmetric if $\mathbf{A}_{i_1,\ldots,i_m} = \mathbf{A}_{\mathrm{perm}\{i_1,\ldots,i_m\}}$ for all permutations of $i_1,\ldots,i_m$. $\mathbf{A}$ can be described by an $m$th order polynomial $f(x)$ as follows

$$
\begin{aligned}
f(x) &\equiv \mathbf{A}x^m \\
&:= \sum_{i_1,\ldots,i_m=1}^{n} \mathbf{A}_{i_1,\ldots,i_m} x_{i_1} \ldots x_{i_m}
\end{aligned}
\tag{4.6}
$$

where $x$ can be regarded as an $m$th order $n$-dimensional tensor of rank one. If the polynomial $f(x)$ is positive semi-definite (PSD), then $\mathbf{A}$ is said to be PSD.

The real solutions $x$ and $\lambda$ of

$$
\begin{cases}
\mathbf{A}x &= \lambda x \\
x^T x &= 1
\end{cases}
\tag{4.7}
$$

are called the Z-eigenvectors and Z-eigenvalues respectively. If and only if all Z-eigenvalues of $\mathbf{A}$ are positive, $\mathbf{A}$ is PSD. If a second order tensor is symmetric, then it has only real eigenvalues with real eigenvectors. However this is not true for higher order supersymmetric tensors. Therefore it is important to emphasise that it is the real solutions that are Z-eigenvalues and Z-eigenvectors (the complete set, including complex solutions are denoted H-eigenvalues and H-eigenvectors).

The symmetric hyper-determinant $\det(\mathbf{A})$ of the super-symmetric tensor $\mathbf{A}$ is defined with an irreducible polynomial in $\mathbf{A}_{i_1,\ldots,i_m}$ which vanishes when $x \in C^n$ and $x \neq 0$ such that $f(x) = 0$ and $\nabla f(x) = 0$. If $m = 2$ this coincides with the conventional determinant.

An extension of the Kronecker delta is defined according to

$$
\delta_{i_1,\ldots,i_m} =
\begin{cases}
1, & \text{if } i_1 = \ldots = i_m \\
0, & \text{otherwise}
\end{cases}
\tag{4.8}
$$

An $m$th order $n$-dimensional tensor is called the $m$th unit tensor if its elements are $\delta_{i_1,\ldots,i_m}$ for $i_1,\ldots,i_m = 1$ and is denoted $\mathbb{I}$. Additionally, $\det(\mathbb{I}) = 1$ to specify sign and size of the symmetric hyper-determinant.

If $m$ is even, the Z-eigenvalues of $\mathbf{A}$ are the real solutions $\lambda$ to

$$
\phi(\lambda) = \det(\mathbf{A} - \lambda \mathbb{I}).
\tag{4.9}
$$

$\phi$ is called the characteristic polynomial of $\mathbf{A}$. The number of Z-eigenvalues is strictly less than $m^2 - m + 1$.

### Finding the Eigenvalues

In this section, the method suggested in [13] for finding the Z-eigenvalues and Z-eigenvectors is summarised.

The Z-eigenvalues and eigenvectors are found by finding the real solutions to the equation system

$$\begin{cases} \sum_{i=1}^{4}\sum_{j=0}^{4-i} i d_{ij} x_1^{i-1} x_2^j x_3^{4-i-j} & = 4\lambda x_1 \\ \sum_{i=0}^{4}\sum_{j=1}^{4-i} j d_{ij} x_1^i x_2^{j-1} x_3^{4-i-j} & = 4\lambda x_2 \\ \sum_{i=0}^{4}\sum_{j=0}^{3-i} (4-i-j) d_{ij} x_1^i x_2^j x_3^{3-i-j} & = 4\lambda x_3 \\ x_1^2 + x_2^2 + x_3^2 & = 1 \end{cases} \tag{4.10}$$

Here $d_{ij}$ denotes the 15 unique elements of a fourth order super-symmetric tensor $\mathbf{D}$.

The solutions can be divided into four cases described below, that are solved separately, and contribute to the set of eigenvalues.

**Case 1:** The elements in the eigenvector $x_2 = x_3 = 0$ which correspond to $d_{3,1} = d_{3,0} = 0$ and thus $x_1 = \pm 1$, $\lambda = d_{4,0}$.

**Case 2:** The elements in the eigenvector $x_1 = x_3 = 0$ which correspond to $d_{1,3} = d_{0,3} = 0$ and thus $x_2 = \pm 1$, $\lambda = d_{0,4}$.

**Case 3:** If $x_3 = 0$, and $x_1, x_2 \neq 0$ then by eliminating $\lambda$ (4.10) is simplified into the equation system

$$\begin{cases} \sum_{i=1}^{4} i d_{i,4-i} t^{i-1} & = \sum_{i=0}^{3} (4-i) d_{i,4-i} t^{i+1} \\ \sum_{i=0}^{3} d_{i,3-i} t^i & = 0 \end{cases} \tag{4.11}$$

where $t = x_1/x_2$. If the two equations have common solutions $t$, then $x_1 = \frac{t}{\sqrt{1+t^2}}$, $x_2 = \frac{\pm 1}{\sqrt{1+t^2}}$, $x_3 = 0$ and $\lambda = d(\vec{x})$.

**Case 4:** If $x_3 \neq 0$ then the resulting equation system is

$$\begin{cases} \sum_{i=1}^{4}\sum_{j=0}^{4-i} i d_{ij} u^{i-1} v^j & = \sum_{i=0}^{4}\sum_{j=0}^{3-i} (4-i-j) d_{ij} u^{i+1} v^j \\ \sum_{i=0}^{4}\sum_{j=1}^{4-i} j d_{ij} u^i v^{j-1} & = \sum_{i=0}^{4}\sum_{j=0}^{3-i} (4-i-j) d_{ij} u^i v^{j+1} \end{cases} \tag{4.12}$$

if $\lambda$ is eliminated and $u = x_1/x_3$ and $v = x_2/x_3$. After solving this for $u$ and $v$ the eigenvector and eigenvalues are $x_1 = u/\sqrt{1+u^2+v^2}$, $x_2 = v/\sqrt{1+u^2+v^2}$, $x_3 = \pm 1/\sqrt{1+u^2+v^2}$ and $\lambda = d(\vec{x})$.

These four cases cover all possible combinations. In some implementations there have been suggestions that additional combinations of $\vec{x}$ in *Case 3* is necessary (e.g., $x_1, x_3 \neq 0$ and $x_2 = 0$), but those are actually covered in *Case 4* which include all combinations when $x_3 \neq 0$.

**Table 4.1:** The relation between the fifteen elements in the vector **T** and their relation to the fourth order symmetric tensor **A** used in the implementation of the Z-eigenvalues decomposition from [11]

| | | | | |
|---|---|---|---|---|
| $\mathbf{T}(1)$ | $1 \cdot \mathbf{A}_{3333}$ | | $\mathbf{T}(9)$ | $4 \cdot \mathbf{A}_{1222}$ |
| $\mathbf{T}(2)$ | $4 \cdot \mathbf{A}_{2333}$ | | $\mathbf{T}(10)$ | $6 \cdot \mathbf{A}_{1133}$ |
| $\mathbf{T}(3)$ | $6 \cdot \mathbf{A}_{2233}$ | | $\mathbf{T}(11)$ | $12 \cdot \mathbf{A}_{1123}$ |
| $\mathbf{T}(4)$ | $4 \cdot \mathbf{A}_{2223}$ | | $\mathbf{T}(12)$ | $6 \cdot \mathbf{A}_{1122}$ |
| $\mathbf{T}(5)$ | $1 \cdot \mathbf{A}_{2222}$ | | $\mathbf{T}(13)$ | $4 \cdot \mathbf{A}_{1113}$ |
| $\mathbf{T}(6)$ | $4 \cdot \mathbf{A}_{1333}$ | | $\mathbf{T}(14)$ | $4 \cdot \mathbf{A}_{1112}$ |
| $\mathbf{T}(7)$ | $12 \cdot \mathbf{A}_{1233}$ | | $\mathbf{T}(15)$ | $1 \cdot \mathbf{A}_{1111}$ |
| $\mathbf{T}(8)$ | $12 \cdot \mathbf{A}_{1223}$ | | | |

### 4.4.2 Previous Software Implementations

Two implementations were available, the first one can be found in [11]. This implementations finds the set of eigenvalues and eigenvectors in three different cases. First, the vector **T** that contains the fifteen unique fourth order tensor elements is transformed into a symmetric fourth order tensor **A** according to Table 4.1. The factor corresponds to the multiplicity of the specific element.

Then a fourth order tensor $\bar{\mathbf{A}}$ is calculated element-wise according to

$$\bar{\mathbf{A}}_{ijkl} = \bar{\Delta}_{i:} \cdot \mathbf{A}_{:jkl} \tag{4.13}$$

In the implementation $\Delta = \mathbb{I}$ where $\mathbb{I}$ is the identity matrix which means that $\bar{\mathbf{A}} = \mathbf{A}$.

The eigenvalues are then calculated in three different steps described below. The equations are presented in terms of the vector of the fifteen unique elements to facilitate comparison with the two other implementations.

**Step 1:** If $\mathbf{T}_{14} = \mathbf{T}_{13} = 0$ then $\lambda = \mathbf{T}_{15}$ and $\vec{x} = (1\ 0\ 0)$.

**Step 2:** For $t$ solve the equation system

$$\begin{cases} -\frac{1}{4}\mathbf{T}_{14} \cdot t^4 + (\mathbf{T}_{15} - \frac{1}{2}\mathbf{T}_{12}) \cdot t^3 + \\ +\frac{3}{4}(\mathbf{T}_{14} - \mathbf{T}_9) \cdot t^2 + (\frac{1}{2}\mathbf{T}_{12} - \mathbf{T}5) \cdot t + \frac{1}{4}\mathbf{T}_9 &= 0 \\ \frac{1}{4}\mathbf{T}_6 \cdot t^3 + \frac{1}{4}\mathbf{T}_{11} \cdot t^2 + \frac{1}{4}\mathbf{T}_8 \cdot t + \frac{1}{4}\mathbf{T}_4 &= 0 \end{cases} \tag{4.14}$$

The real solutions $t_i$ gives the eigenvectors $\vec{x}^{(i)}$ and eigenvalues $\lambda_1$ according to $\vec{x}^{(i)} = (t_i\ 0\ 0)/\gamma_i$ where $\gamma_i = \sqrt{t_i^2 + 1}$ and $\lambda = \mathbf{T}_{15} \cdot (t_i/\gamma_i)^4$

**Step 3:** For two variables, $u$ and $v$ equation system

$$\begin{cases} -\frac{1}{4}\mathbf{T}_{13} \cdot u^4 - \frac{1}{4}\mathbf{T}_{11} \cdot u^3 \cdot v + (\mathbf{T}_{15}) - \frac{1}{2}\mathbf{T}_{10}) \cdot u^3 - \frac{1}{4}\mathbf{T}_8 \cdot u^2 \cdot v^2 + \\ \quad + (\frac{3}{4}\mathbf{T}_{14} - \frac{1}{2}\mathbf{T}_7) \cdot u^2 \cdot v + (\frac{3}{4}\mathbf{T}_{13} - \cdot\frac{3}{4}\mathbf{T}_6) \cdot u^2 - \frac{1}{2}\mathbf{T}_3 \cdot u \cdot v^2 - \\ \quad \frac{1}{4}\mathbf{T}_4 \cdot u \cdot v^3 + \frac{1}{2}\mathbf{T}_{12} \cdot u \cdot v^2 + (\frac{1}{2}\mathbf{T}_{11} - \frac{3}{4}\mathbf{T}_2) \cdot u \cdot v + \\ \quad (\frac{1}{2}\mathbf{T}_{10} - \mathbf{T}_1) \cdot u + \frac{1}{4}\mathbf{T}_9 \cdot v^3 + \frac{1}{4}\mathbf{T}_8 \cdot v^2 + \cdot\frac{1}{4}\mathbf{T}_7 \cdot v + \frac{1}{4}\mathbf{T}_6 \quad = \quad 0 \\ -\frac{1}{4}\mathbf{T}_{13} \cdot u^3 \cdot v + \frac{1}{4}\mathbf{T}_{14} \cdot u^3 - \frac{1}{4}\mathbf{T}_{11} \cdot u^2 \cdot v^2 + (\frac{1}{2}\mathbf{T}_{12} - \frac{1}{2}\mathbf{T}_{10}) \cdot u^2 \cdot v + \\ \quad \frac{1}{4}\mathbf{T}_{11} \cdot u^2 - \frac{1}{4}\mathbf{T}_8 \cdot u \cdot v^3 + (\frac{3}{4}\mathbf{T}_9 - \frac{1}{2}\mathbf{T}_7) \cdot u \cdot v^2 + (\frac{1}{2}\mathbf{T}_8 - \\ \quad \frac{3}{4}\mathbf{T}_6) \cdot u \cdot v + \frac{1}{4}\mathbf{T}_7 \cdot u + \frac{3}{4}\mathbf{T}_4 \cdot v^2 - \frac{1}{4}\mathbf{T}_4 \cdot v^4 + (\mathbf{T}_5 - \frac{1}{2}\mathbf{T}_3) \cdot v^3 - \\ \quad \frac{3}{4}\mathbf{T}_2 \cdot v^2 + (\frac{1}{2}\mathbf{T}_3 - \mathbf{T}_1) \cdot v + \frac{1}{4}\mathbf{T}_2 \quad = \quad 0 \end{cases} \tag{4.15}$$

is solved with MATLAB's solver 'solve' and the eigenvectors and eigenvalues are calculated according to $x^{(l)} = (u_l \ v_l \ 1)/\beta_l$ where $\beta_l = \sqrt{u_l^2 + v_l^2 + 1}$ and $\lambda_l = \sum_{i=1}^3 \sum_{j=1}^3 \sum_{k=1}^3 \sum_{m=1}^3 \mathbf{A}_{ijkm} \cdot x(i)^{(l)} x(j)^{(l)} x(k)^{(l)} x(m)^{(l)}$.

This implementation works in most cases, but is sometimes slow. For

$$\mathbf{T} = \quad [1.4751 \ 0.7276 \ -3.9916 \ -0.0061 \ 12.4934 \ -2.7988 \ -7.1486 \ 17.7676$$
$$-3.6968 \ 5.2683 \ 0.0099 \ 18.6609 \ -4.3874 \ 19.5485 \ 5.9023]$$

this takes almost half an hour to solve, but with the later implementation a few seconds. Additionally, if $\mathbf{T}$ consists of only zeros and ones this returns a set of complex solutions with a larger set of eigenvalues than the right amount, e.g. if $\mathbf{T} = [1\ 1\ 0\ 1\ 0\ 0\ 0\ 0\ 0\ 0\ 1\ 0\ 0\ 0\ 0]$ it returns a set of five complex eigenvectors (where the complex part is small but present) instead of three.

The second implementation (by the first author, Alipoor, of [18]) available utilises the case-based method described in Section 4.4.1 using MATLAB's `solve` function for both *Case 3* and *Case 4*. During simulations it occasionally crashed and it was observed that in *Case 4* `solve` utilises back-substitution which can cause division by zero.

### 4.4.3 The Improved Implementation of Z-eigenvalues Decomposition

This uses the cases described in Section 4.4.1 and is based on the implementation by Alipoor. The method to find the solutions to *Case 1-3* was essentially kept, but subcases giving repeated solutions were isolated and removed. One additional step was implemented, confirming that the found solutions solved the original problem in Equation (4.10).

To avoid the back substitution in *Case 4* the computer algebra system `MuPAD` – which is included in MATLAB's Symbolic Math Toolbox – is called directly instead of via `solve`. Since all real solutions to (4.12) are requested the `MuPAD`-function `numeric::polysysroots` is used. This returns a numerical approximation of both real and complex solutions and to isolate the real solution a tolerance of $10^{-12}$ is set. All complex solutions with an

imaginary part larger than the tolerance are removed, and if the imaginary part is smaller the solution is considered to be real.

After removing the repeated solutions and verified that they all are solutions to the original problem (4.10), the eigenvalues and eigenvectors are ordered with largest eigenvalue first.

## 4.5   Results of FA-estimations

Here a representative selection of the FA-estimation-results is presented. The complete set of results can be found in Appendix B.

### 4.5.1   Results for one Fibre FA-Estimations
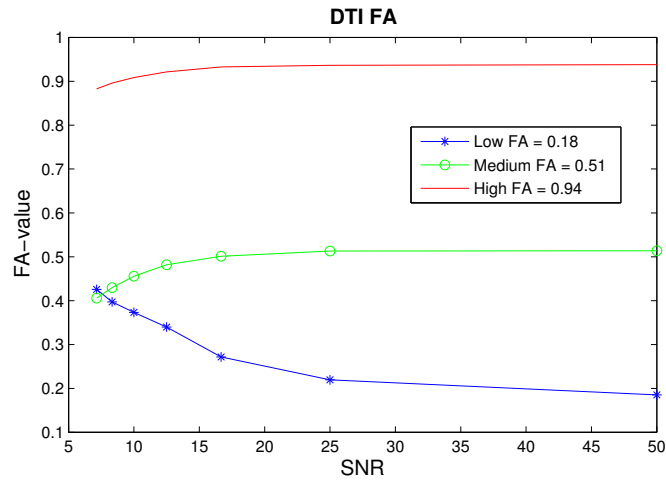


**Figure 4.1:** FA estimated with DTI, ground truth FA: $FA_{low} = 0.18$, $FA_{med} = 0.51$ and $FA_{high} = 0.94$.

In one fibre simulations the results of FA for DTI are presented in Figure 4.1, where when ground truth FA is high, the estimated FA-value was accurate. For the two lower FA-values, the estimates were more sensitive to noise, and the signal from the low ground truth FA-value was overestimated for SNR below 20. For the lowest SNR-level the low FA-value was estimated to be higher than the medium FA-value.

The three FA-values generated from the bi-Gaussian model were for low and medium FA overestimated, but all three were close to ground truth for the high FA-value. The most accurate result was acquired from $FA_{min}$ (see Figure 4.2). For $FA_{min}$ the medium FA-value was consistently higher than the ground truth FA-value, and the high-FA-value was slightly underestimated.

Both definitions for the fourth order model overestimated the medium and slightly underestimated the low. Qi's definition was close to ground truth for the high FA-value.
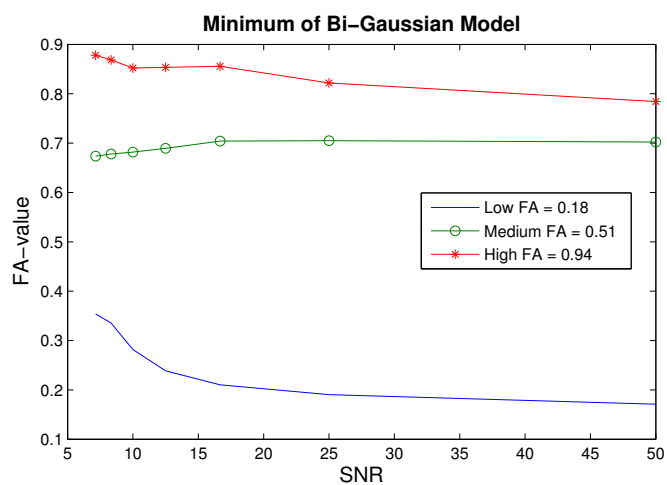
**Figure 4.2:** Minimum of FA's estimated with bi-Gaussian model, ground truth FA: $FA_{low} = 0.18$, $FA_{med} = 0.51$ and $FA_{high} = 0.94$.

In Figure 4.3 the results from $FA_{Qi}$ are plotted.
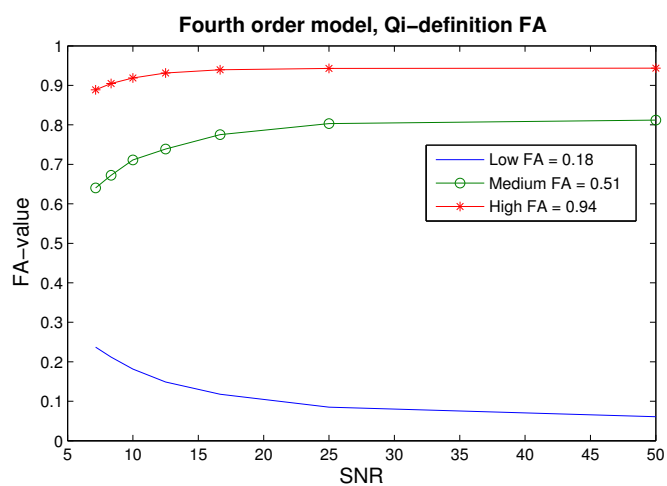


**Figure 4.3:** FA-values estimated with Qi's FA-definition for the fourth order model, ground truth FA: $FA_{low} = 0.18$, $FA_{med} = 0.51$ and $FA_{high} = 0.94$.

### 4.5.2 Results for two Fibre FA-Estimations

Consistently for all models, was that when one fibre had low FA-value, there was a very low dependence on crossing angle, e.g. see Figure B.21, B.23, and many others in Appendix B.

#### DTI

For DTI, when no ground truth tensor had low FA, the estimated FA decreased with increasing crossing angle. The higher the ground truth FA-values were, the more the estimated FA decreased with increasing crossing angle. This behaviour can be seen in Figure 4.4 where both synthetic fibres had high FA-value.
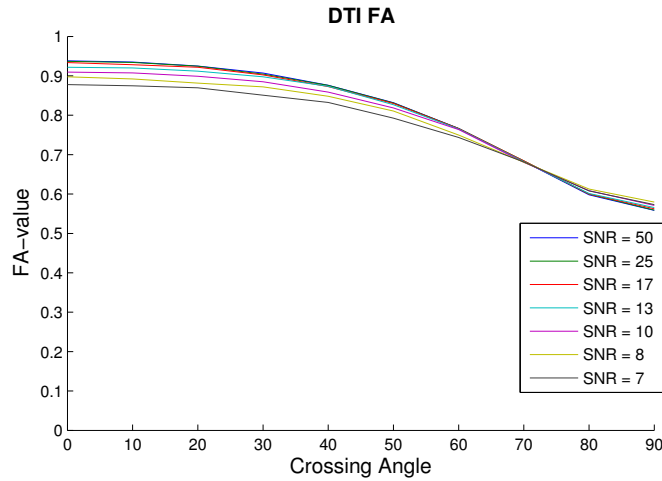


**Figure 4.4:** Synthetic signal, two fibres with $FA_1 = FA_2 = 0.94$, DTI FA-estimation.

#### Bi-Gaussian model

The three bi-Gaussian FA-definitions were insensitive to the crossing angle. Excluding the high-high structure, when comparing the estimated FA-value to the mean of the ground truth FA-values both $FA_{max}$ and $FA_{mean}$ were overestimated. In Figure 4.5 the $FA_{mean}$ of high-low and medium-medium-structure is plotted and the resulting FA values are all higher than the mean of the ground truth FA-values.

#### Fourth Order Model

Figure 4.6 show a typical result of the fourth order FA-estimations. When the crossing angle increases from $50°$ to $70°$ the estimated FA-value decreases rapidly. This behaviour was noted in all simulations when no fibre had low ground truth FA-value. In this rapid FA-estimation drop, the relation between SNR and FA changed. For crossing angles
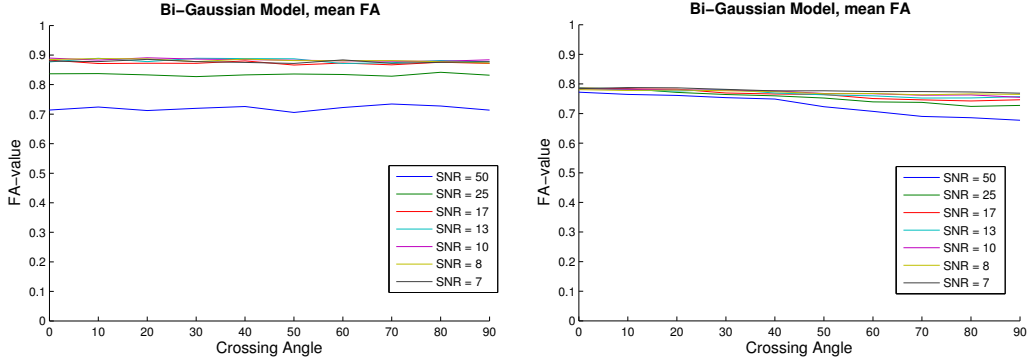
**(a)** Synthetic signal, two fibres with $FA_1 = 0.94$ and $FA_2 = 0.18$. Mean of FA's estimated with the bi-Gaussian model. Ranged random initialisation.

**(b)** Synthetic signal, two fibres with $FA_1 = 0.94$ $FA_2 = 0.51$. Mean of FA's estimated with the bi-Gaussian model. Ranged random initialisation.

**Figure 4.5:** Bi-Gaussian model, synthetic signal, two fibres with $FA_1 = 0.94$ $FA_2 = 0.51$.

lower than $50°$ the FA-value increased with increasing SNR, but for angles higher than $70°$ the FA-value decreased with increasing SNR. If we compare DTI and the fourth order model, both methods' FA-values decrease with increasing SNR, $FA_{Qi}$ lowest value is approximately the same as the lowest DTI, and $FA_{MA}$ is lower than DTI.
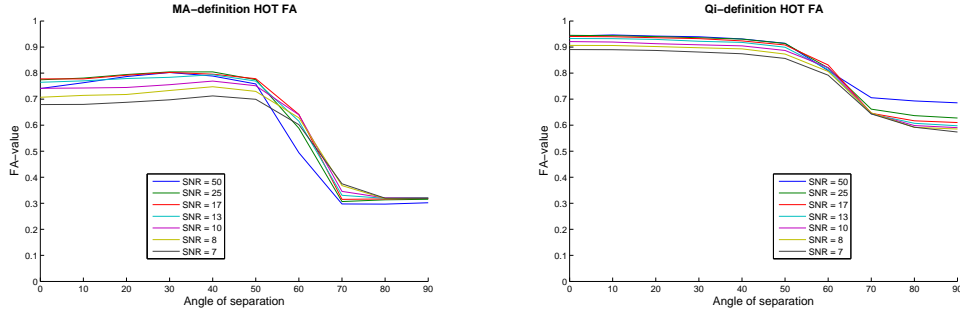


**(a)** Synthetic signal, two fibres with $FA_1 = FA_2 = 0.94$. FA's estimated with MA's FA-definition for the fourth order model.

**(b)** Synthetic signal, two fibres with $FA_1 = FA_2 = 0.94$. FA's estimated with Qi's FA-definition for the fourth order model. .

**Figure 4.6:** Fourth order tensor model, synthetic signal, two fibres with $FA_1 = FA_2 = 0.94$.

It was also observed that for perpendicular fibres the fourth order estimated FA-values was lower for the high-high fibre configuration than for high-medium. Compare Figure 4.6 and Figure 4.7.
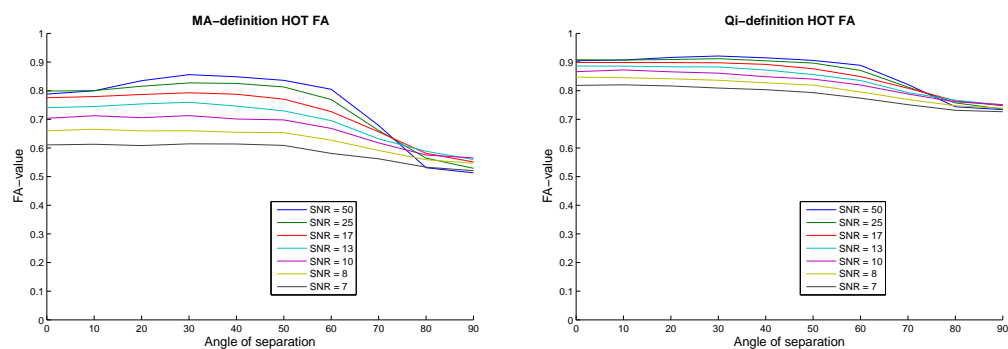
**(a)** Synthetic signal, two fibres with $FA_1 = 0.94$ and $FA_2 = 0.51$ FA's estimated with MA's FA-definition for the fourth order model.

**(b)** Synthetic signal, two fibres with $FA_1 = 0.94$ and $FA_2 = 0.51$. FA's estimated with Qi's FA-definition for the fourth order model.

**Figure 4.7:** Fourth order tensor model, synthetic signal, two fibres with $FA_1 = 0.94$ and $FA_2 = 0.51$.

### 4.5.3 Results of Real Data FA-Estimations

In Figure 4.8 the conventional FA-map is shown. The non-Gaussian FA-maps were compared to this, given that no ground truth FA-values is available for real data.
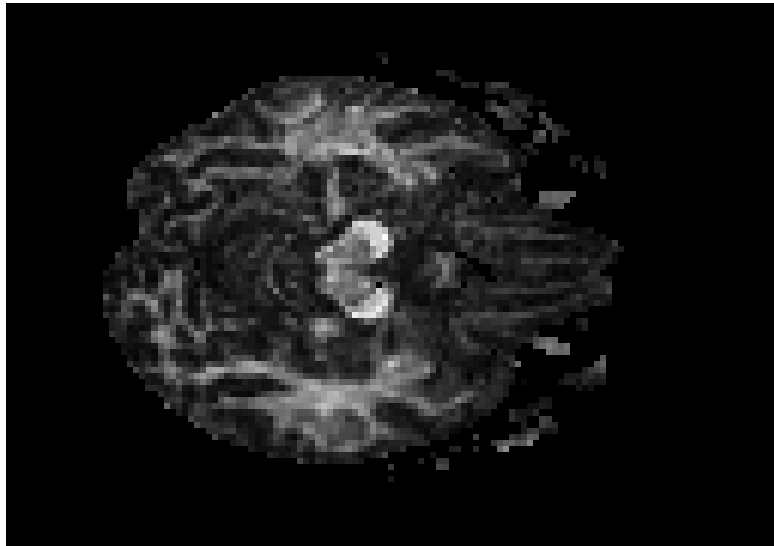


**Figure 4.8:** The conventional FA from DTI.

For the bi-Gaussian model (see Figure 4.9), in many voxels an FA-value could not be estimated since neither of the estimated tensors was PSD. For these voxels the FA-value was set to zero, which turns out black in the image. This problem was not as significant for the synthetic signal, since many estimates and noise realisations for each structure was performed, and the non-PSD tensors could simply be ignored. However, if that artefact is put aside, the map is brighter than Figure 4.8 and has less contrast (ignoring black voxels).

The fourth order model was fitted to the signal in two different ways. The first method described in Section 3.2.3, used for model evaluation of the fourth order tensor model in Chapter 3, yielded the FA-map shown in Figure 4.10. The contrast is much lower than in Figure 4.8. The second method, described in Section 4.3.3, yielded an FA-map with higher contrast (see Figure 4.11). The areas with high anisotropy (the bright areas) in this map, corresponds well with the DTI-FA-map. However the fourth order FA-map has fewer high anisotropic areas. Remember from the synthetic signal FA-maps for the fourth order model, that when the crossing angle increased to above 70° the FA-value rapidly decreased.

**Figure 4.9:** The mean FA of the two FA from bi-Gaussian model.
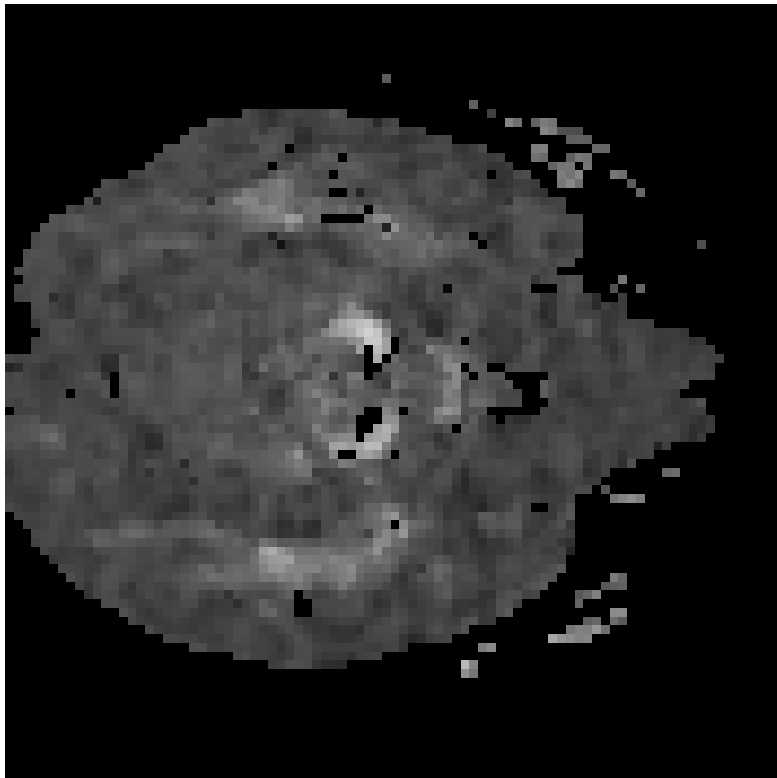


**Figure 4.10:** The Qi definition of FA from HOT, filtered with Gaussian window of 4 voxel size, fitted to the CT-ODF.
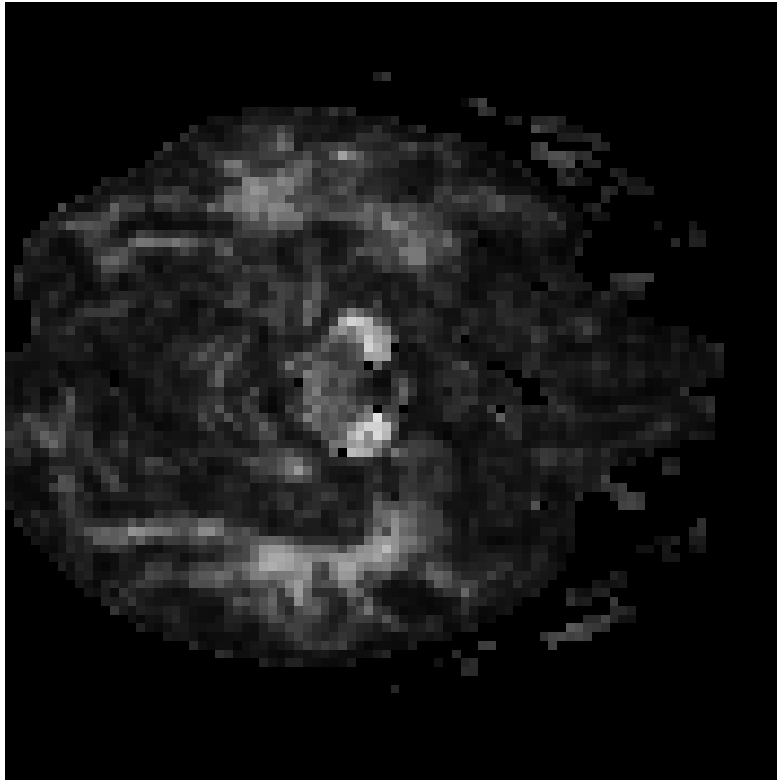
**Figure 4.11:** The Qi definition of FA from HOT, filtered with Gaussian window of 4 voxel size, fitted to the ADC-profile.

## 4.6 Conclusions, Discussion and Improvement of FA-estimations

The first and easiest conclusion to draw from these experiments is that the FA-estimations for the three models give different results. FA computed from DTI, as previously mentioned, decreases with increasing crossing angle. It is well known that the conventional FA measure is lower in complex structures such as fibre crossings [20]. The three FA-definitions for the bi-Gaussian model are all invariant to the crossing angle. If this could be utilised the FA-value would not decrease in a complex area. However, since the bi-Gaussian FA-definitions consistently overestimates low anisotropy areas it is difficult to know if the FA-value reflects the ground truth or if it overestimates it. Consequently the bi-Gaussian FA-estimates are less informative than DTI FA-values. One possible improvement is to include a PSD-constraint in the model-fit used for the bi-Gaussian model. This would eliminate the negative eigenvalues and at the very least, remove the black voxels from the real data FA-maps. Furthermore, since the negative eigenvalues from the synthetic data simply are ignored and the mean values are calculated out of those estimated eigenvalues that are positive, the resulting FA-maps could be rather different from those presented above. The effect of a PSD constraint would be interesting to evaluate and could be a continuation of the results presented here.

The two FA-estimates derived from the fourth order tensor model were both approximately invariant to the crossing angle below 50° and above 70° and exhibit rapid decrease in-between those two angles. The real data FA-maps for the fourth order model have fewer areas of bright areas, indicating less information than in the DTI FA-maps. One possible reason for this is that for DTI only six parameters were estimated, compared to 13 parameters for the fourth order model. The relation between number of measurements and parameters to estimate is for DTI larger than five, for the fourth order tensor model the relation is smaller than three. For future improvements it would be interesting to see if a larger number of gradient directions would improve the fourth order FA-maps and if they would provide more (but still accurate information) than the DTI FA-map.

In discussions with dr. Ylva Lilja MD and PhD-student and Mohammad Alipoor, Lic. and PhD-student (see Section 4.1.2 for a presentation of their research) during the this research it was concluded that, clinically speaking, the desired behaviour is that an increased crossing angle naturally decreases the FA-value. The distinction between white matter-integrity and fibre-structure is key here. If the characteristic of interest is integrity, then the increase of crossing angle, probably should not decrease the integrity-value because whether or not the white matter fibres are crossing or not does not decrease their integrity. If instead the characteristic of interest is fibre structure, then increased crossing angle (and an increase of directions) is consistent with loss of structure and the measure should decrease. This was highlighted in [3].

For future work, the inclusion of a fraction of occupancy estimation for both the bi-Gaussian model and the fourth order model should be explored. For the bi-Gaussian model this requires multi-shell signal acquisition, but in a synthetic environment that

is just a matter of more simulation time. This could then lead to a more sophisticated FA-measure where the fraction between the fibres (Fraction of Occupancy – FoO) could be included as a weight to their respective eigenvalues. For the fourth order model, the current normalising factor $\nu$ (see Equation (4.4) and Equation (4.5)) give the same weight to all eigenvalues. If the FoO's of these eigenvalues were known many small eigenvalues with low FoO would have less impact on the resulting FA value.

The concept of a scalar measure that provides information about the underlying structure is good, but what exactly it should reflect is still an open question. Nevertheless this does not preclude the possibility of generalising the definition of FA for DTI to non-Gaussian models. However if such a measure has good accuracy and can differentiate between integrity and structure, white and grey matter, it would be superior to FA from DTI.

# 5

# Summary and Conclusions

I N THIS CHAPTER the thesis and the work presented in it is summarised in Section 5.1. The major contributions and findings are presented in Section 5.2 and the conclusions in Section 5.3, and finally opportunities for further research in Section 5.5.

## 5.1 Thesis Summary

**Chapter 1** Introduces DWI (Diffusion Weighted Imaging) and DTI (Diffusion Tensor Imaging), and how it can be used to image the brain neural tracts in vivo. The more complex models than DTI are introduced. The scalar FA (Fractional Anisotropy) derived from DWI data is described, and that it can be used as a tool to determine the progress of diseases like MS (Multiple Sclerosis) and Alzheimer's Disease, or to demonstrate the improvement of white matter integrity after tumour removal. The chapter also states the two major aims of the thesis:

*The first aim* was to compare the conventional Gaussian diffusion model with two non-Gaussian diffusion models, the bi-Gaussian and the fourth-order tensor, for single and crossing fibre architectures.

*The second aim* was to explore the concept of FA and to evaluate existing FA definitions for the three models chosen in the first aim.

and its objectives:

i) To generate synthetic data to simulate a single voxel, a single fibre (for three different FA values), and two crossing fibres (for six FA combinations, and a range of crossing angles).

ii) To fit each model to this data and evaluate the quality of the fit in terms of the three measures: signal deviation, angle deviation and tensor element deviation.

iii) To review the physical meaning and significance of FA.

iv) To develop a robust and accurate implementation of the Z-eigenvalue decomposition algorithm needed for the FA estimation for high order tensors.

v) To investigate and compare FA definitions for the bi-Gaussian and fourth-order tensor models, empirically (using both the earlier synthetic data and real brain DWI data), to the second-order definition.

**Chapter 2** Reviews the concept of diffusion, what DWI is and how it can be used to measure diffusion. The three diffusion models explored in the thesis are presented.

**Chapter 3** Addresses objectives i) and ii) associated with the first aim of the thesis. The framework used for synthesising the signal is presented. It evaluates how well the three models perform in terms of signal deviation, angle deviation and tensor element deviation and how these quality measures are calculated is described. The resulting measures are presented and the models compared.

**Chapter 4** Addresses objectives iii), iv) and v) associated with the second aim of the thesis. In particular the concept of FA and what FA means is discussed. The protocol for synthesising signals with known FA is described as well as how to estimate the FA values for the three different models. Z-eigenvalue decomposition of high order tensors is discussed and a new implementation presented. The results of the FA value estimations for the three models are presented and compared.

## 5.2 Key Contributions and Findings

- The fourth-order tensor model is found to consistently have lower signal deviation than the bi-Gaussian and second-order tensor models, however not necessarily lower angular deviation.

- When estimating the direction of one fibre with the bi-Gaussian model, the model generates one direction that fits well with the underlying structure and one that does not.

- The experimental results for the synthetic data show that the FA-definition for the second-order tensor in general yields FA-values close to true FA for one fibre and close to the mean value of true FA for two fibres. The bi-Gaussian FA-definitions all tend to overestimate the true FA for both one and two fibres. The fourth-order definitions yield FA-values that correlate well with true FA for one fibre and for two fibres with a small crossing angle, but decreases with increasing crossing angle. In the real data experiments the DTI-FA maps are more detailed than both the bi-Gaussian and the fourth order model maps.

- The thesis presents an implementation of the Z-eigenvalue decomposition that is more robust and more accurate compared to the existing open-source implementation.

## 5.3 Conclusions

This thesis explored how the two non-Gaussian models, the bi-Gaussian and the fourth order model, compared to DTI, estimate the structure that forms the signal in DWI. This was evaluated in Section 3.4 in terms of three measures: signal deviation, angle deviation and tensor element deviation.

It was observed that all three models perform well in terms of signal deviation, but despite this the angle deviation can be large. This indicates that if only signal deviation is used as a measure of quality when evaluating a model, the model may describe fibre-directions that align poorly with the true direction.

The fourth order model performs well when the simulated crossing angle is larger than 70°. However decreasing the angle from 70° the angle deviation increases rapidly. The large angle deviation for low crossing angles can to some extent be explained by the limitation that the number of fibres is not estimated. This can be seen in the one fibre simulations where the fourth order model estimates the fibre direction well. For one fibre simulations DTI and the fourth order model performed very similar with respect to describing the main direction.

The bi-Gaussian model experiences the same trends as the fourth order model. Larger crossing angles results in lower angle deviation. This can also be related to the fact that the number of fibres is not estimated. Given that two tensors always were estimated when using the bi-Gaussian model, two directions were always estimated even for the single fibre simulations. It was observed that one of these tensors described the direction well, but the other did not. If the model included an estimation of the fraction of occupancy for the two Gaussians the tensor with a large angular deviation would possibly have had a much smaller weight than the tensor with the good angular fit.

For all models the angular deviation increased when the FA decreased. When the fibre direction was less prominent the angle-deviation increased.

In the second part, three FA-definitions for the bi-Gaussian model and two for the fourth order model were compared to the conventional FA-estimate developed for DTI. The results (see Section 4.5) show that the three FA-estimates for the bi-Gaussian model were all more independent of the crossing angle than for the fourth order model and DTI. But, to the bi-Gaussian model's disadvantage, the FA-value were consistently overestimated both for single fibre and crossing fibre simulations.

For the fourth order model the estimated FA-value decreased rapidly when the crossing angle increased from 50° to 70°. This behaviour was most prominent for higher FA-values. For perpendicular fibres, the high-high FA-simulation resulted in a lower estimated FA-value than the high-medium FA-simulation.

## 5.4 Limitations

The real data was obtained at Sahlgrenska University Hospital, with a single $b = 0$ acquisition, and a single-shell acquisition with $b = 800$ s/mm$^2$ using 32 gradient directions. Single-shell image acquisitions sets a limit in the model describing the diffusion to one exponential. To estimate the fraction of occupancy (FoO) constants $A_1$ and $A_2$ in Equation (2.8) of the exponential terms, more than one $b$-value must be used (i.e. multi-shell acquisitions) [7]. Consequently the FoO of the bi-Gaussian model was assumed to be known.

The bi-Gaussian model was fitted using non-linear least squares (Levenberg-Marquardt algorithm) to obtain estimates for the two second order tensors $\mathbf{D}_1$ and $\mathbf{D}_2$ according to Equation 3.15. There is no requirement on the solution that the tensors are PSD (Positive Semi Definite). The FA-estimations of the non-PSD tensors are set to zero, which explains the many black voxels in the real data FA-estimations (see Figure 4.9 in Section 4.5.3 and Figure C.2 – C.4 in Appendix C).

For the fourth order model, the method used to estimate the direction of diffusion did not include an estimation of how many directions are present in each voxel. Instead the number of main directions was assumed to be known.

## 5.5 Further Research

For the real data FA-maps the non-PSD tensors contributed to the large number of voxels where an FA-value could not be calculated. For future work both a PSD constraint and an estimation of number of fibres as well as fraction of occupancy for those fibres is suggested to be included.

For further development of the bi-Gaussian model, estimations of the constants (the fraction of occupancy) $A_1$ and $A_2$ in Equation 2.8 should be included. In order to achieve this more than one $b$-value must be used (i.e. multi-shell acquisitions) [7].

A larger set of gradient-directions during real data image acquisition could provide a better comparison between the FA-maps generated from DTI and the two FA-definitions (used in this thesis) for the fourth order tensor. In this thesis for the real data analysis, 32 gradient directions was used. This gave 32 equations to estimate 6 unknowns for DTI, and the same number of equations but 15 unknowns for the fourth order model. This could be a reason to why the FA-map generated from DTI provided more detail than the FA-map generated from the fourth order model.

If the performance of the fourth order model is further investigated in terms of angle deviation, an estimation of number of fibres should be included. As for now artefacts occur when the synthetic fibre directions almost coincide.

# Bibliography

[1] Derek K. Jones and Mara Cercignani. *Diffusion MRI, Theory, Methods and Applications.* Oxford University Press., 2011.

[2] Stephan E. Maier, Sridhar Vajapeyam, Hatsuho Mamata, Carl-Fredrik Westin, Ferenc A. Jolesz, and Robert V. Mulkern. Biexponential diffusion tensor analysis of human brain diffusion data. *Magnetic Resonance in Medicine*, 51(2):321–330, 02 2004.

[3] Derek K. Jones, Thomas R. Knösche, and Robert Turner. White matter integrity, fiber count, and other fallacies: The do's and don'ts of diffusion MRI. *NeuroImage*, 73(0):239 – 254, 2013.

[4] Gwenaëlle Douaud, Saâd Jbabdi, Timothy E.J. Behrens, Ricarda A. Menke, Achim Gass, Andreas U. Monsch, Anil Rao, Brandon Whitcher, Gordon Kindlmann, Paul M. Matthews, and Stephen Smith. DTI measures in crossing-fibre areas: Increased diffusion anisotropy reveals early white matter alteration in MCI and mild Alzheimer's disease. *NeuroImage*, 55(3):880 – 890, 2011.

[5] Gavin P. Winston. The physical and biological basis of quantitative parameters derived from diffusion MRI. *Quantitative Imaging in Medicine and Surgery*, 2(4), 2012.

[6] Peter J. Basser, James Mattiello, and Dennis LeBihan. Estimation of the effective self-diffusion tensor from the NMR spin echo. *Journal of Magnetic Resonance, Series B*, 103(3):247 – 254, 1994.

[7] Benoit Scherrer and Simon K. Warfield. Parametric representation of multiple white matter fascicles from cube and sphere diffusion MRI. *PLoS ONE*, 7(11):e48232, 11 2012.

[8] Angelos Barmpoutis, Bing Jian, Baba C. Vemuri, and Timothy M. Shepherd. Symmetric positive 4th order tensors and their estimation from diffusion weighted MRI. In Nico Karssemeijer and Boudewijn Lelieveldt, editors, *Information Processing in*

*Medical Imaging*, volume 4584 of *Lecture Notes in Computer Science*, pages 308–319. Springer Berlin Heidelberg, 2007.

[9] David S. Tuch, Timothy G. Reese, Mette R. Wiegell, Nikos Makris, John W. Belliveau, and Van J. Wedeen. High angular resolution diffusion imaging reveals intravoxel white matter fiber heterogeneity. *Magnetic Resonance in Medicine*, 48(4):577–582, 2002.

[10] Mohammad Alipoor, Irene Yu-Hua Gu, Andrew J. H. Mehnert, Ylva Lilja, and Daniel Nilsson. Optimal diffusion tensor imaging with repeated measurements. In Kensaku Mori, Ichiro Sakuma, Yoshinobu Sato, Christian Barillot, and Nassir Navab, editors, *MICCAI (1)*, volume 8149 of *Lecture Notes in Computer Science*, pages 687–694. Springer, 2013.

[11] Angelos Barmpoutis. Tutorial on diffusion tensor MRI using MATLAB. *Electronic Edition, University of Florida*, 2010.

[12] Derek K. Jones. The effect of gradient sampling schemes on measures derived from diffusion tensor MRI: A Monte Carlo study. *Magnetic Resonance in Medicine*, 51(4):807–815, 2004.

[13] Liqun Qi, Gaohang Yu, and Ed X. Wu. Higher order positive semidefinite diffusion tensor imaging. *SIAM Journal on Imaging Sciences*, 3(3):416–433, 2010.

[14] Stefan Lienhard, James G. Malcolm, Carl-Frederik Westin, and Yogesh Rathi. A full bi-tensor neural tractography algorithm using the unscented Kalman filter. *EURASIP Journal on Advances in Signal Processing*, 2011(1):1–10, 2011.

[15] Angelos Barmpoutis and Baba C. Vemuri. A unified framework for estimating diffusion tensors of any order with symmetric positive-definite constraints. *In Proceedings of ISBI10: IEEE International Symposium on Biomedical Imaging*, pages 1385–1388, 14-17 April 2010.

[16] Liqun Qi, Gaohang Yu, and Yi Xu. Nonnegative diffusion orientation distribution function. *Journal of Mathematical Imaging and Vision*, 45(2):103–113, 2013.

[17] Vikas Gulani, Andrew G. Webb, Ian D. Duncan, and Paul C. Lauterbur. Apparent diffusion tensor measurements in myelin-deficient rat spinal cords. *Magnetic Resonance in Medicine*, 44:191–195, 2001.

[18] Mohammad Alipoor, Irene Yu-Hua Gu, Andrew J.H. Mehnert, Ylva Lilja, and Daniel Nilsson. On high order tensor-based diffusivity profile estimation. In *Engineering in Medicine and Biology Society (EMBC), 2013 35th Annual International Conference of the IEEE*, pages 93–96, July 2013.

[19] Liqun Qi. Eigenvalues of a real supersymmetric tensor. *Journal of Symbolic Computation*, 40(6):1302 – 1324, 2005.

[20] Alex D. Leow, Liang Zhan, Siwei Zhu, Nathan Hageman, Ming-Chang Chiang, Marina Barysheva, Arthur W. Toga, K.L. McMahon, G.I. de Zubicaray, M.J. Wright, and Paul M. Thompson. White matter integrity measured by fractional anisotropy correlates poorly with actual individual fiber anisotropy. In *Biomedical Imaging: From Nano to Macro, 2009. ISBI '09. IEEE International Symposium on*, pages 622–625, 2009.

# A

# Plots of Quality Measures

## A.1   One Fibre Structure

### A.1.1   Angle Deviation
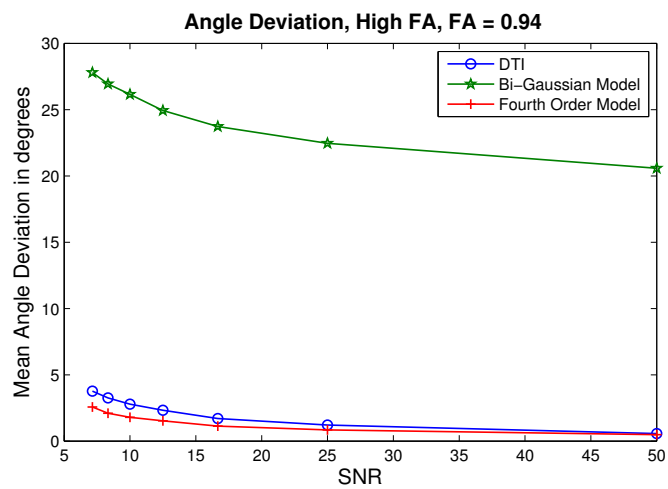


**Figure A.1: Description:** Mean angle deviation, one fibre. Ground truth FA= 0.94. **Comment:** Both fourth order and DTI have low angle deviation. The bi-Gaussian model's large angle deviation is due to model-structure-mismatch.
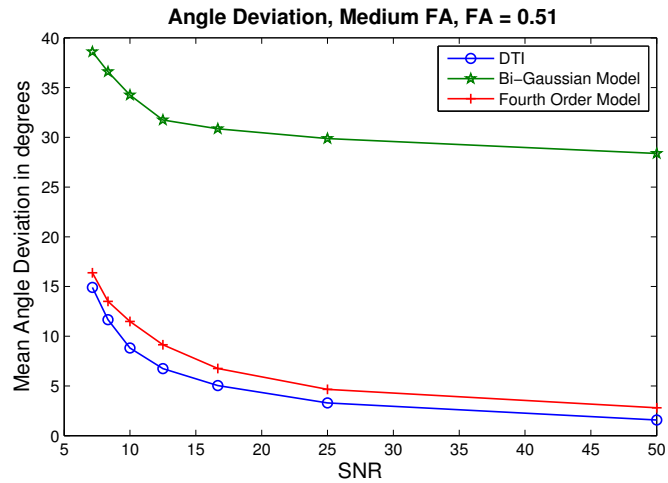
**Figure A.2: Description:** Mean angle deviation, one fibre. Ground truth FA= 0.51.
**Comment:** Both fourth order and DTI have low angle deviation. The bi-Gaussian model's
large angle deviation is due to model-structure-mismatch.
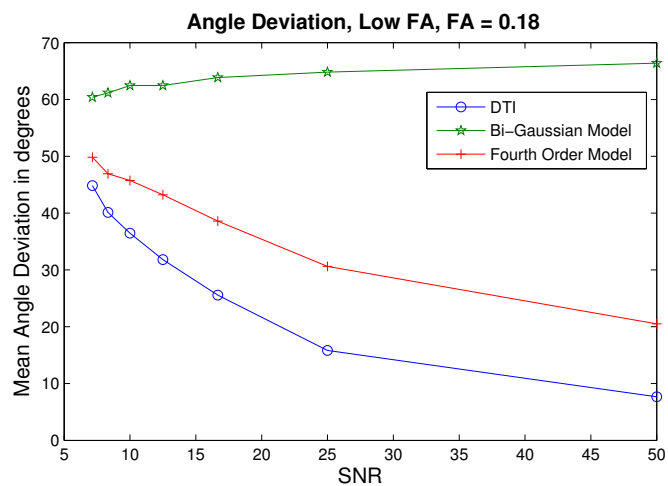


**Figure A.3: Description:** Mean angle deviation, one fibre. Ground truth FA= 0.18.
**Comment:** For the fourth order model and DTI the mean angle deviation decreases with
increased SNR. With FA= 0.18, which is the mean FA for grey matter, this is expected.

### A.1.2   Signal Deviation
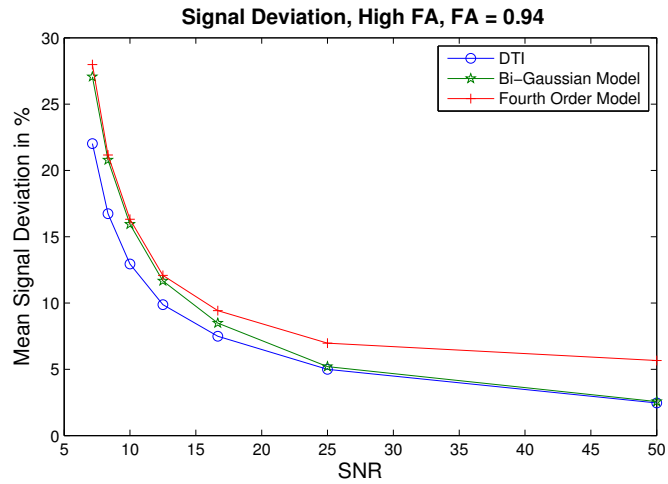


**Figure A.4: Description:** Mean signal deviation, one fibre. Ground truth FA= 0.94. **Comment:** For all models signal deviation decreases with increasing SNR, DTI has lowest signal deviation.
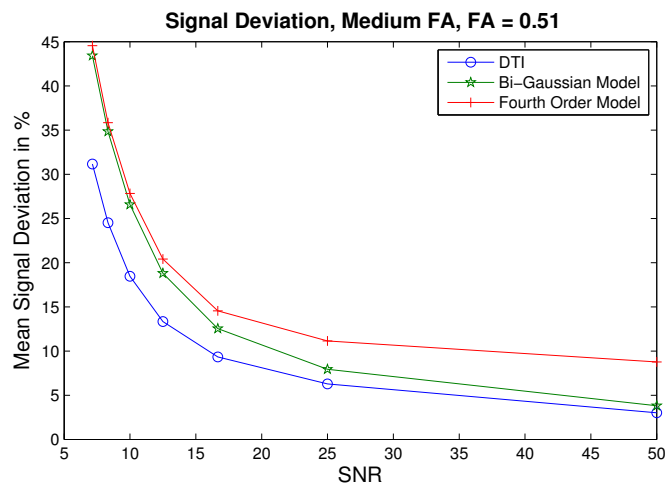


**Figure A.5: Description:** Mean signal deviation, one fibre. Ground truth FA= 0.51. **Comment:** For all methods signal deviation decreases with increased SNR, DTI has lowest signal deviation. Same trend as in Figure A.4
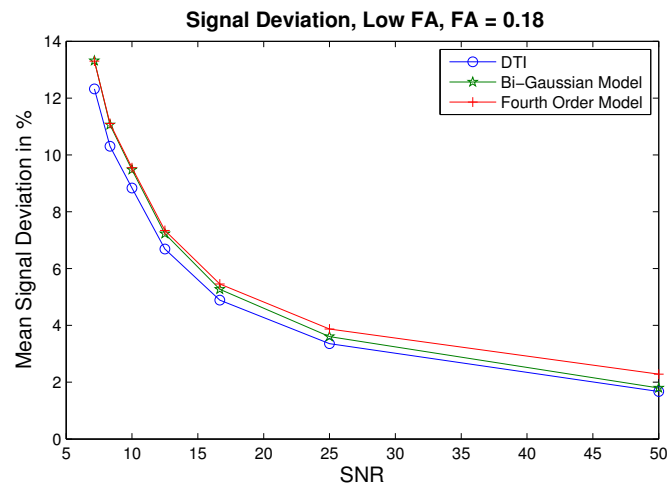
**Figure A.6: Description:** Mean signal deviation, one fibre. Ground truth FA= 0.18. **Comment:** For all methods signal deviation decreases with increased SNR, DTI has lowest signal deviation.

62

### A.1.3 Tensor Element Deviation
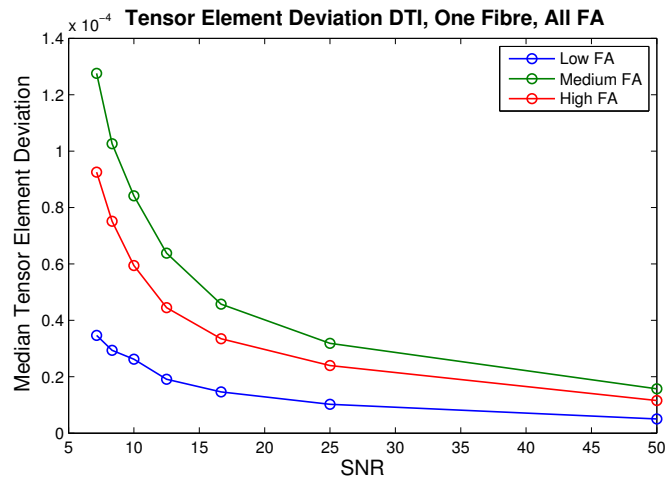


**Figure A.7: Description:** Median tensor element deviation, one fibre, DTI. Ground truth $FA_{low} = 0.18$, $FA_{medium} = 0.51$ and $FA_{high} = 0.94$.
**Comment:** The magnitude of the deviation is the same order of magnitude as a typical tensor element (that is $17 \cdot 10^{-4}$ in simulations), and decreases with increasing SNR.

## A.2 Two Fibre Structure

### A.2.1 Angle Deviation

**High-High FA Fibre Structure**
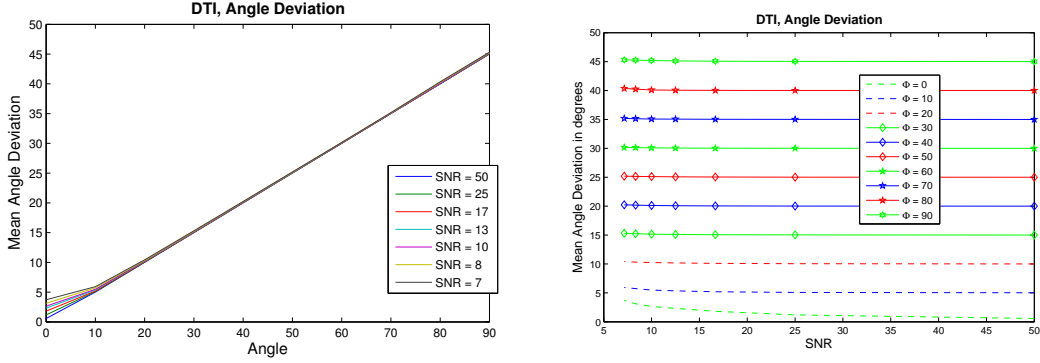


**(a) Description:** Angle deviation as function of fibre crossing angle.

**(b) Description:** Angle deviation as function of SNR.

**Figure A.8: Description:** Angle deviation for DTI. Ground truth $FA_1 = 0.94$ and $FA_2 = 0.94$.
**Comment:** SNR has little impact on the result, somewhat more for crossing angle below 10°. Crossing angle has large impact on the angle deviation, which is expected due to the mismatch between the model and the underlying structure when two tensors are estimated with one.
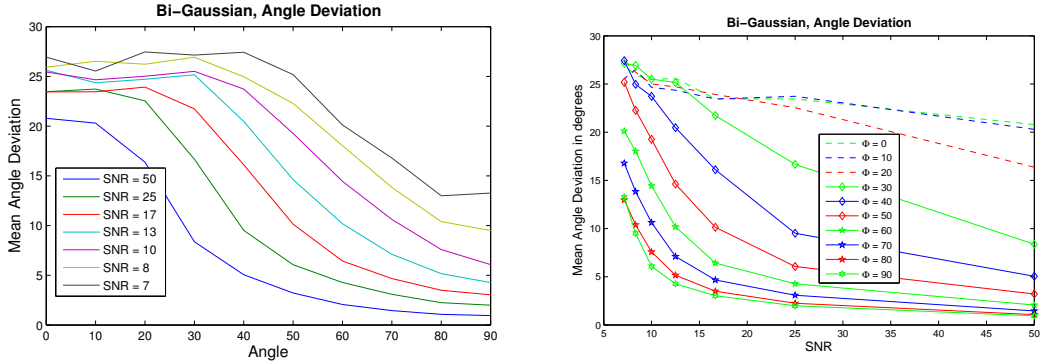


**(a) Description:** Bi-Gaussian model, ranged random initialisation, angle deviation as function of fibre crossing angle.

**(b) Description:** Bi-Gaussian model, ranged random initialisation, angle deviation as function of SNR.

**Figure A.9: Description:** Bi-Gaussian model, random initialisation, angle deviation for bi-Gaussian model estimation. Ground truth $FA_1 = 0.94$ and $FA_2 = 0.94$.
**Comment:** Both crossing angle and SNR have large impact on the angular error. With increasing crossing angle and SNR the angle deviation decreases.
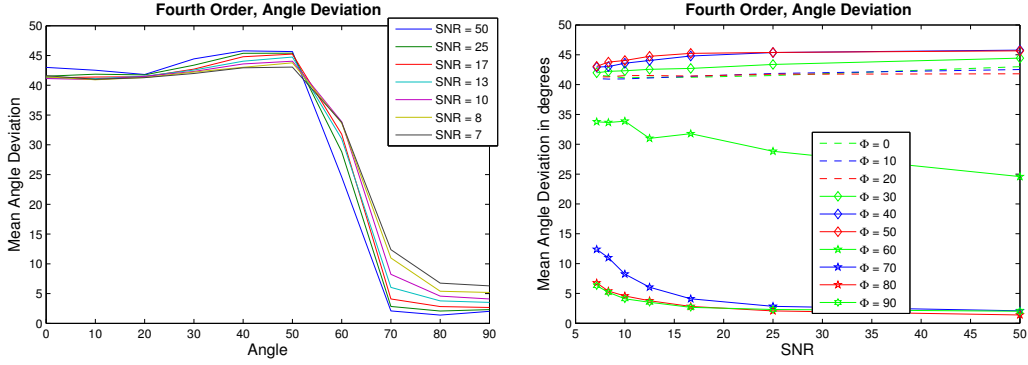
**(a) Description:** Fourth order model, angle deviation as function of fibre crossing angle.

**(b) Description:** Fourth order model, angle deviation as function of SNR.

**Figure A.10: Description:** Angle deviation as function of fibre crossing angle for fourth order tensor estimation. Ground truth $FA_1 = 0.94$ and $FA_2 = 0.94$.

**Comment:** SNR has little impact overall, but most for angles higher than 70°, when the angular error is small. For angles below 70° the angle deviation is large.

## High-Medium FA Fibre Structure



**(a) Description:** Angle deviation as function of fibre crossing angle.

**(b) Description:** Angle deviation as function of SNR.
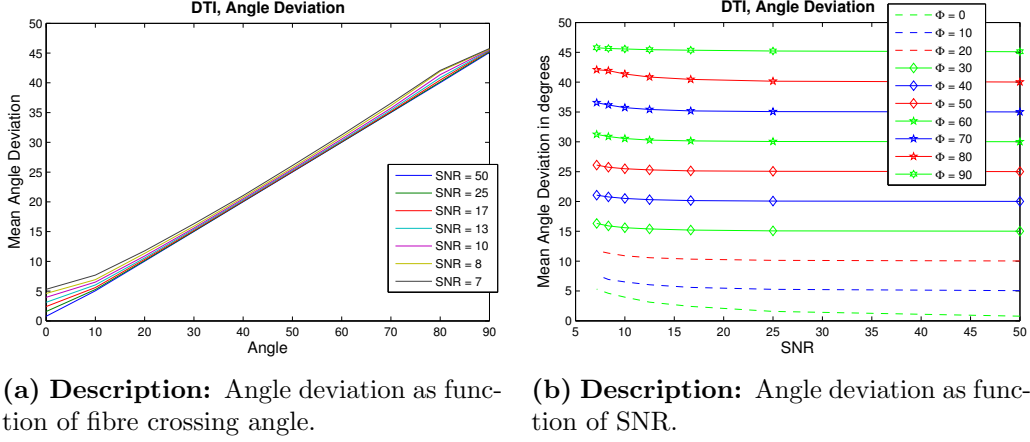
**Figure A.11: Description:** Angle deviation for DTI. Ground truth $FA_1 = 0.94$ and $FA_2 = 0.51$.
**Comment:** SNR has little impact on the deviation, most for crossing angle below 10°. Crossing angle has large impact on the angle deviation, which is expected due to the mismatch between the model and the underlying structure.



**(a) Description:** Bi-Gaussian model, ranged random initialisation, angle deviation as function of fibre crossing angle.

**(b) Description:** Bi-Gaussian model, ranged random initialisation, angle deviation as function of SNR.
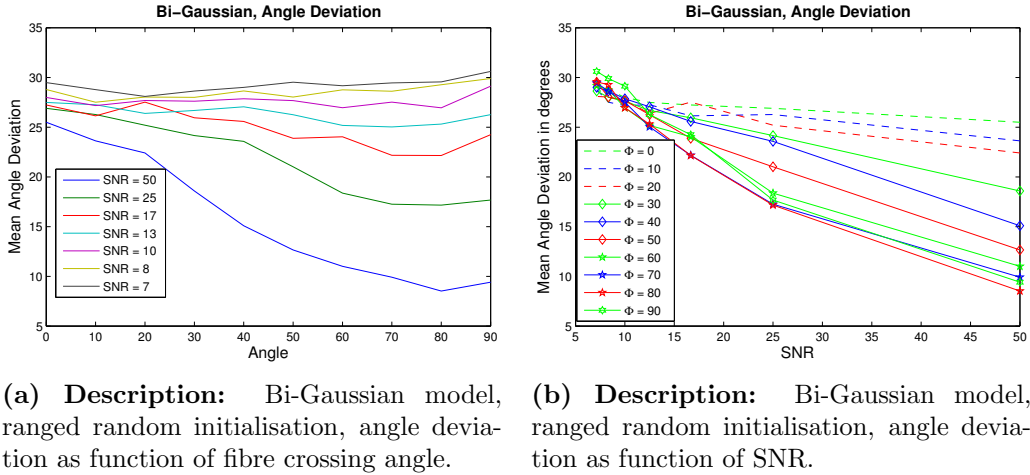
**Figure A.12: Description:** Bi-Gaussian model, ranged random initialisation. Ground truth $FA_1 = 0.94$ and $FA_2 = 0.51$.
**Comment:** Both crossing angle and SNR have large impact on the angular error. For SNR above 25 the angle deviation decreases with increasing crossing angle.
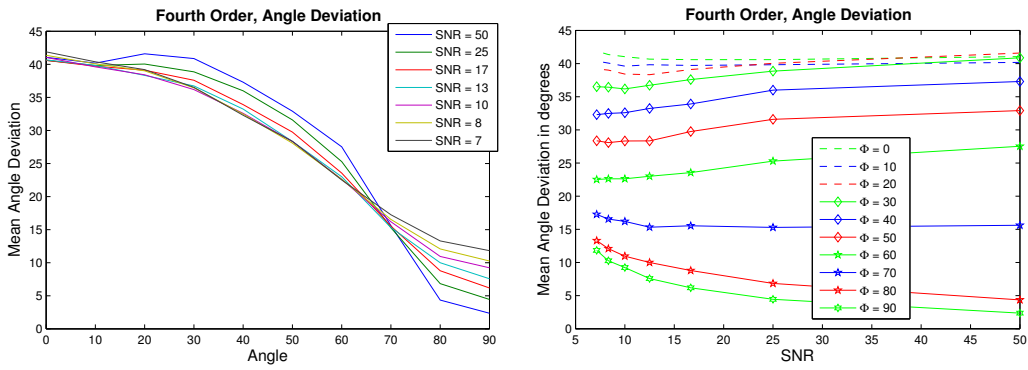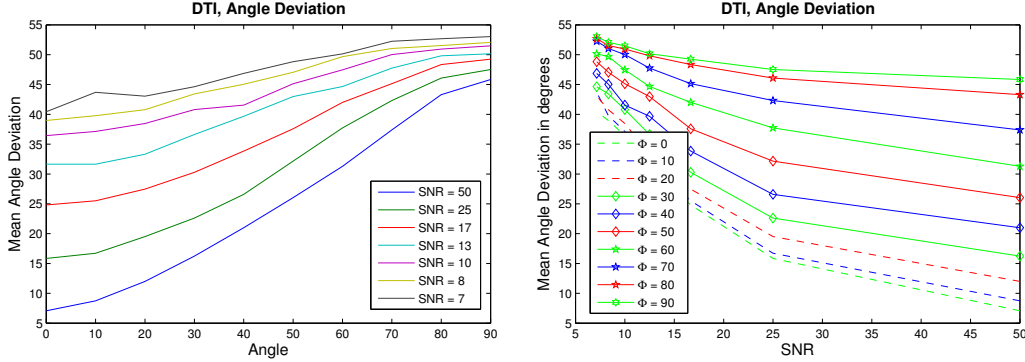
**(a) Description:** Fourth order model, angle deviation as function of fibre crossing angle.

**(b) Description:** Fourth order model, angle deviation as function of SNR.

**Figure A.13: Description:** Fourth order model, angle deviation as function of fibre crossing angle for fourth order tensor estimation. Ground truth $FA_1 = 0.94$ and $FA_2 = 0.51$. **Comment:** SNR has little impact overall, but largest for angles higher than 70°, where the angular error is small. The angle deviation increases with decreasing crossing angle. When crossing angle is lower than 60° the angle deviation decreases with decreasing SNR, above 60° the relation is reversed.
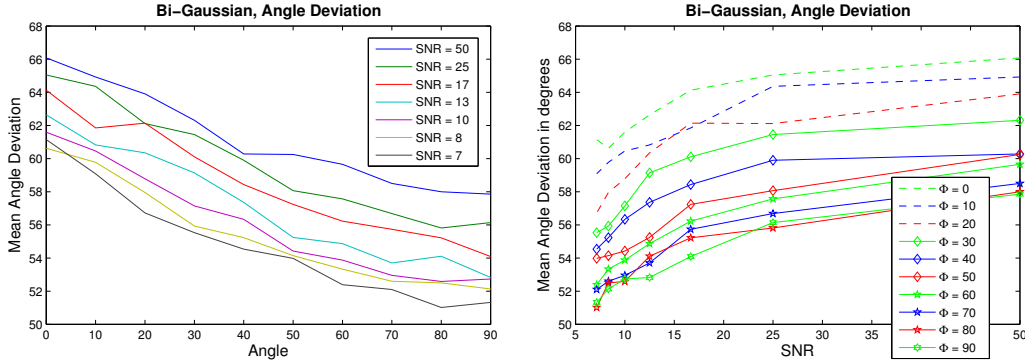
## High-Low FA Fibre Structure
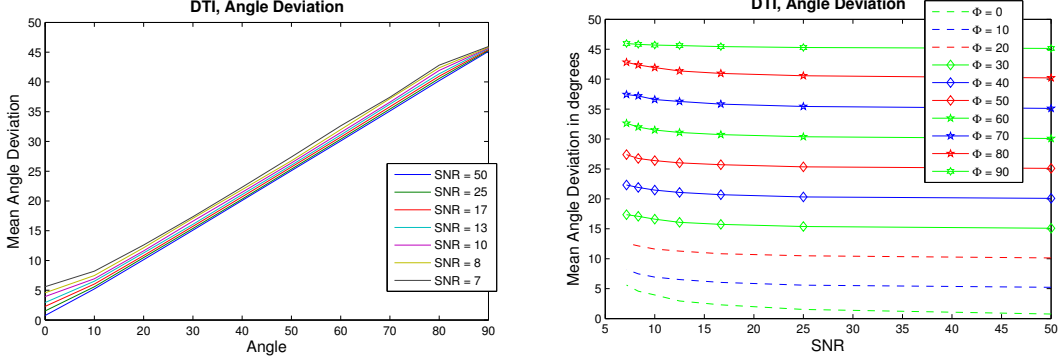


**(a) Description:** DTI, angle deviation as function of fibre crossing angle.

**(b) Description:** DTI, angle deviation as function of SNR.

**Figure A.14:** **Description:** Angle deviation for DTI. Ground truth $FA_1 = 0.94$ and $FA_2 = 0.18$.

**Comment:** SNR has little impact on the result, but more than for high-high FA fibre structure, compare with Figure A.8a. Crossing angle has large impact on the angle deviation, which is expected due to the mismatch between the model and the und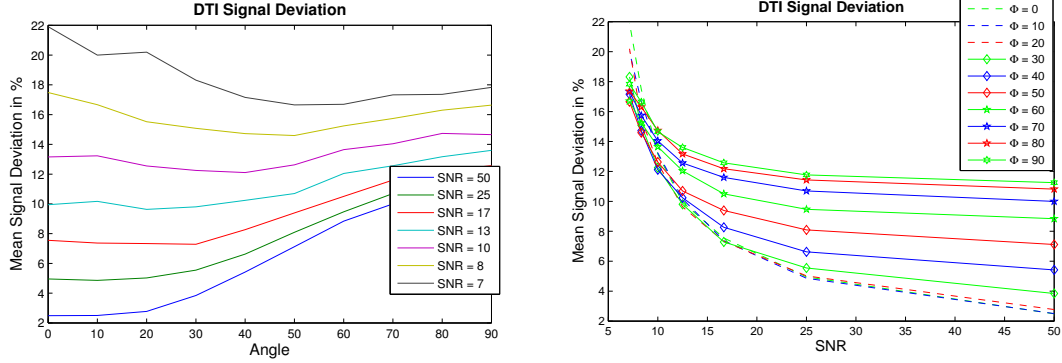erlying structure when two tensors are estimated with one. The angle deviation increases with increasing crossing angle.
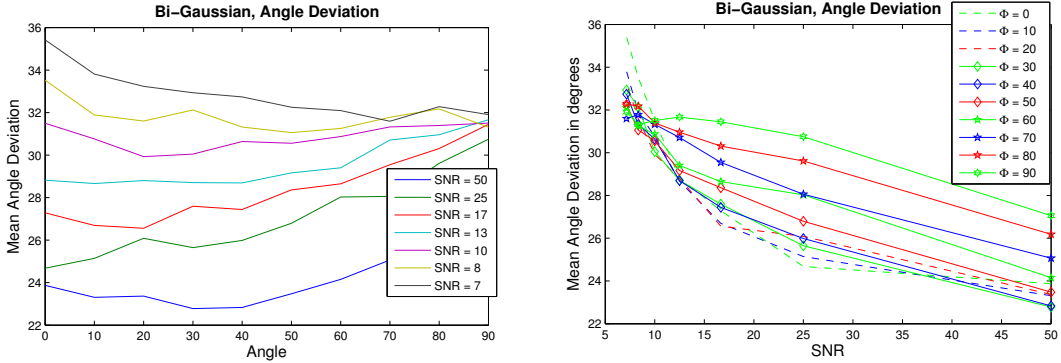


**(a) Description:** Bi-Gaussian model, ranged random initialisation, angle deviation as function of fibre crossing angle.

**(b) Description:** Bi-Gaussian model, ranged random initialisation, angle deviation as function of SNR.

**Figure A.15:** **Description:** Ranged random initialisation, angle deviation for the bi-Gaussian model. Ground truth $FA_1 = 0.94$ and $FA_2 = 0.18$.

**Comment:** Angle deviation decreases with increasing SNR, crossing angle has little impact but for SNR above 10 the angle deviation increases with increasing crossing angle.
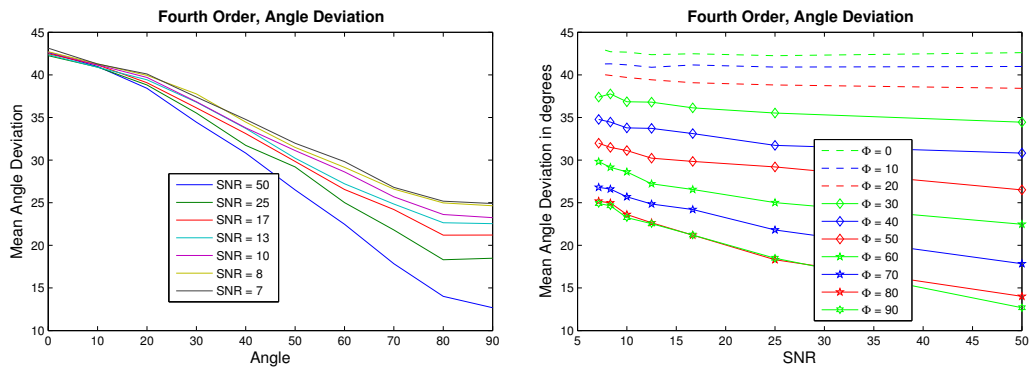
**(a) Description:** Fourth order model, angle deviation as function of fibre crossing angle.

**(b) Description:** Fourth order model, angle deviation as function of SNR.

**Figure A.16: Description:** Angle deviation for fourth order tensor estimation. Ground truth $FA_1 = 0.94$ and $FA_2 = 0.18$.

**Comment:** Angle deviation decreases with increasing SNR and crossing angle.

## Medium-Medium FA Fibre Structure
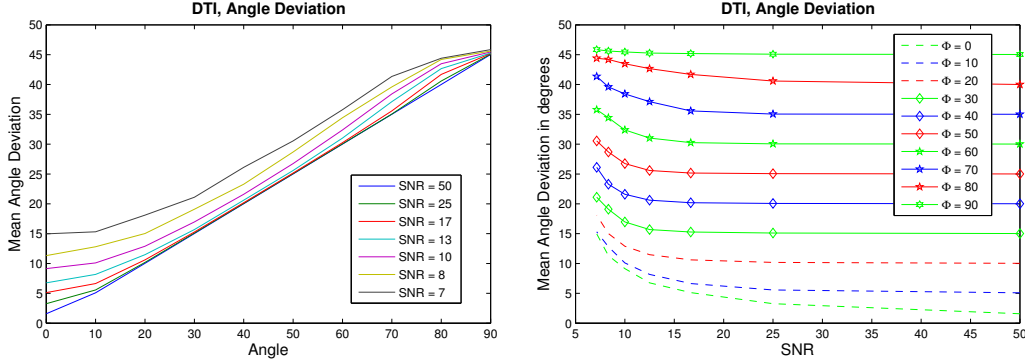


**(a) Description:** DTI, angle deviation as function of fibre crossing angle.

**(b) Description:** DTI, angle deviation as function of SNR.

**Figure A.17: Description:** Angle deviation for DTI. Ground truth $FA_1 = 0.51$ and $FA_2 = 0.51$.

**Comment:** SNR has little impact on the result, somewhat more for crossing angle below $10°$. With increased crossing angle the angle deviation increases almost linearly, the high dependence on crossing angle is expected due to the model-structure mismatch.
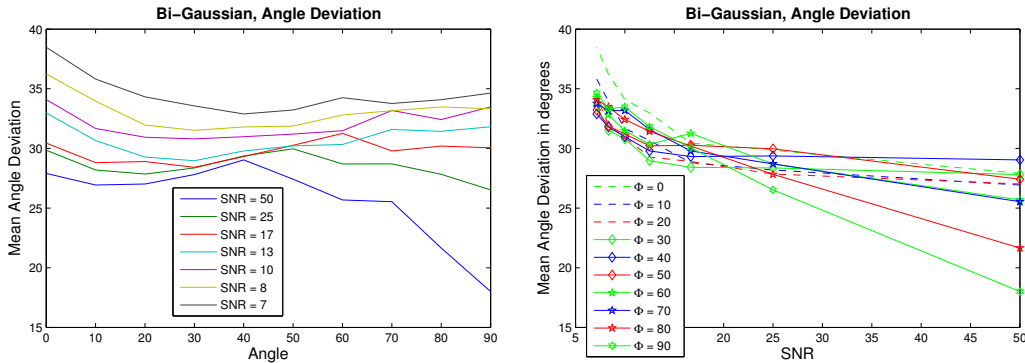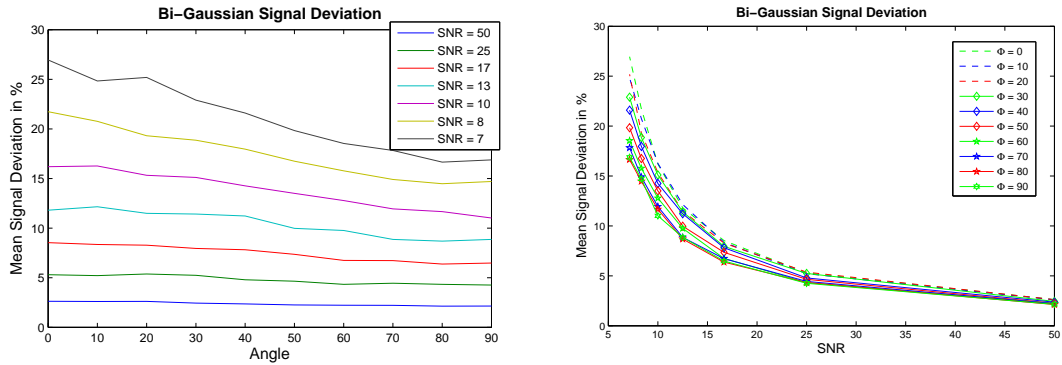


**(a) Description:** Bi-Gaussian model, random initialisation, angle deviation as function of fibre crossing angle.

**(b) Description:** Bi-Gaussian model, random initialisation, angle deviation as function of SNR.

**Figure A.18: Description:** Random initialisation, angle deviation for bi-Gaussian model estimation. Ground truth $FA_1 = 0.51$ and $FA_2 = 0.51$.

**Comment:** Angle deviation decreases with increasing SNR.
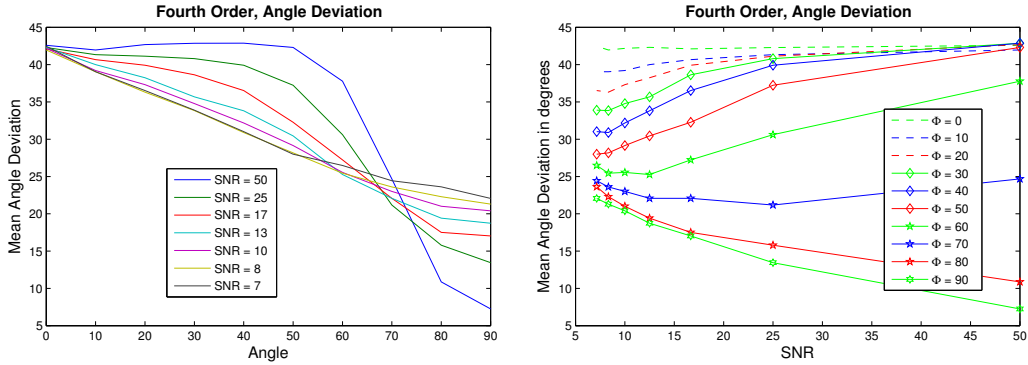
**(a) Description:** Fourth order model, angle deviation as function of fibre crossing angle.

**(b) Description:** Fourth order model, angle deviation as function of SNR.

**Figure A.19: Description:** Angle deviation as function of fibre crossing angle for fourth order tensor estimation. Ground truth $FA_1 = 0.51$ and $FA_2 = 0.51$.

**Comment:** Angle deviation decreases with increasing crossing angle. For crossing angles larger than $70°$ increasing the SNR will decrease the angle deviation, but for crossing angles lower than $60°$ the relationship is reversed.

## Medium-Low FA Fibre Structure



**(a) Description:** DTI, angle deviation as function of fibre crossing angle.

**(b) Description:** DTI, angle deviation as function of SNR.
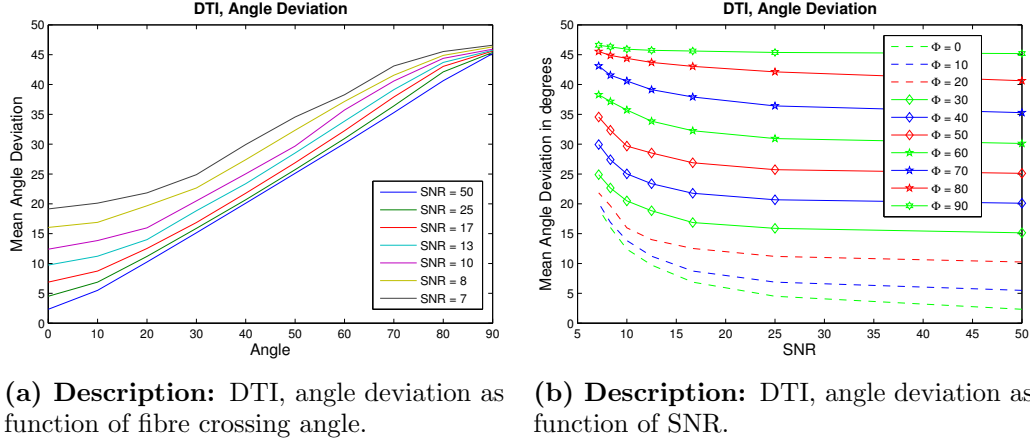
**Figure A.20: Description:** Angle deviation for DTI. Ground truth $FA_1 = 0.51$ and $FA_2 = 0.18$.

**Comment:** With increasing crossing angle the angle deviation increases almost linearly, a high dependence is expected due to the structure-model mismatch. The angle deviation increases with decreasing SNR.



**(a) Description:** Bi-Gaussian model, random initialisation, angle deviation as function of fibre crossing angle.

**(b) Description:** Bi-Gaussian model, random initialisation, angle deviation as function of SNR.
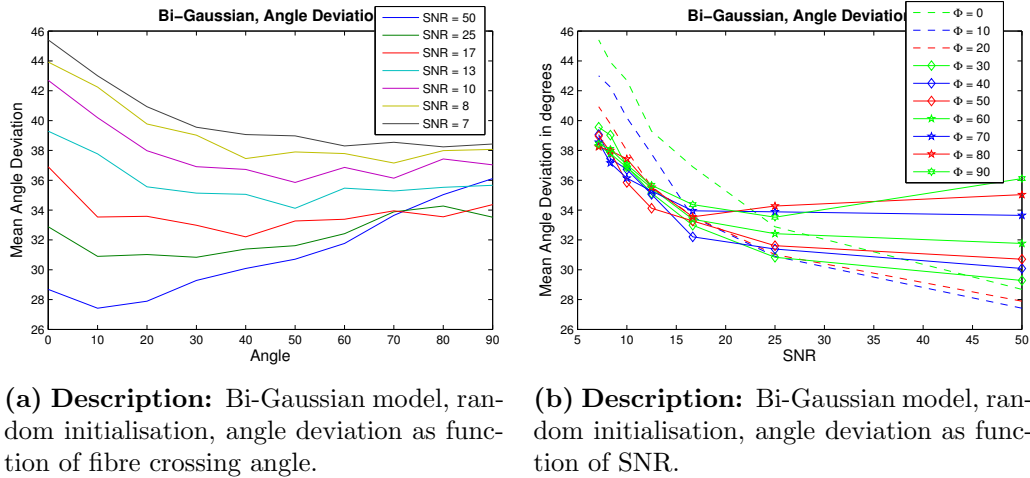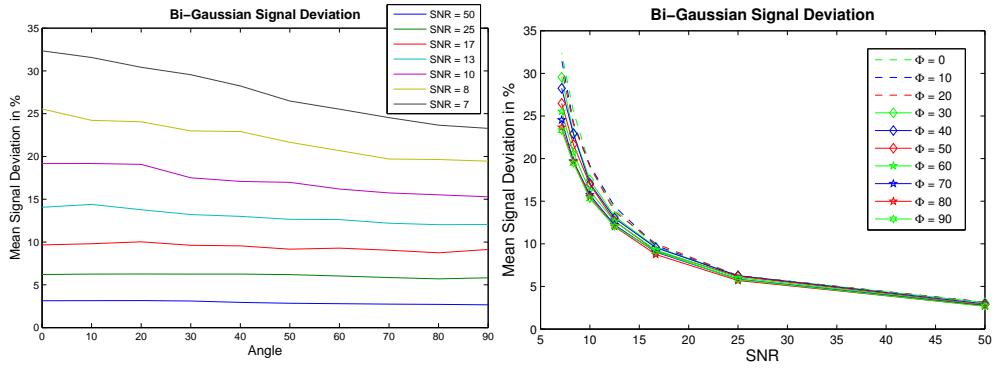
**Figure A.21: Description:** Random initialisation, angle deviation for bi-Gaussian model estimation. Ground truth $FA_1 = 0.51$ and $FA_2 = 0.18$.

**Comment:** Angle deviation is large for all SNR's and crossing angles, but decreases with with increasing SNR for crossing angles below $70°$.
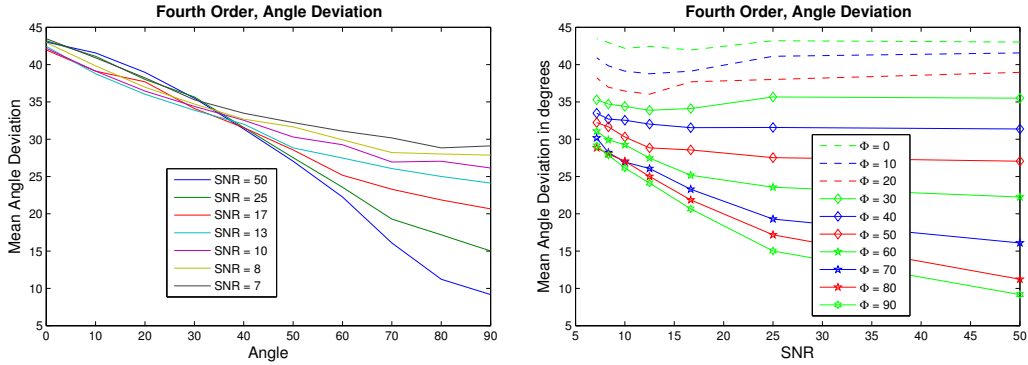
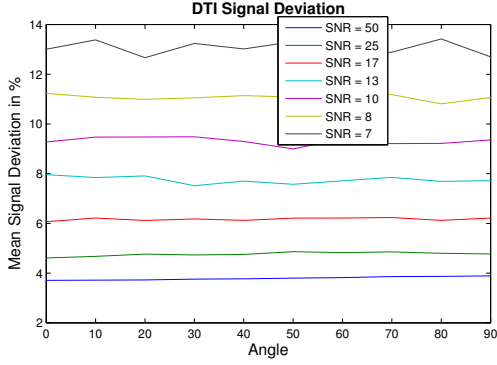**(a) Description:** Fourth order model, angle deviation as function of fibre crossing angle.

**(b) Description:** Fourth order model, angle deviation as function of SNR.

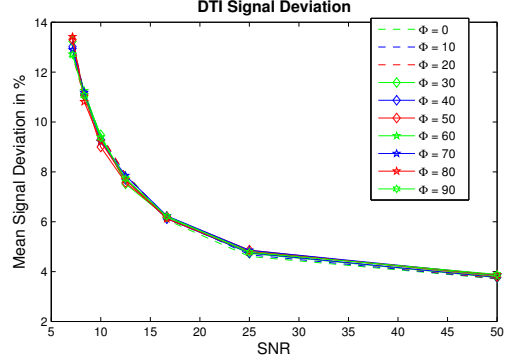**Figure A.22: Description:** Angle deviation as function of fibre crossing angle for fourth order tensor estimation. Ground truth $FA_1 = 0.51$ and $FA_2 = 0.18$.

**Comment:** SNR has little impact overall, however most for angles larger than $70°$, where the angular error is small. For angles lower than $70°$ the angular resolution with this model is poor.
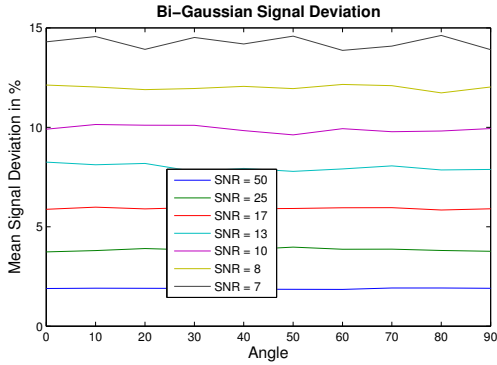
**Low-Low FA Fibre Structure**



**(a) Description:** Angle deviation as function of fibre crossing angle.

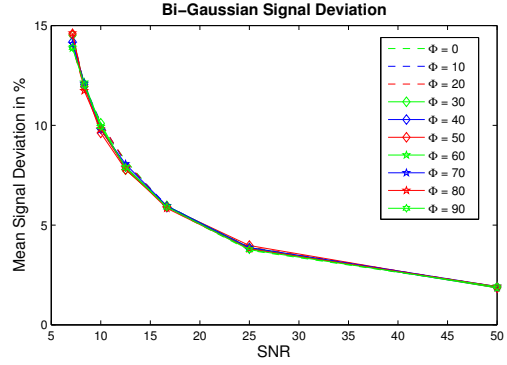**(b) Description:** Angle deviation as function of SNR.

**Figure A.23: Description:** Angle deviation for DTI. Ground truth $FA_1 = 0.18$ and $FA_2 = 0.18$.

**Comment:** SNR has little impact on the result, somewhat more for crossing angle below $10°$. Crossing angle has large impact on the angle deviation, which is expected due to the mismatch between the model and the underlying structure when two tensors are estimated with one.



**(a) Description:** Bi-Gaussian model, ranged random initialisation, angle deviation as function of fibre crossing angle.

**(b) Description:** Bi-Gaussian model, ranged random initialisation, angle deviation as function of SNR.

**Figure A.24: Description:** Ranged random initialisation, angle deviation for bi-Gaussian model estimation. Ground truth $FA_1 = 0.18$ and $FA_2 = 0.18$.

**Comment:** Angle deviation increases with increasing SNR and decreasing crossing angle.
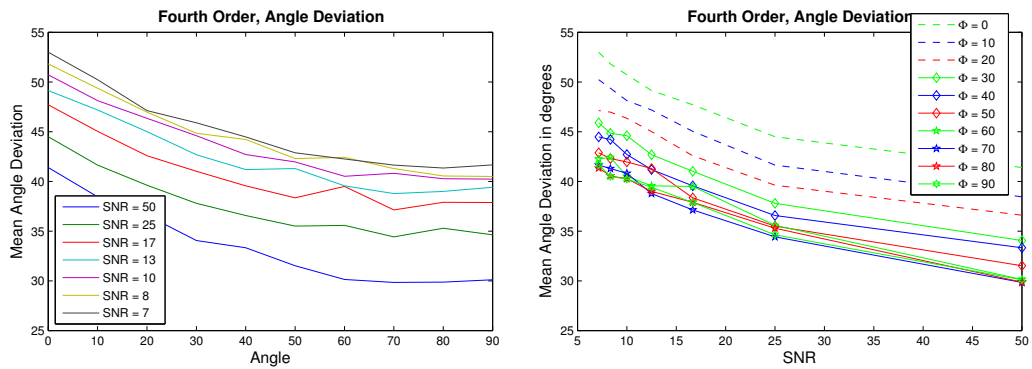
**(a) Description:** Fourth order model, angle deviation as function of fibre crossing angle.

**(b) Description:** Fourth order model, angle deviation as function of SNR.

**Figure A.25: Description:** Angle deviation as function of fibre crossing angle for fourth order tensor estimation. Ground truth $FA_1 = 0.18$ and $FA_2 = 0.18$.
**Comment:** Angle deviation decreases with increasing SNR and crossing angle.

## A.2.2 Signal Deviation

### High-High FA Fibre Structure
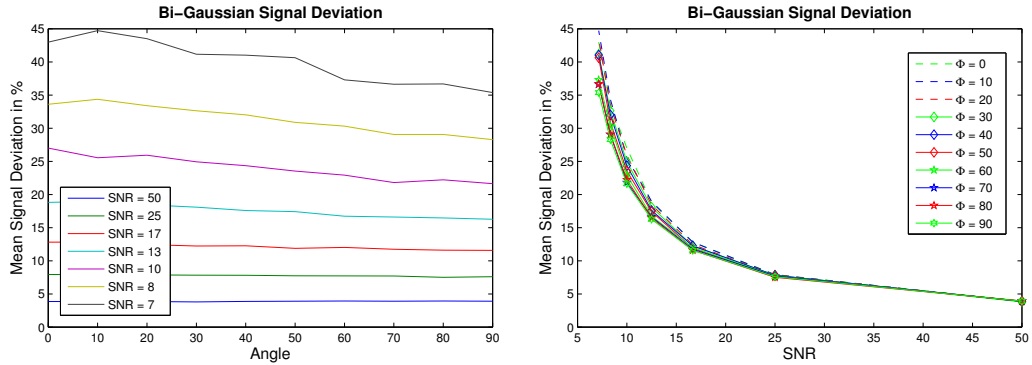


**(a) Description:** DTI, signal deviation as function of fibre crossing angle.

**(b) Description:** DTI, signal deviation as function of SNR.

**Figure A.26: Description:** Signal deviation for DTI. Ground truth $FA_1 = 0.94$ and $FA_2 = 0.94$.
**Comment:** Model-structure mismatch, two fibres are estimated with one second order tensor. The signal deviation decreases with increasing SNR. For SNR above 10 the signal deviation increases with increasing crossing angle.



**(a) Description:** Bi-Gaussian model, ranged random initialisation, signal deviation as function of fibre crossing angle.

**(b) Description:** Bi-Gaussian model, ranged random initialisation, signal deviation as function of SNR.

**Figure A.27: Description:** Random initialisation, signal deviation for bi-Gaussian model estimation. Ground truth $FA_1 = 0.94$ and $FA_2 = 0.94$.
**Comment:** Model and structure match. The signal deviation decreases with increasing SNR.
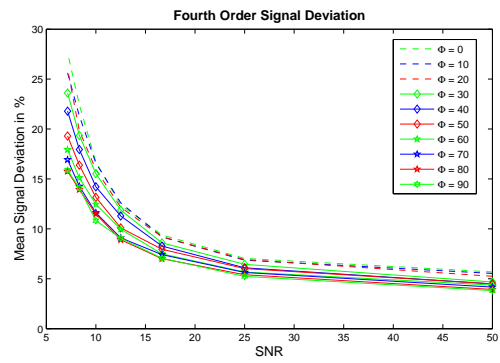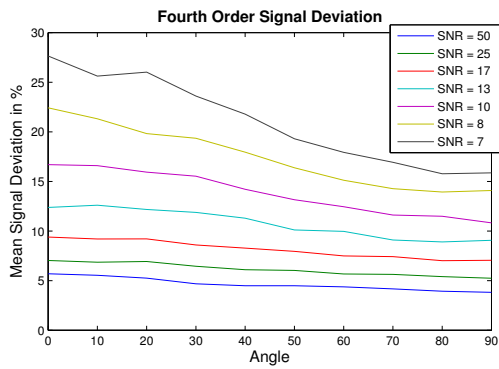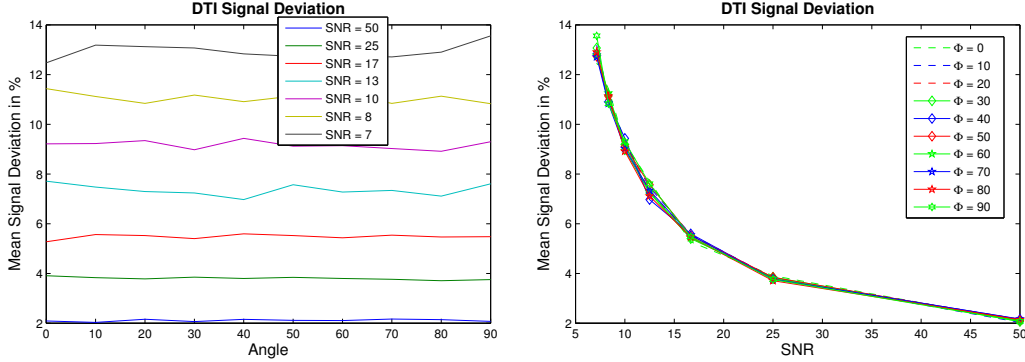
**(a) Description:** Fourth order model, signal deviation as function of fibre crossing angle.

**(b) Description:** Fourth order model, signal deviation as function of SNR.

**Figure A.28: Description:** Signal deviation for HOT estimation. Ground truth $FA_1 = 0.94$ and $FA_2 = 0.94$.

**Comment:** Signal deviation decreases with increasing SNR.
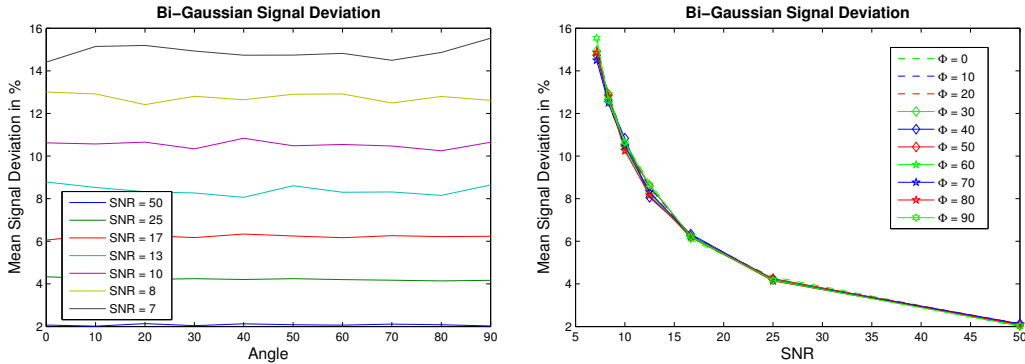
77

**High-Medium FA Fibre Structure**



**(a) Description:** Signal deviation as function of fibre crossing angle.

**(b) Description:** Signal deviation as function of SNR.
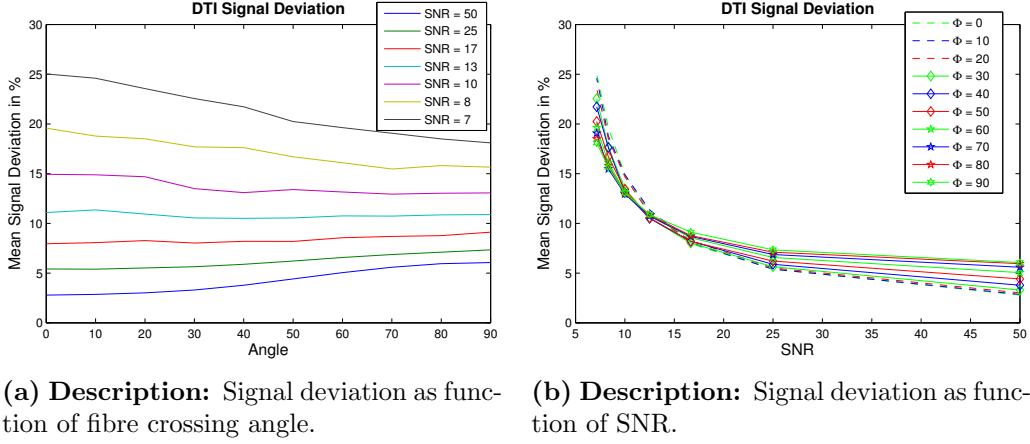
**Figure A.29: Description:** Signal deviation for DTI. Ground truth $FA_1 = 0.94$ and $FA_2 = 0.51$.

**Comment:** Model-structure mismatch. Signal deviation decreases with increasing SNR. For SNR above 13 signal deviation increases with increasing crossing angle, and for SNR below 13 the signal deviation decreases with increasing crossing angle.



**(a) Description:** Bi-Gaussian model, ranged random initialisation, signal deviation as function of fibre crossing angle.

**(b) Description:** Bi-Gaussian model, ranged random initialisation, signal deviation as function of SNR.

**Figure A.30: Description:** Random initialisation, signal deviation for bi-Gaussian model estimation. Ground truth $FA_1 = 0.94$ and $FA_2 = 0.51$.

**Comment:** Signal deviation decreases with increasing SNR, and when SNR is above 17 decreases with increasing crossing angle.
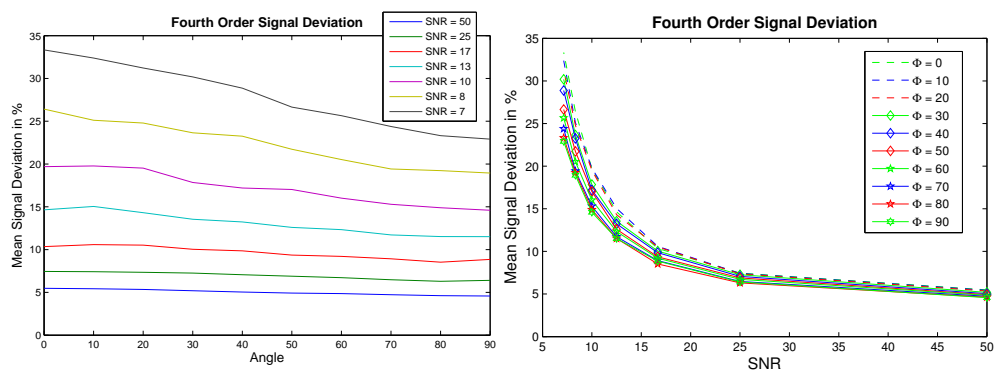
**(a) Description:** Fourth order model, signal deviation as function of fibre crossing angle.

**(b) Description:** Fourth order model, signal deviation as function of SNR.

**Figure A.31: Description:** Signal deviation for fourth order tensor estimation. Ground truth $FA_1 = 0.94$ and $FA_2 = 0.51$.
**Comment:** Signal deviation decreases with increasing SNR, and when SNR is above 17 decreases with increasing crossing angle.

**High-Low FA Fibre Structure**



**(a) Description:** DTI, signal deviation as function of fibre crossing angle.

**(b) Description:** DTI, signal deviation as function of SNR.

**Figure A.32: Description:** Signal deviation for DTI. Ground truth $FA_1 = 0.94$ and $FA_2 = 0.18$.
**Comment:** Signal deviation decreases with increasing SNR, but is close to independent on crossing angle. Similar result as presented in Figure A.33 and Figure A.34.



**(a) Description:** Bi-Gaussian model, ranged random initialisation, signal deviation as function of fibre crossing angle.

**(b) Description:** Bi-Gaussian model, ranged random initialisation, signal deviation as function of SNR.

**Figure A.33: Description:** Random initialisation, signal deviation for bi-Gaussian model estimation. Ground truth $FA_1 = 0.94$ and $FA_2 = 0.18$.
**Comment:** Signal deviation decreases with increasing SNR, but independent of crossing angle. Similar result as presented in Figure A.32 and Figure A.34.
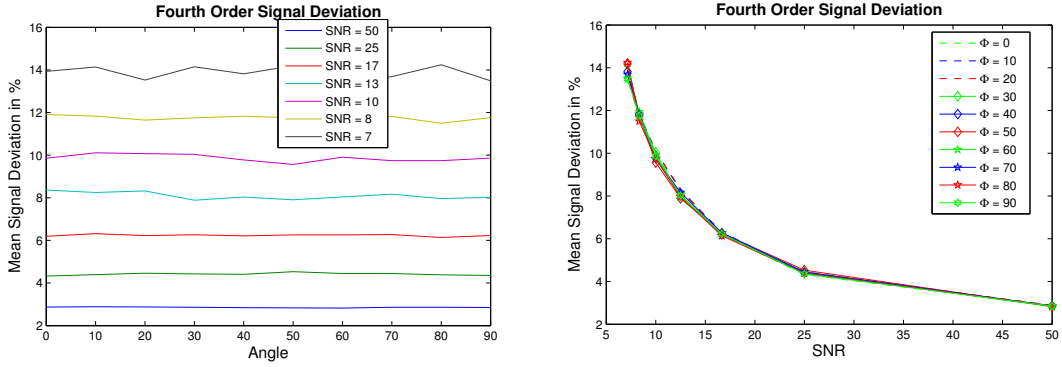
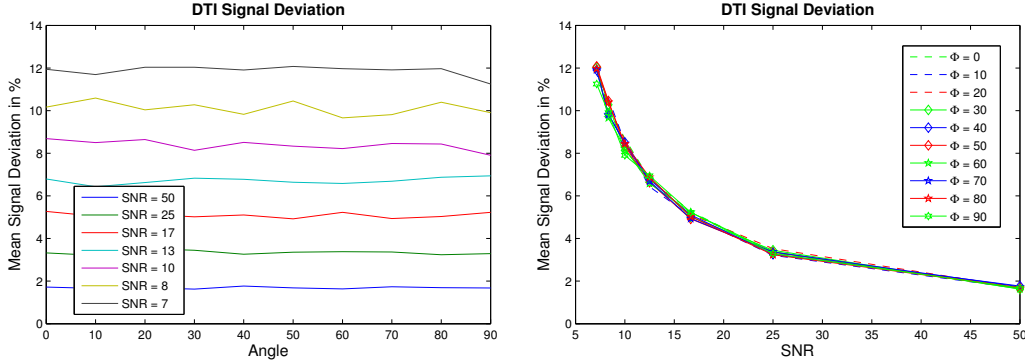**(a) Description:** Fourth order model, signal deviation as function of fibre crossing angle.

**(b) Description:** Fourth order model, signal deviation as function of SNR.

**Figure A.34: Description:** Signal deviation for fourth order tensor estimation. Ground truth $FA_1 = 0.94$ and $FA_2 = 0.18$.

**Comment:** Signal deviation decreases with increasing SNR, but is close to independent on crossing angle. Similar result as presented in Figure A.32 and Figure A.33.

**Medium-Medium FA Fibre Structure**
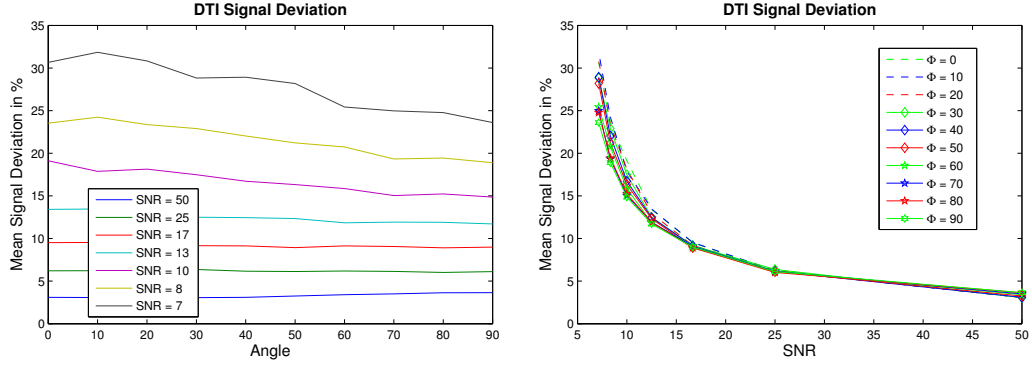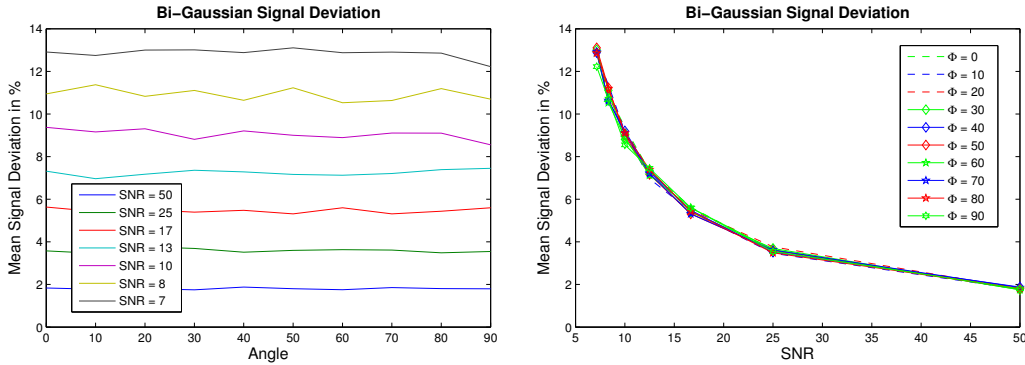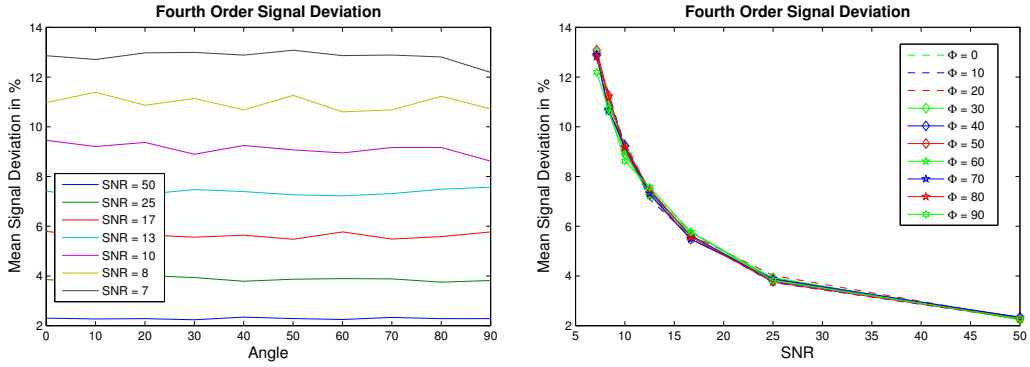
**Signal Deviation**



**(a) Description:** DTI, signal deviation as function of fibre crossing angle.

**(b) Description:** DTI, signal deviation as function of SNR.

**Figure A.35: Description:** Signal deviation for DTI. Ground truth FA$_1$ = 0.51 and FA$_2$ = 0.51.
**Comment:** Signal deviation decreases with increasing SNR and for SNR below 13 with increasing crossing angle. Similar result as presented in Figure A.36 and Figure A.37.



**(a) Description:** Bi-Gaussian model, ranged random initialisation, signal deviation as function of fibre crossing angle.

**(b) Description:** Bi-Gaussian model, ranged random initialisation, signal deviation as function of SNR.

**Figure A.36: Description:** Random initialisation, signal deviation for bi-Gaussian model estimation. Ground truth FA$_1$ = 0.51 and FA$_2$ = 0.51.
**Comment:** Signal deviation decreases with increasing SNR and for SNR below 13 with increasing crossing angle. Similar result as presented in Figure A.35 and Figure A.37.
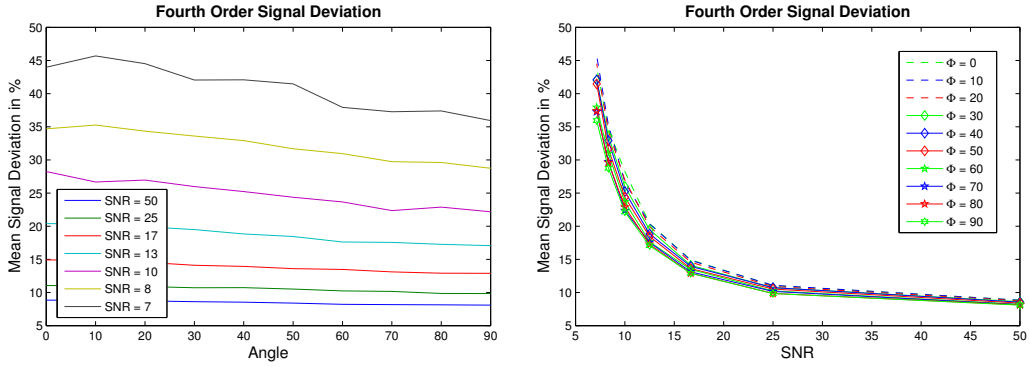
**(a) Description:** Fourth order model, signal deviation as function of fibre crossing angle.

**(b) Description:** Fourth order model, signal deviation as function of SNR.

**Figure A.37: Description:** Signal deviation for fourth order tensor estimation. Ground truth $FA_1 = 0.51$ and $FA_2 = 0.51$.

**Comment:** Signal deviation decreases with increasing SNR and for SNR below 13 with increasing crossing angle. Similar result as presented in Figure A.35 and Figure A.36.

**Medium-Low FA Fibre Structure**



**(a) Description:** DTI, signal deviation as function of fibre crossing angle.

**(b) Description:** DTI, signal deviation as function of SNR.

**Figure A.38: Description:** Signal deviation for DTI. Ground truth $FA_1 = 0.51$ and $FA_2 = 0.18$.

**Comment:** Signal deviation decreases with increasing SNR and is close to independent of crossing angle. Similar results as presented in Figure A.39 and Figure A.40.



**(a) Description:** Bi-Gaussian model, signal deviation as function of fibre crossing angle.

**(b) Description:** Bi-Gaussian model, signal deviation as function of SNR.

**Figure A.39: Description:** Random initialisation, signal deviation for bi-Gaussian model estimation. Ground truth $FA_1 = 0.51$ and $FA_2 = 0.18$.

**Comment:** Signal deviation decreases with increasing SNR and is close to independent of crossing angle. Similar results as presented in Figure A.38 and Figure A.40.
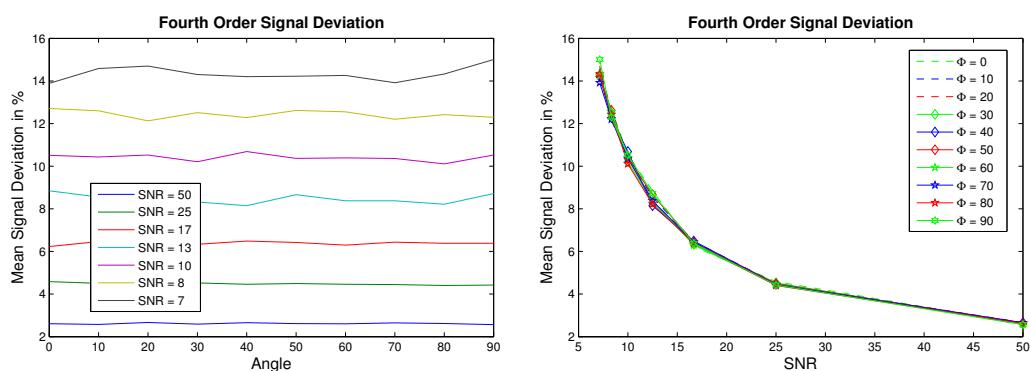
**(a) Description:** Fourth order model, signal deviation as function of fibre crossing angle.

**(b) Description:** Fourth order model, signal deviation as function of SNR.

**Figure A.40: Description:** Signal deviation for fourth order tensor estimation. Ground truth $FA_1 = 0.51$ and $FA_2 = 0.18$.

**Comment:** Signal deviation decreases with increasing SNR and is close to independent of crossing angle. Similar results as presented in Figure A.38 and Figure A.39.

**Low-Low FA Fibre Structure**

**Signal Deviation**



**(a) Description:** DTI, signal deviation as function of fibre crossing angle.



**(b) Description:** DTI, signal deviation as function of SNR.

**Figure A.41: Description:** Signal deviation for DTI. Ground truth $FA_1 = 0.18$ and $FA_2 = 0.18$.
**Comment:** Signal deviation decreases with increasing SNR and is close to independent of crossing angle. Similar results as presented in Figure A.42 and Figure A.43.



**(a) Description:** Bi-Gaussian model, signal deviation as function of fibre crossing angle.



**(b) Description:** Bi-Gaussian model, signal deviation as function of SNR.

**Figure A.42: Description:** Signal deviation for bi-Gaussian model estimation. Ground truth $FA_1 = 0.18$ and $FA_2 = 0.18$.
**Comment:** Signal deviation decreases with increasing SNR and is close to independent of crossing angle. Similar results as presented in Figure A.41 and Figure A.43.

**(a) Description:** Fourth order model, signal deviation as function of fibre crossing angle.

**(b) Description:** Signal deviation as function of SNR.

**Figure A.43: Description:** Signal deviation for fourth order tensor estimation. Ground truth $FA_1 = 0.18$ and $FA_2 = 0.18$.
**Comment:** Signal deviation decreases with increasing SNR and is close to independent of crossing angle. Similar results as presented in Figure A.41 and Figure A.42.

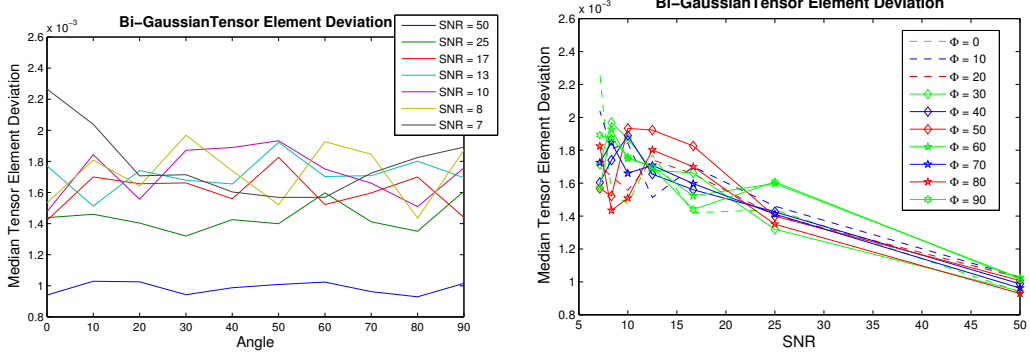### A.2.3 Tensor Element Deviation

**High-High FA Fibre Structure**
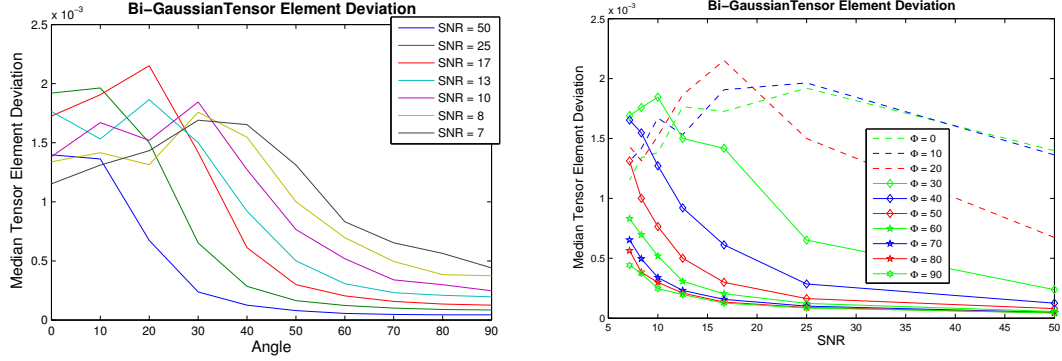


**(a) Description:** Bi-Gaussian model, tensor element deviation as function of fibre crossing angle. Ranged random initialisation. High-high FA fibre structure.

**(b) Description:** Bi-Gaussian model, tensor element deviation as function of SNR. Ranged random initialisation. High-high FA fibre structure.

**Figure A.44: Description:** Tensor element deviation for bi-Gaussian model estimation. Ground truth $FA_1 = 0.94$ and $FA_2 = 0.94$.

**Comment:** A typical tensor element is of order $10^{-4}$, the tensor element deviation decreases with increasing SNR and crossing angle.

## High-Medium FA Fibre Structure
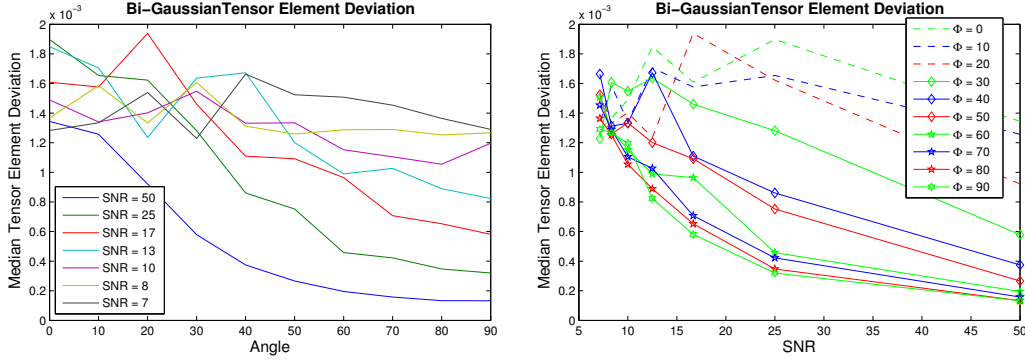


**(a) Description:** Bi-Gaussian model, tensor element deviation as function of fibre crossing angle. Ranged random initialisation. High-medium FA fibre structure.

**(b) Description:** Bi-Gaussian model, tensor element deviation as function of SNR. Ranged random initialisation. High-medium FA fibre structure.

**Figure A.45: Description:** Tensor element deviation for bi-Gaussian model estimation. Ground truth $FA_1 = 0.94$ and $FA_2 = 0.51$.
**Comment:** A typical tensor element is of order $10^{-4}$, the tensor element deviation decreases with increasing crossing angle and SNR.

## High-Low FA Fibre Structure
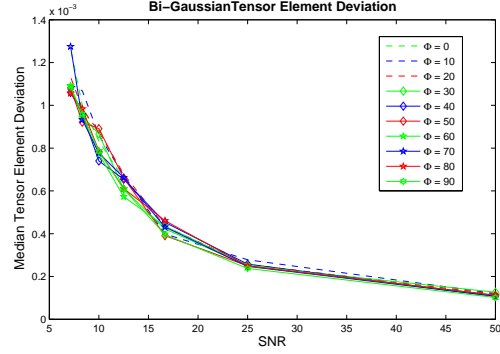


**(a) Description:** Bi-Gaussian model, tensor element deviation as function of fibre crossing angle. Ranged random initialisation. High-low FA fibre structure.

**(b) Description:** Bi-Gaussian model, tensor element deviation as function of SNR. Ranged random initialisation. High-low FA fibre structure.

**Figure A.46: Description:** Tensor element deviation for bi-Gaussian model estimation. Ground truth $FA_1 = 0.94$ and $FA_2 = 0.18$.

**Comment:** A typical tensor element is of order $10^{-4}$, the tensor element deviation decreases with increasing SNR and is close to independent of crossing angle.

**Medium-Medium FA Fibre Structure**
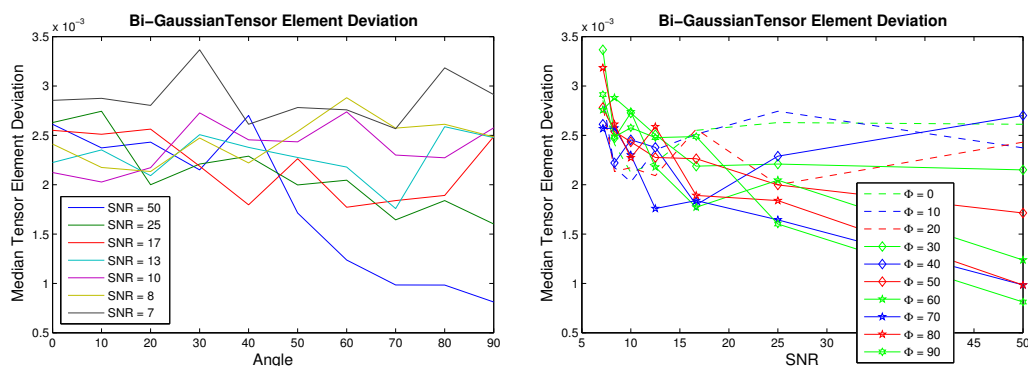


**(a) Description:** Bi-Gaussian model, tensor element deviation as function of fibre crossing angle. Ranged random initialisation. Medium-medium FA fibre structure.

**(b) Description:** Bi-Gaussian model, tensor element deviation as function of SNR. Ranged random initialisation. Medium-medium FA fibre structure.

**Figure A.47: Description:** Tensor element deviation for bi-Gaussian model estimation. Ground truth $FA_1 = 0.51$ and $FA_2 = 0.51$.

**Comment:** A typical tensor element is of order $10^{-4}$. For crossing angles larger than $50°$ the tensor element deviation decreases with increasing SNR.

## Medium-Low FA Fibre Structure
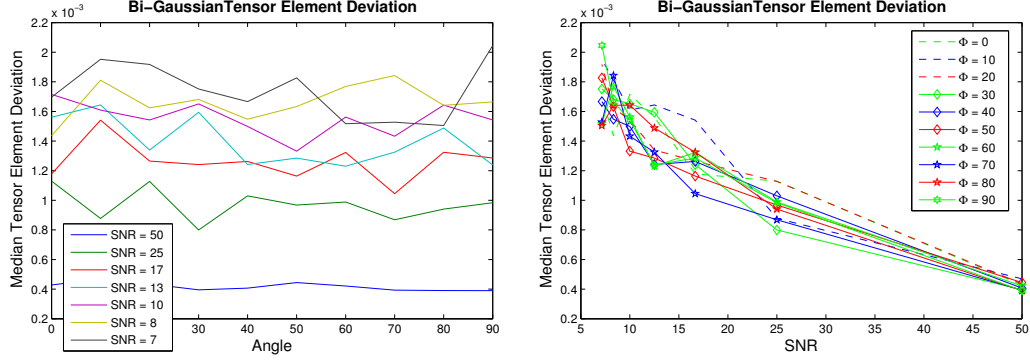


**(a) Description:** Bi-Gaussian model, tensor element deviation as function of fibre crossing angle. Ranged random initialisation. Medium-low FA fibre structure.

**(b) Description:** Bi-Gaussian model, tensor element deviation as function of SNR. Ranged random initialisation. Medium-low FA fibre structure.

**Figure A.48: Description:** Tensor element deviation for bi-Gaussian model estimation. Ground truth $FA_1 = 0.51$ and $FA_2 = 0.18$.
**Comment:** A typical tensor element is of order $10^{-4}$, the tensor element deviation decreases with increasing SNR.

**Low-Low FA Fibre Structure**



**(a) Description:** Bi-Gaussian model, tensor element deviation as function of fibre crossing angle. Ranged random initialisation. Low-low FA fibre structure.

**(b) Description:** Bi-Gaussian model, tensor element deviation as function of SNR. Ranged random initialisation. Low-low FA fibre structure.

**Figure A.49: Description:** Tensor element deviation for bi-Gaussian model estimation. Ground truth $FA_1 = 0.18$ and $FA_2 = 0.18$.
**Comment:** A typical tensor element is of order $10^{-4}$, the tensor element deviation decreases with increasing crossing angle.

93

# B

# Plots of FA-values

## B.1 One Fibre Structure
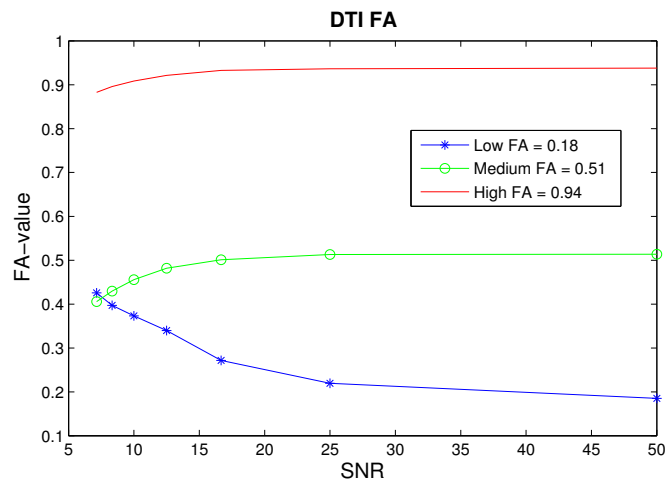


**Figure B.1: Description:** FA estimated with DTI, ground truth FA: $FA_{low} = 0.18$, $FA_{med} = 0.51$ and $FA_{high} = 0.94$.
**Comment:** Model and structure match, estimated FA approaches ground truth FA with increasing SNR.
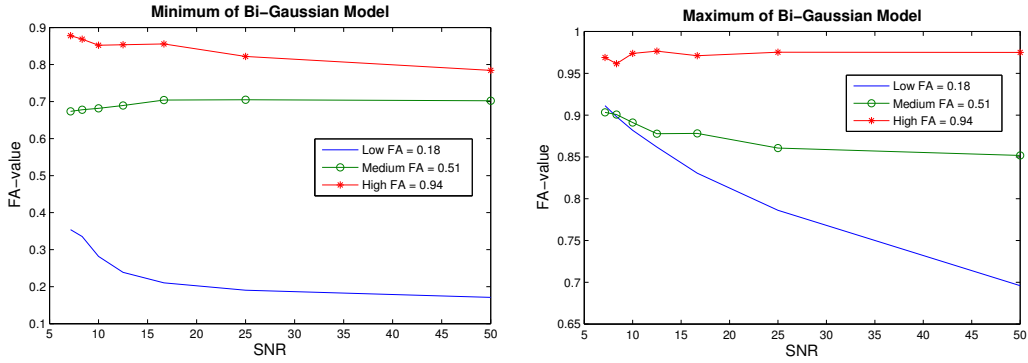
**(a) Description:** Minimum of FA's estimated with bi-Gaussian model, ground truth FA: $FA_{low} = 0.18$, $FA_{med} = 0.51$ and $FA_{high} = 0.94$.
**Comment:** High FA-estimation is more underestimated with increased SNR, medium FA-estimation consistently overestimates, and low FA-estimation approaches ground truth FA with increased SNR.

**(b) Description:** Maximum of FA's estimated with bi-Gaussian model, ground truth FA: $FA_{low} = 0.18$, $FA_{med} = 0.51$ and $FA_{high} = 0.94$.
**Comment:** High FA-estimation approaches ground truth FA with increased SNR, medium and low FA-estimation consistently overestimates, low FA-estimation decreases with increasing SNR.

**Figure B.2: Description:** FA's estimated with bi-Gaussian model, ground truth FA: $FA_{low} = 0.18$, $FA_{med} = 0.51$ and $FA_{high} = 0.94$.
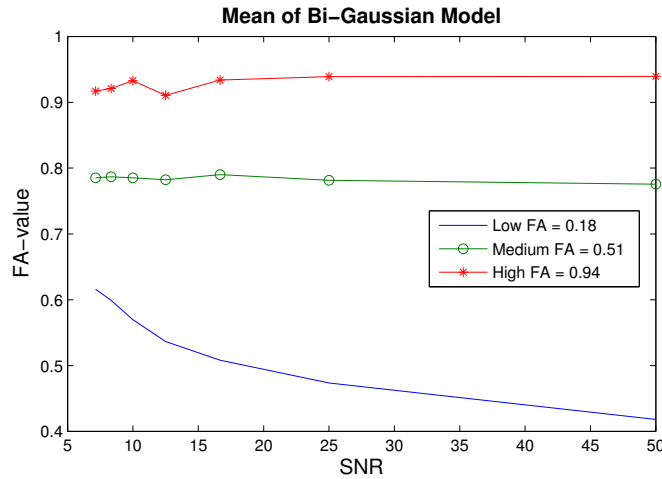


**Figure B.3: Description:** Mean of FA's estimated with bi-Gaussian model, ground truth FA: $FA_{low} = 0.18$, $FA_{med} = 0.51$ and $FA_{high} = 0.94$.
**Comment:** High FA-estimation approaches ground truth FA with increased SNR, medium and low FA-estimation consistently overestimates, low FA-estimation decreases with increasing SNR.
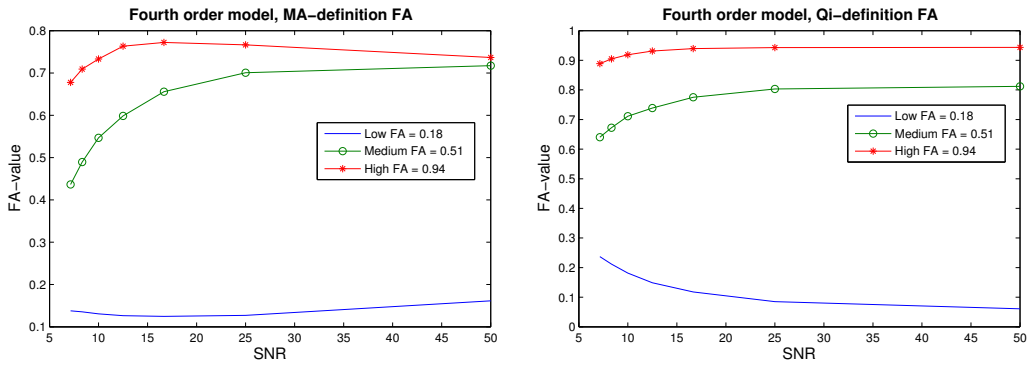
**(a) Description:** FA's estimated with MA's FA-definition for the fourth order tensor model, ground truth FA: $FA_{low} = 0.18$, $FA_{med} = 0.51$ and $FA_{high} = 0.94$.
**Comment:** High FA-estimation consistently underestimates, medium FA-estimation consistently overestimates, low FA-estimation consistently underestimates.

**(b) Description:** FA's estimated with Qi's FA-definition for the fourth order model, ground truth FA: $FA_{low} = 0.18$, $FA_{med} = 0.51$ and $FA_{high} = 0.94$.
**Comment:** High FA-estimation approaches ground truth FA with increased SNR, medium FA-estimation consistently overestimates, low FA-estimation underestimates for SNR above 8 and decreases with increasing SNR.

**Figure B.4: Description:** FA's estimated with Qi's and MA's FA-definitions for the fourth order tensor model.

## B.2  Two Fibre Structure

### B.2.1  High-High FA Fibre Structure
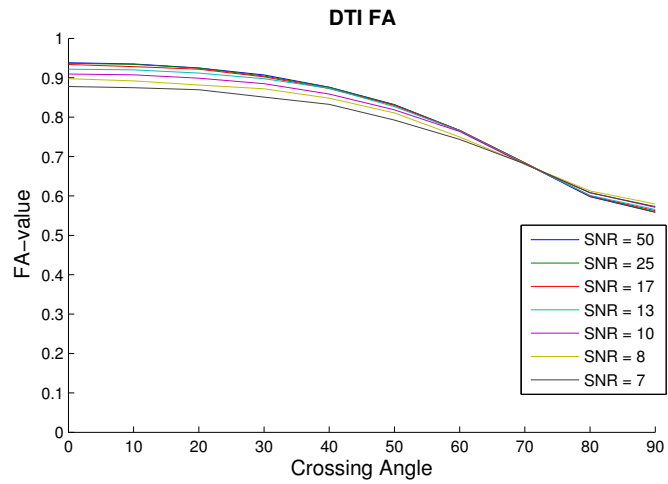


**Figure B.5: Description:** Synthetic signal, two fibres with $FA_1 = FA_2 = 0.94$, DTI FA-estimation.
**Comment:** For parallel fibres the estimated FA is close to the mean of the two ground truth FA-values, for increasing crossing angle the estimated FA decreases.

97
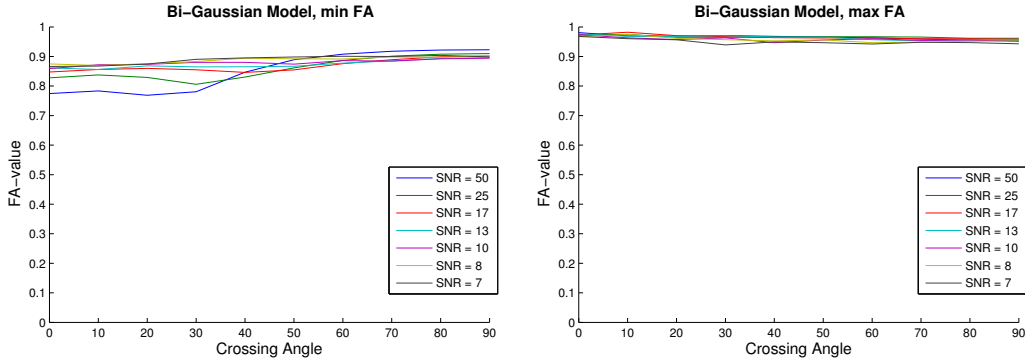
**(a) Description:** Synthetic signal, two fibres with $FA_1 = FA_2 = 0.94$. Minimum of FA's estimated with bi-Gaussian model. Ranged random initialisation.

**Comment:** With increasing SNR, the FA decreases with decreasing crossing angle for angles below $50°$. Close to mean of ground truth FA-values, but slightly underestimated.

**(b) Description:** Synthetic signal, two fibres with $FA_1 = FA_2 = 0.94$. Maximum of FA's estimated with bi-Gaussian model. Ranged random initialisation.

**Comment:** The estimated FA is independent of the crossing angle and close to mean of ground truth FA but slightly overestimated.

**Figure B.6: Description:** Synthetic signal, two fibres with $FA_1 = FA_2 = 0.94$, minimum and maximum of FA's estimated with the bi-Gaussian model.
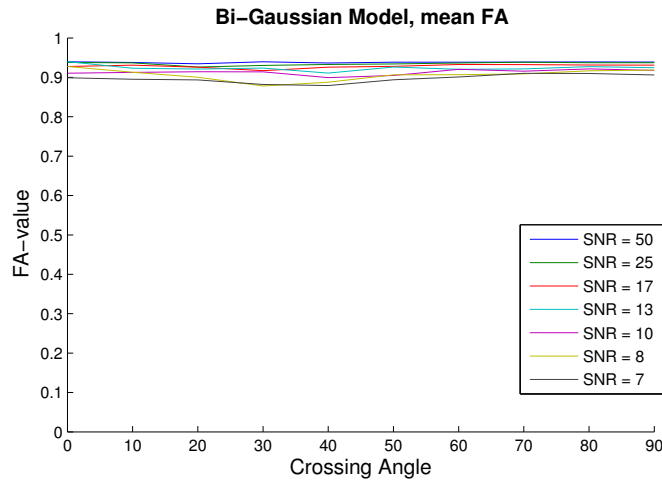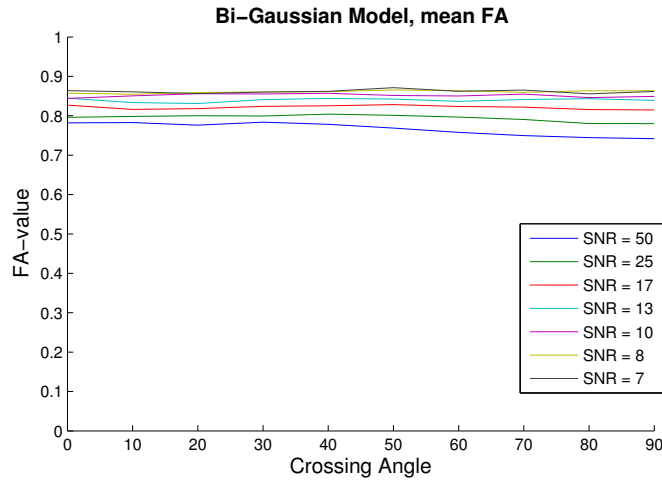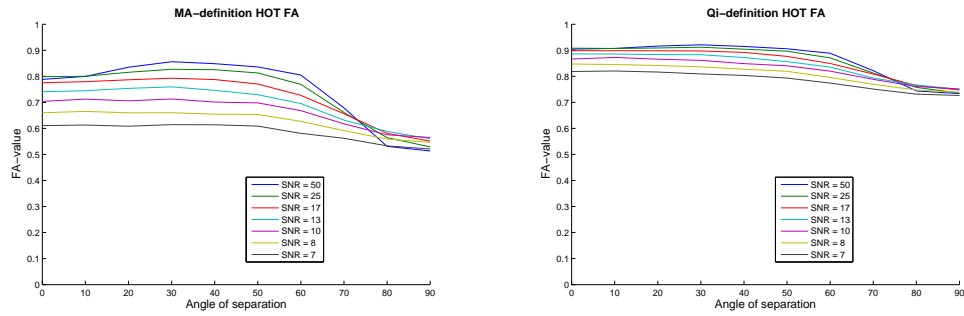


**Figure B.7: Description:** Synthetic signal, two fibres with $FA_1 = FA_2 = 0.94$. Mean of FA's estimated with the bi-Gaussian model. Ranged random initialisation.

**Comment:** The estimated FA is independent of the crossing angle and close to the mean of ground truth FA's, with the best result for the highest SNR.
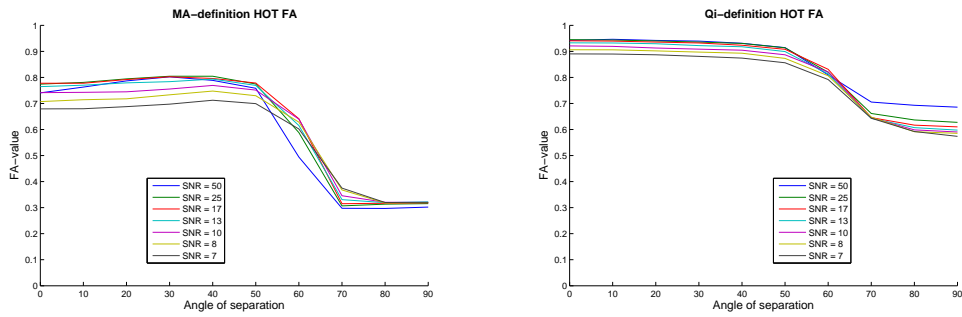
**(a) Description:** Synthetic signal, two fibres with $FA_1 = FA_2 = 0.94$. FA's estimated with MA's FA-definition for the fourth order model.

**Comment:** With crossing angle increasing from $50°$ to $70°$, FA decreases, below $50°$ the estimated FA is lower than ground truth mean FA, and for crossing angle above $70°$ much lower.

**(b) Description:** Synthetic signal, two fibres with $FA_1 = FA_2 = 0.94$. FA's estimated with Qi's FA-definition for the fourth order model.

**Comment:** With crossing angle increasing from $50°$ to $80°$, FA decreases, below $50°$ the estimated FA-values is close to the mean ground truth-FA, and above $80°$ it is lower than ground truth-FA.

**Figure B.8: Description:** Fourth order tensor model, synthetic signal, two fibres with $FA_1 = FA_2 = 0.94$.
**Comment:** For both definitions, for increased SNR the estimated FA is closer to the mean ground truth FA.
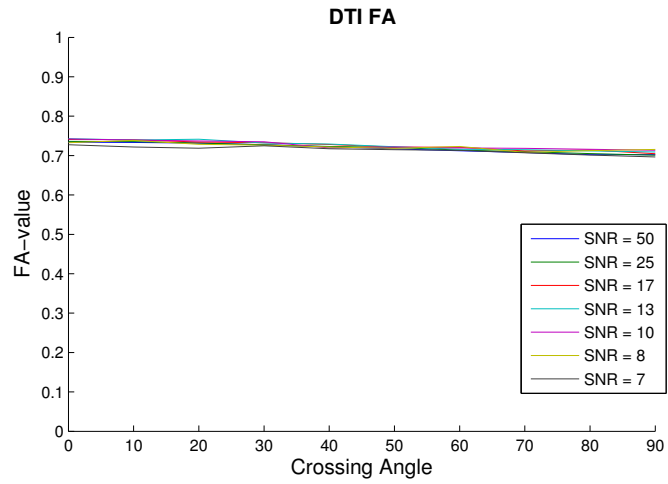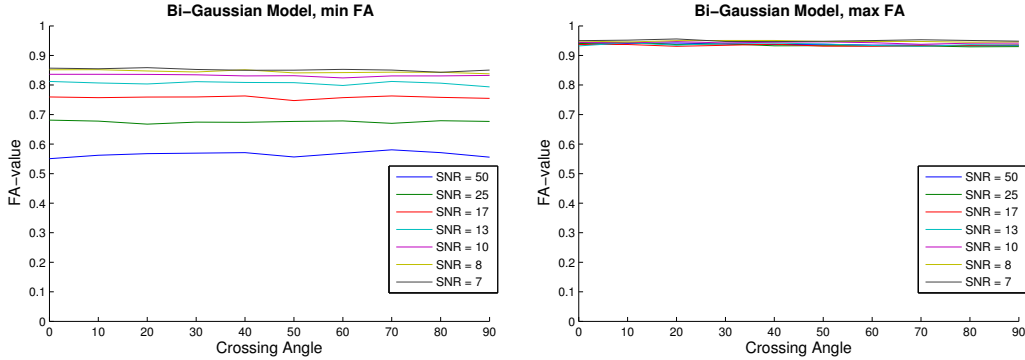
## B.2.2   High-Medium FA Fibre Structure
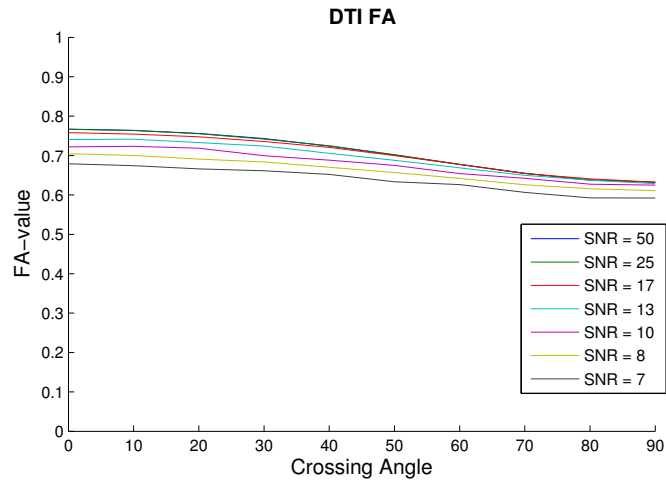


**Figure B.9: Description:** Synthetic signal, two fibres with $FA_1 = 0.94$ and $FA_2 = 0.51$, DTI FA-estimation.
**Comment:**   Estimated FA decreases with increasing crossing angle and increases with increasing SNR. Estimated FA is close to the mean of ground truth FA.
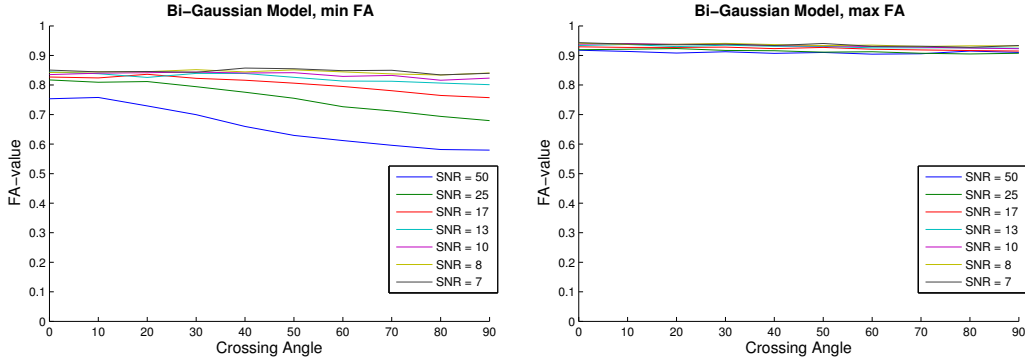
**(a) Description:** Synthetic signal, two fibres with FA$_1$ = 0.94 and FA$_2$ = 0.51. Minimum of FA's estimated with bi-Gaussian model. Ranged random initialisation.
**Comment:** With increasing crossing angle and SNR above 13 FA decreases. Compared to minimum of ground truth FA, estimated FA is overestimated.

**(b) Description:** Synthetic signal, two fibres with FA$_1$ = 0.94 and FA$_2$ = 0.51. Maximum of FA's estimated with bi-Gaussian model. Ranged random initialisation.
**Comment:** Estimated FA is close to constant at maximum of ground truth maximum FA.

**Figure B.10: Description:** Synthetic signal, two fibres with FA$_1$ = 0.94 and FA$_2$ = 0.51, minimum and maximum of FA's estimated with the bi-Gaussian model.
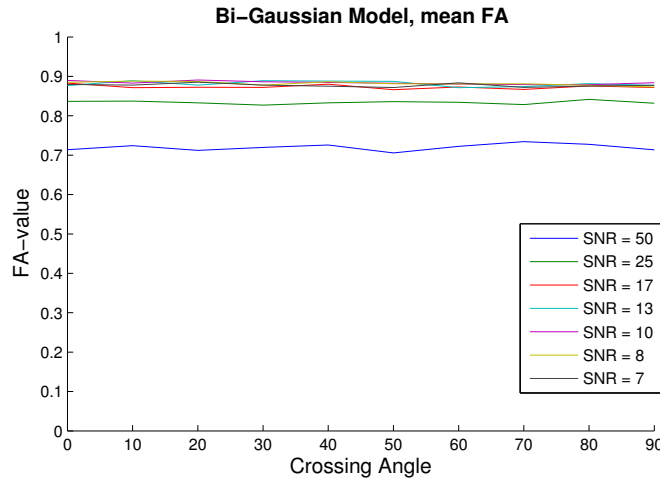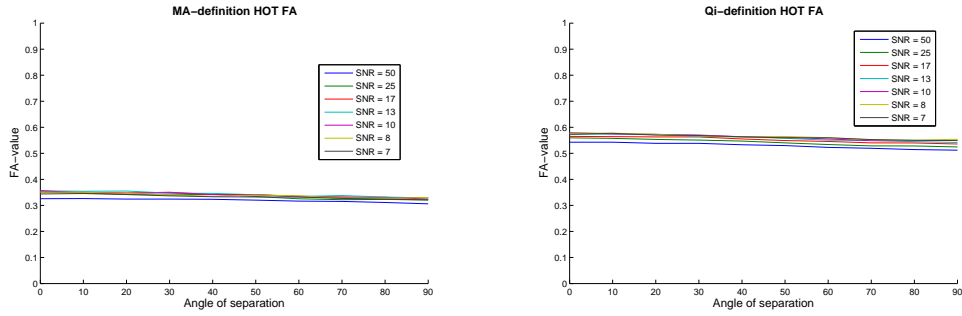


**Figure B.11: Description:** Synthetic signal, two fibres with FA$_1$ = 0.94 and FA$_2$ = 0.51. Mean of FA's estimated with the bi-Gaussian model. Ranged random initialisation.
**Comment:** Crossing angle has little impact on FA, with increasing SNR FA decreases. Estimated FA is consistently higher than mean ground truth FA.

101

**(a) Description:** Synthetic signal, two fibres with $FA_1 = 0.94$ and $FA_2 = 0.51$ FA's estimated with MA's FA-definition for the fourth order model.

**Comment:** For crossing angles above 70° and SNR above 13 FA decreases with increasing crossing angle and SNR. Below 70° and SNR 13 FA instead increases with increasing SNR.

**(b) Description:** Synthetic signal, two fibres with $FA_1 = 0.94$ and $FA_2 = 0.51$. FA's estimated with Qi's FA-definition for the fourth order model.

**Comment:** For crossing angle above 60° estimated FA decreases with increasing crossing angle.

**Figure B.12: Description:** Fourth order tensor model, synthetic signal, two fibres with $FA_1 = 0.94$ and $FA_2 = 0.51$.
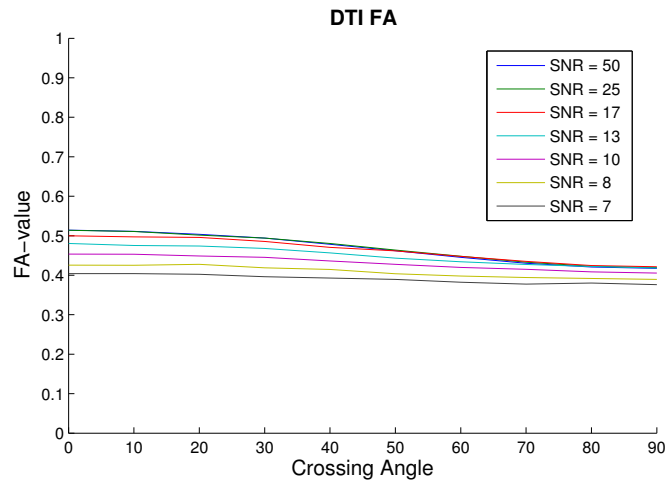
### B.2.3 High-Low FA Fibre Structure



**Figure B.13: Description:** Synthetic signal, two fibres with $FA_1 = 0.94$ and $FA_2 = 0.18$, DTI FA-estimation.
**Comment:** Estimated FA decreases slightly with increasing crossing angle. Compared to mean of ground truth FA, FA is consistently overestimated.

**(a) Description:** Synthetic signal, two fibres with $FA_1 = 0.94$ and $FA_2 = 0.18$. Minimum of FA's estimated with bi-Gaussian model. Ranged random initialisation.
**Comment:** Estimated FA decreases with increasing SNR.

**(b) Description:** Synthetic signal, two fibres with $FA_1 = 0.94$ and $FA_2 = 0.18$. Maximum of FA's estimated with bi-Gaussian model. Ranged random initialisation.
**Comment:** Estimated FA is constant close to maximum ground truth FA for all crossing angles and SNR.

**Figure B.14: Description:** Synthetic signal, two fibres with $FA_1 = 0.94$ and $FA_2 = 0.18$, minimum and maximum of FA's estimated with the bi-Gaussian model.
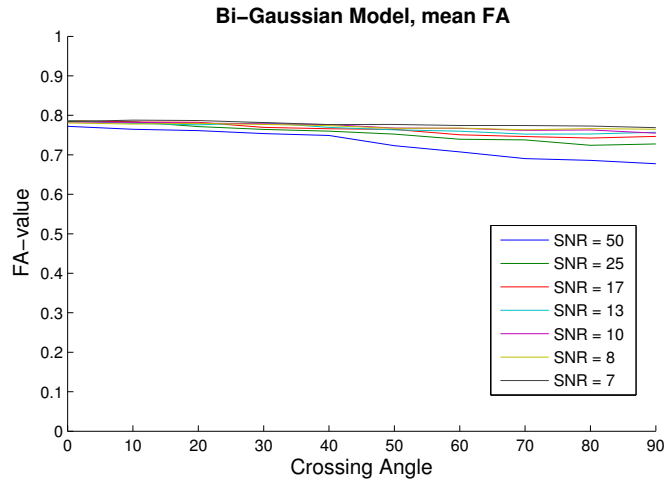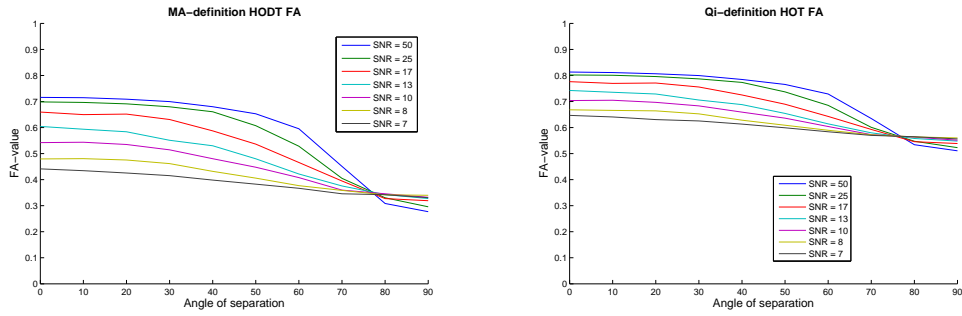


**Figure B.15: Description:** Synthetic signal, two fibres with $FA_1 = 0.94$ and $FA_2 = 0.18$. Mean of FA's estimated with the bi-Gaussian model. Ranged random initialisation.
**Comment:** For SNR 50 and 25 estimated FA is lower than for the other SNR. Compared to mean of ground truth FA, estimated FA is consistently overestimated.

**(a) Description:** Synthetic signal, two fibres with $FA_1 = 0.94$ and $FA_2 = 0.18$. FA's estimated with MA's FA-definition for the fourth order model.
**Comment:** Compared to mean of ground truth FA, the estimated FA is consistently underestimated.

**(b) Description:** Synthetic signal, two fibres with $FA_1 = 0.94$ and $FA_2 = 0.18$. FA's estimated with Qi's FA-definition for the fourth order model.
**Comment:** Estimated FA decreases some for increasing crossing angle and SNR, and is close to mean of ground truth FA.

**Figure B.16: Description:** Fourth order tensor model, synthetic signal, two fibres with $FA_1 = 0.94$ and $FA_2 = 0.18$.
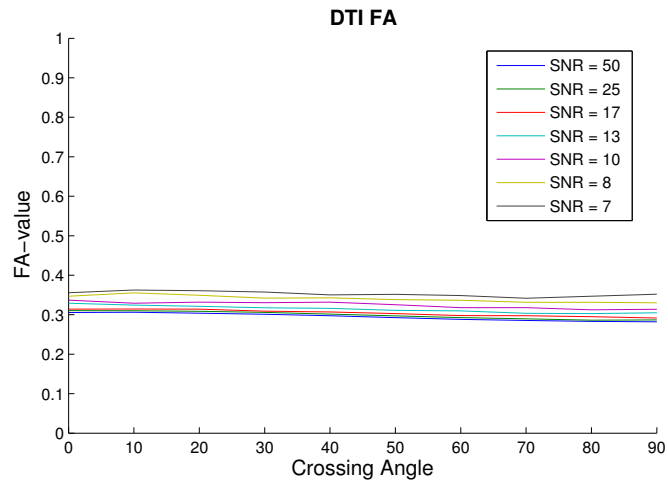
105

### B.2.4 Medium-Medium FA Fibre Structure



**Figure B.17: Description:** Synthetic signal, two fibres with $FA_1 = FA_2 = 0.51$, DTI FA-estimation.
**Comment:** Estimated FA decreases with decreasing SNR, for high SNR decreases with increasing crossing angle, a little lower than ground truth mean FA.
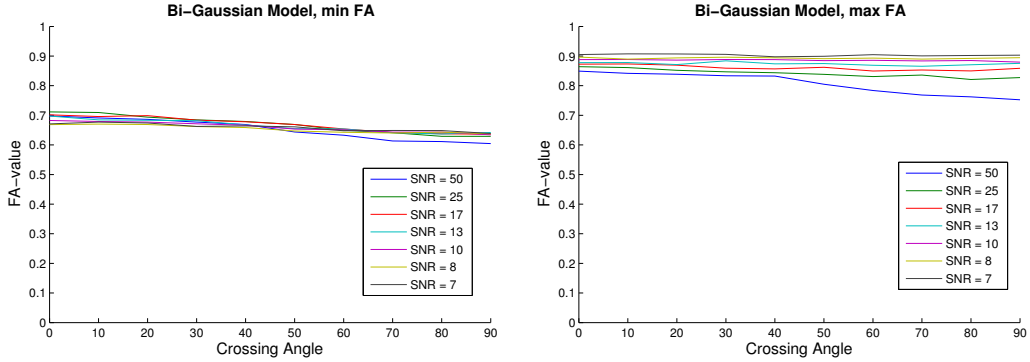
**(a) Description:** Synthetic signal, two fibres with $FA_1 = FA_2 = 0.51$ . Minimum of FA's estimated with bi-Gaussian model. Ranged random initialisation.
**Comment:** Estimated FA is consistently higher than both ground truth FA-values.

**(b) Description:** Synthetic signal, two fibres with $FA_1 = FA_2 = 0.51$ . Maximum of FA's estimated with bi-Gaussian model. Ranged random initialisation.
**Comment:** Estimated FA decreases with increasing SNR, but is consistently much higher than ground truth FA for both fibres.

**Figure B.18: Description:** Synthetic signal, two fibres with $FA_1 = FA_2 = 0.51$, minimum and maximum of FA's estimated with the bi-Gaussian model. Ranged random intialisation.



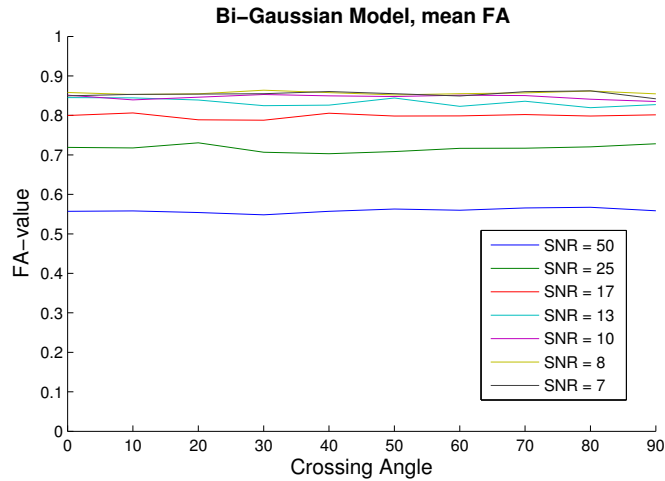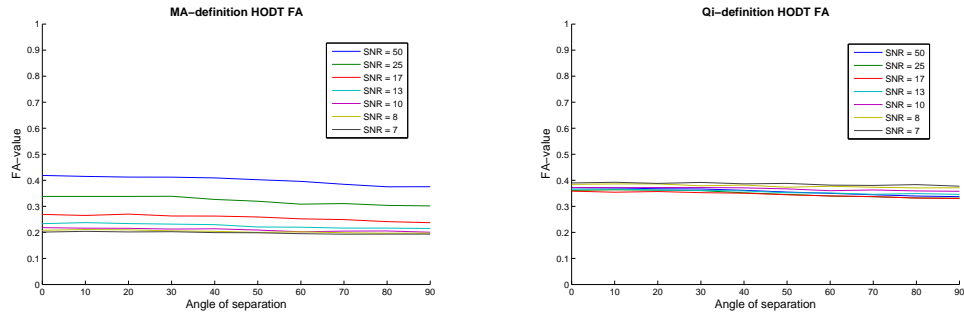**Figure B.19: Description:** Synthetic signal, two fibres with $FA_1 = FA_2 = 0.51$. Mean of FA's estimated with the bi-Gaussian model. Ranged random initialisation.
**Comment:** Estimated FA is consistently higher than both ground truth FA-values

**(a) Description:** Synthetic signal, two fibres with $FA_1 = FA_2 = 0.51$ FA's estimated with MA's FA-definition for the fourth order model.

**Comment:** For crossing angles below $70°$ estimated FA increases with increasing SNR, for crossing angle above $80°$ estimated FA increases with decreasing SNR and is lower than mean of ground truth FA. For small crossing angles and high SNR estimated FA is high compared to mean of ground truth FA.

**(b) Description:** Synthetic signal, two fibres with $FA_1 = FA_2 = 0.51$ FA's estimated with Qi's FA-definition for the fourth order model.

**Comment:** For crossing angles below $70°$ estimated FA increases with increasing SNR, for crossing angle above $80°$ estimated FA increases with decreasing SNR. Estimated FA is consistently higher than mean of ground truth FA.

**Figure B.20: Description:** Fourth order tensor model, synthetic signal, two fibres with $FA_1 = FA_2 = 0.51$.

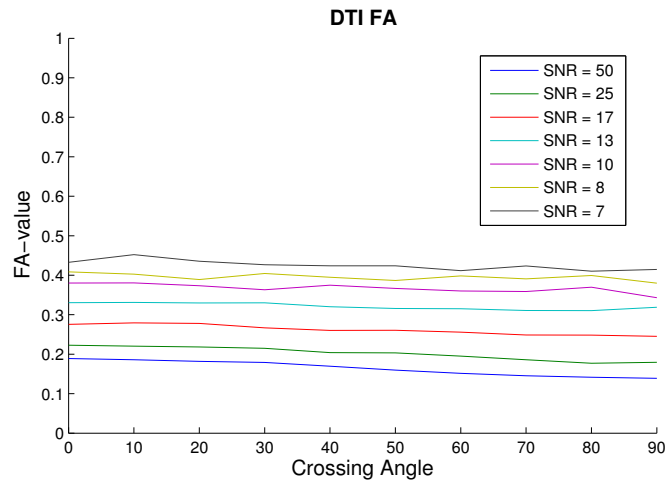## B.2.5   Medium-Low FA Fibre Structure



**Figure B.21: Description:** Synthetic signal, two fibres with $FA_1 = 0.51$ and $FA_2 = 0.18$, DTI FA-estimation.
**Comment:**   Estimated FA decreases with increasing SNR.
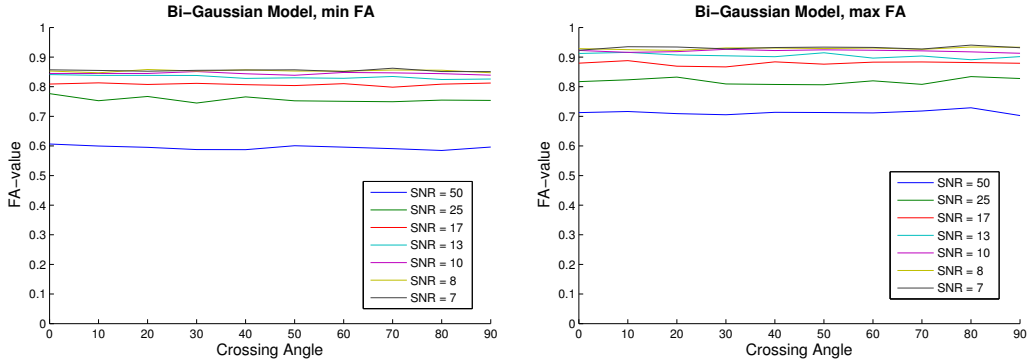
**(a) Description:** Synthetic signal, two fibres with $FA_1 = 0.51$ and $FA_2 = 0.18$. Minimum of FA's estimated with bi-Gaussian model. Ranged random initialisation.
**Comment:** Estimated FA decreases with increasing SNR and is consistently higher than mean of ground truth FA.

**(b) Description:** Synthetic signal, two fibres with $FA_1 = 0.51$ and $FA_2 = 0.18$. Minimum of FA's estimated with bi-Gaussian model. Ranged random initialisation.
**Comment:** Estimated FA decreases with increasing SNR and is consistently higher than mean of ground truth FA.

**Figure B.22: Description:** Synthetic signal, two fibres with $FA_1 = 0.51$ and $FA_2 = 0.18$, minimum and maximum of FA's estimated with the bi-Gaussian model. Ranged random intialisation.



**Figure B.23: Description:** Synthetic signal, two fibres with $FA_1 = 0.51$ and $FA_2 = 0.18$. Mean of FA's estimated with the bi-Gaussian model. Ranged random initialisation.
**Comment:** Estimated FA decreases with increasing SNR and is consistently higher than mean of ground truth FA.

**(a) Description:** Synthetic signal, two fibres with $FA_1 = 0.51$ and $FA_2 = 0.18$. FA's estimated with MA's FA-definition for the fourth order model.
**Comment:** Estimated FA increases with increasing SNR.

**(b) Description:** Synthetic signal, two fibres with $FA_1 = 0.51$ and $FA_2 = 0.18$. FA's estimated with Qi's FA-definition for the fourth order model.
**Comment:** Estimated FA is close to mean of ground truth FA for all crossing angles and SNR.

**Figure B.24: Description:** Ground truth FA's are $FA_1 = 0.51$ and $FA_2 = 0.18$.

111

## B.2.6  Low-Low FA Fibre Structure



**Figure B.25:  Description:** Synthetic signal, two fibres with $FA_1 = FA_2 = 0.18$, DTI FA-estimation.
**Comment:** Estimated FA decreases with increasing SNR, the highest SNR is close to mean ground truth FA, the lower the SNR the more overestimated FA is.
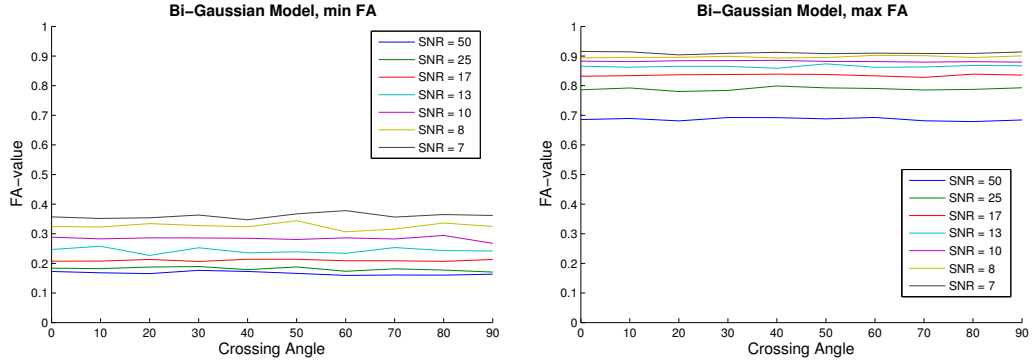
**(a) Description:** Synthetic signal, two fibres with $FA_1 = FA_2 = 0.18$. Minimum of FA's estimated with bi-Gaussian model. Ranged random initialisation.
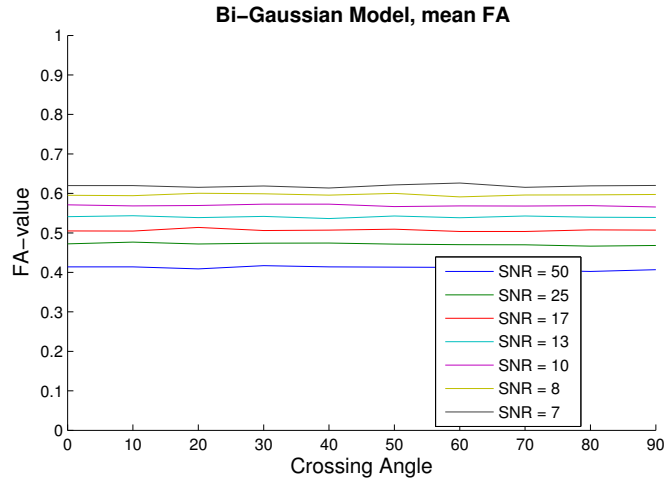**Comment:** Estimated FA decreases with increasing SNR.

**(b) Description:** Synthetic signal, two fibres with $FA_1 = FA_2 = 0.18$. Maximum of FA's estimated with bi-Gaussian model. Ranged random initialisation.
**Comment:** Estimated FA decreases with increasing SNR and is consistently much higher than both ground truth FA-values.

**Figure B.26: Description:** Synthetic signal, two fibres with $FA_1 = FA_2 = 0.18$, minimum and maximum of FA's estimated with the bi-Gaussian model. Ranged random intialisation.
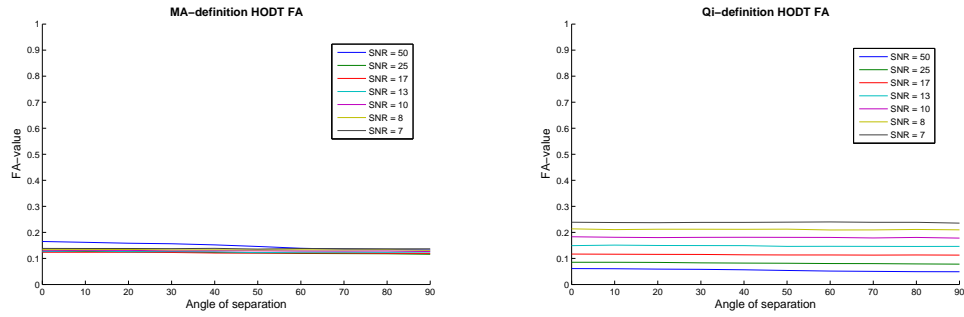


**Figure B.27: Description:** Synthetic signal, two fibres with $FA_1 = FA_2 = 0.18$. Mean of FA's estimated with the bi-Gaussian model. Ranged random initialisation.
**Comment:** Estimated FA decreases with increasing SNR and is consistently higher than both ground truth FA-values.

**(a) Description:** Synthetic signal, two fibres with $FA_1 = FA_2 = 0.18$. FA's estimated with MA's FA-definition for the fourth order model.
**Comment:** Estimated FA is lower than both ground truth FA-values for all crossing angles and SNR.

**(b) Description:** Synthetic signal, two fibres with $FA_1 = FA_2 = 0.18$. FA's estimated with Qi's FA-definition for the fourth order model.
**Comment:** Estimated FA decreases with increasing SNR.

**Figure B.28: Description:** Ground truth FA's are $FA_1 = FA_2 = 0.18$.

# C

# FA Maps from Real DWI-Data
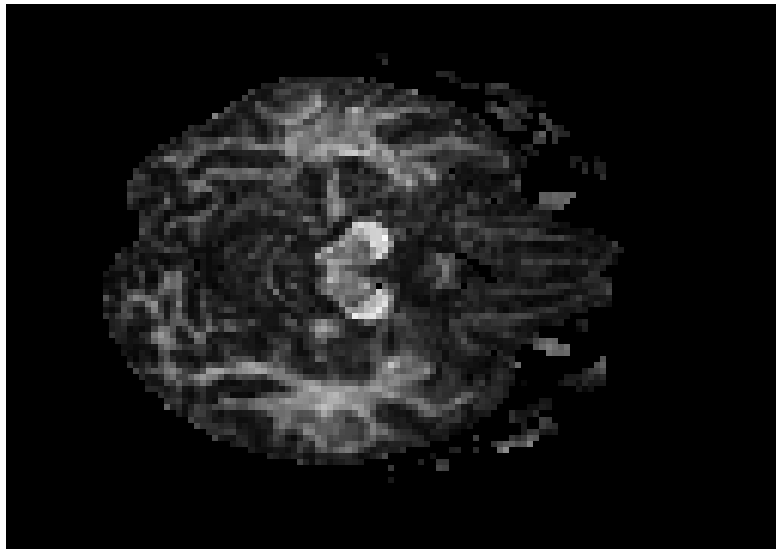


**Figure C.1: Description:** The conventional FA from DTI. Real DWI-data.
**Description:** Compared to the real data results from the bi-Gaussian model, see Figures C.2, C.3 and C.4, and the HOT model, see Figures C.5 and C.6, this reveals more information about the brain structure.
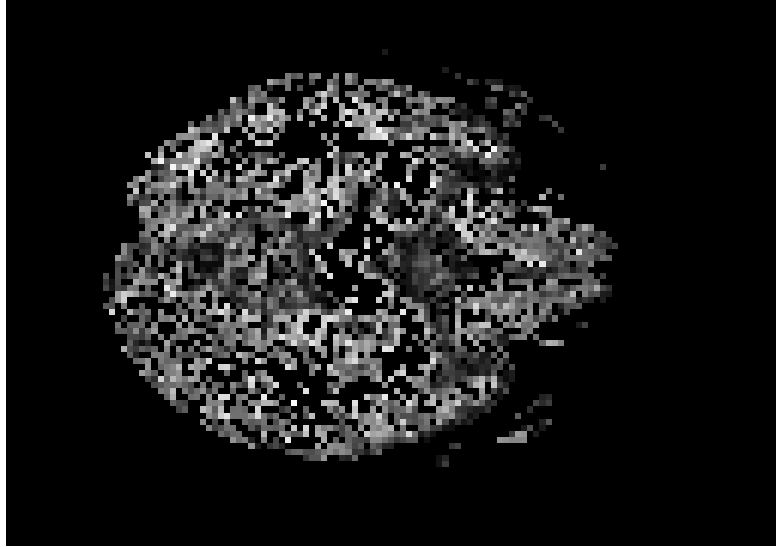
**Figure C.2: Description:** The minimum FA of the two FA-values from bi-Gaussian model.
**Comment:** Many voxels are black, indicating that one of the estimated tensors are not PSD resulting in that the lowest FA-value is zero.



**Figure C.3: Description:** The maximum FA of the two FA-values from bi-Gaussian model.
**Comment:** Fewer black voxels than compared to Figure C.2, but much brighter than Figure C.1. Difficult to see structures.
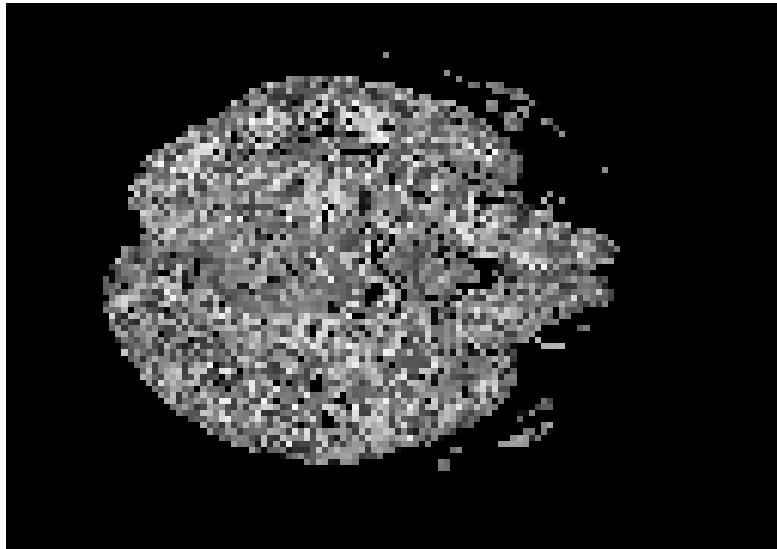
**Figure C.4: Description:** The mean FA of the two FA from bi-Gaussian model.
**Comment:**  Fewer black voxels than compared to Figure C.2, but difficult to see structures.
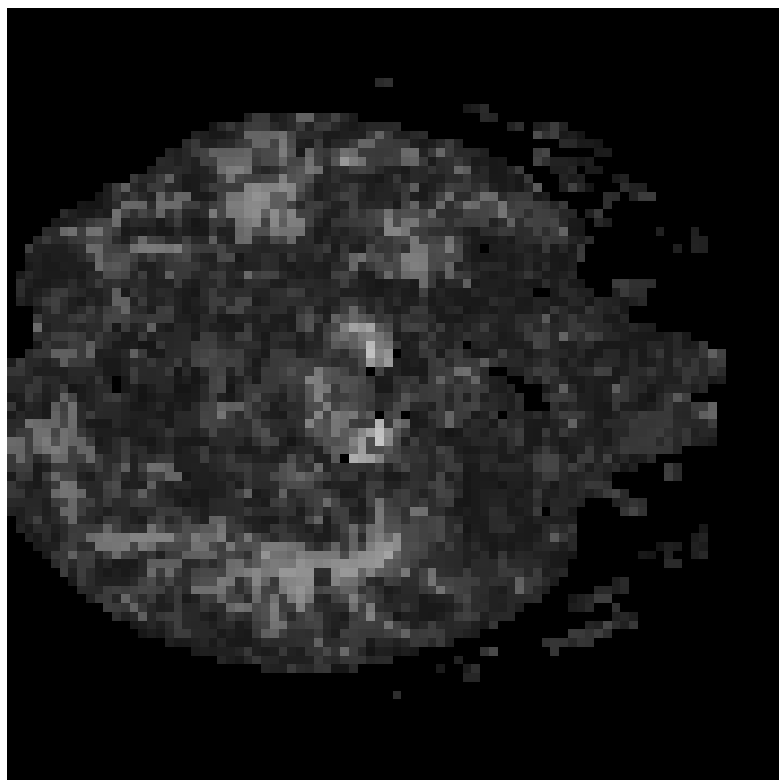
**Figure C.5: Description:** The MA definition of FA from HOT, filtered with Gaussian window of 4 voxel size.
**Comment:** Compared with Figure C.1 fewer structures are visible, but more structures than in Figure C.4.
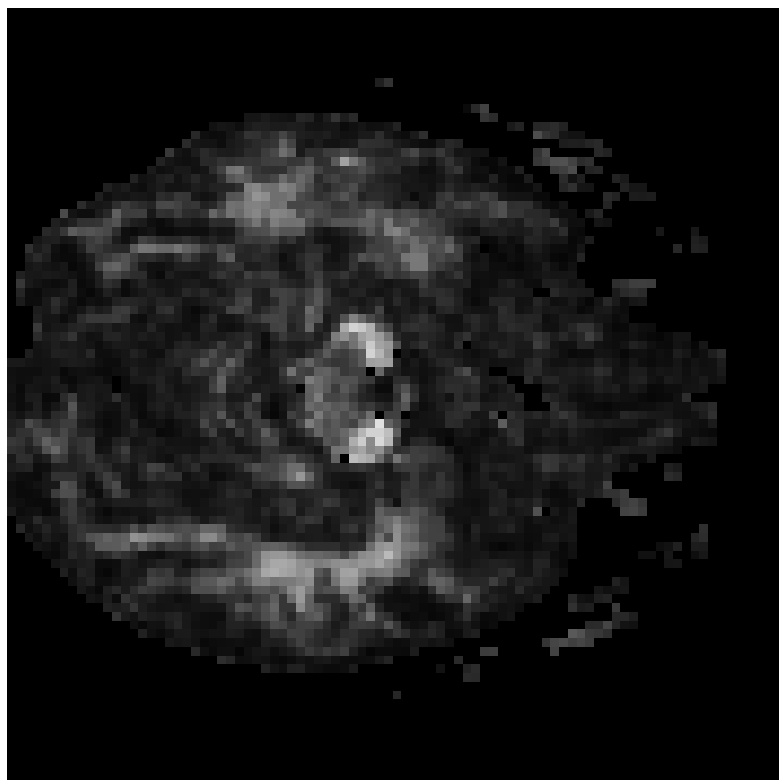
**Figure C.6: Description:** The Qi definition of FA from HOT, filtered with Gaussian window of 4 voxel size.
**Comment:** Compared to Figure C.1 fewer structures are visible, but more structures than in Figure C.4. Compare with Figure C.5.